Chiral Acyl Radicals Generated by Visible Light Enable Stereoselective Access to 3,3-Disubstituted Oxindoles: Application toward the Synthesis of (–)- and (+)-Physovenine

by

Josef Späth

Supervised by

Dr Wade Petersen

And Co-supervised by

Professor Roger Hunter

Dissertation presented for the Degree

Master of Science

Department of Chemistry

University of Cape Town

Rondebosch, Cape Town

7701

December 2023

Acknowledgments

I possess tremendous gratitude for the role my supervisor, Dr Wade Petersen, served in the production of this work. In addition to directly connecting me to funding, constant guidance and explorable ideas throughout the process, he also supplied the various essential roles of teacher, role model, (occasional) first aider and hype man.

My co-supervisor, Professor Roger Hunter deserves praise as his wise and detailed input was instrumental at various stages in the overall construction of this thesis and the publication that preceded it.

Additional thanks are due to the individuals who supplied the most help to me within the laboratory, particularly Meghan Oddy and especially Dr Dan Kusza. Both contributed significantly to the development of my skills in that setting, as well as providing immediate companionship for the numerous hours spent in the lab. This category of acknowledgement should also be extended to the rest of the Petersen group, who all individually played some part in the completion of this work.

Finally, thanks go out to my friends and family (and roommate's cat), who continue to be receptive, supportive, and constructive in all cases.

Declaration

I know the meaning of plagiarism and declare that **"Chiral Acyl Radicals Generated by Visible Light Enable Stereoselective Access to 3,3-Disubstituted Oxindoles: Application toward the Synthesis of (–)- and (+)-Physovenine"** is my own work and has not been previously presented for the award of any degree at any university. All sources of information are cited and fully referenced.

Signature: Signed by candidate

Abstract

Radical species serve as powerful tools for carbon-carbon bond formation in synthetic organic chemistry. Such species can be formed in an efficient and environmentally friendly manner by way of photoredox catalysis, which uses a photocatalyst in conjunction with visible light (typically) to generate the necessary environment for radical generation under extremely mild conditions.

This work outlines the development of a novel imidazolidinone-derived acyl radical, generated under photoredox catalysis, and its application toward the stereoselective synthesis of 3,3-disubstituted oxindoles via an addition-cyclisation cascade sequence to acrylamide precursors. Six oxindoles were produced in up to 85% yield, with moderate diastereoselectivity of up to 2.2:1, but which could be easily separated by standard chromatography to yield pure diastereomers. Mechanistic studies, by virtue of TEMPO-trapping experiments provided strong support for the existence of the proposed acyl-radical, and further synthetic utility of the research was demonstrated in the formal synthesis of the natural product (–)-physovenine, a member of the biologically active cyclotryptamine alkaloid

Glossary of Terms

g Grams

mg milligrams

mL Millilitres

µL Microlitres

mmol millimoles

nm Nanometres

h/hrs Hours

ppm Parts per million

eq. Equivalents

hv light energy

Hz Hertz

ΔG Change in Gibbs Free Energy

W Watts

°C Degrees Celsius

rt Room temperature

Ar Argon

ACN Acetonitrile

DCM Dichloromethane

DMF Dimethylformamide

DMSO Dimethyl sulfoxide

EtOAc Ethyl Acetate

EtOH Ethanol

MeOH Methanol

Hex Hexanes

PC Photocatalyst

HOMO Highest occupied molecular orbital

SOMO Singly occupied molecular orbital

LUMO Lowest unoccupied molecular orbital

bpy Bipyridine ligand

ppy Phenylpyridine ligand

S_0 Singlet ground state

S_1 Singlet excited state

T_1 Triplet excited state

IC Internal conversion

ISC Intersystem crossing

EnT Energy transfer

SET Single electron transfer

HAT Hydrogen atom transfer

PCET Proton coupled electron transfer

E_{ox} Energy of oxidation half reaction

E_{red} Energy of reduction half reaction

TLC Thin-layer chromatography

NMR Nuclear magnetic resonance

HRMS High resolution mass spectrometry

IR Infrared

J Coupling constant

LED Light emitting diode

ppy phenylpyridine ligand

SCE Saturated calomel electrode

Table of Contents

Introduction

1. Photoredox Chemistry: History and Context

Chemical transformations often require a measured input of energy to occur; there are many transformations which would be thermodynamically favourable, were it not for the need to surmount a kinetic barrier. Traditionally, chemists achieve this energy requirement by way of heating. Photochemistry, however, supplies this energy by way of light, tapping into the energy stored in the electromagnetic field oscillations of photons.

Photosynthesis, the process where organisms trap the energy in light to be used to power the chemical reactions necessary for survival, has likely existed for upwards of 2 billion years.[1]

Plants have since developed complex photosystems of proteins and individual molecules that harvest and make use of light energy for metabolism; the most important being the chlorophyll pigments. Chlorophyll B is shown as a representative example (**Figure 1.1)**.

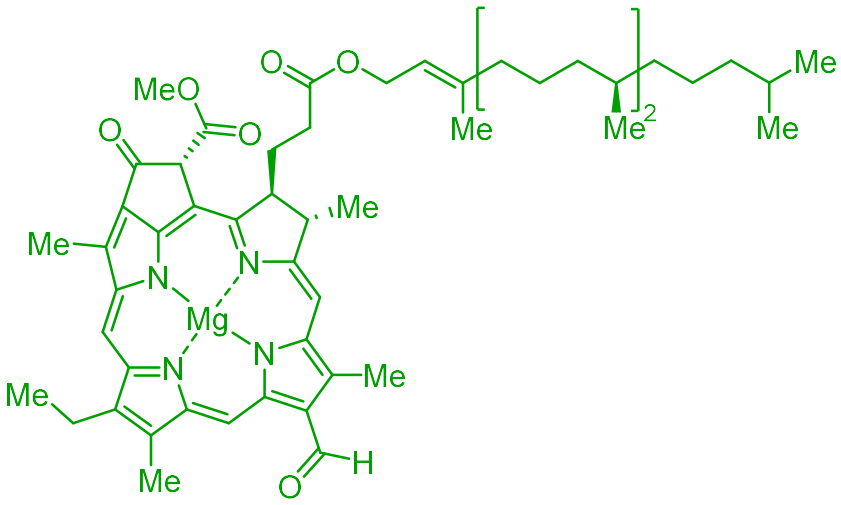

Figure 1.1: *Chlorophyll B, one of numerous chlorophylls present in plants.*

Upon exposure to light, chlorophyll enters an excited state through absorption of an incident photon (photoexcitation), and this initiates a series of electron transfer processes which carries the photon energy to the reaction centre of the photosystem; ultimately driving metabolism. Importantly, the chlorophylls are always reduced back to their electronic ground state (by removing electrons from water), enabling them to restart the cycle.[2] The field of

photocatalysis is inspired by this process, with various compounds being used in place of chlorophylls to absorb light, thereby supplying energy to a chemical reaction. While photosynthesis is an "uphill" process, thermodynamically speaking (ΔG>0), photocatalysis generally features a thermodynamically favourable (ΔG<0) process where the reaction is catalysed by a photocatalyst[3] — molecules that accelerate and/or facilitate chemical processes when exposed to light.

The Photophysics of Photocatalysts

Within the context of chemical synthesis, numerous photocatalysts have been developed since the early days of photochemistry. Broadly speaking, these are either transition metal complexes or purely organic dyes (**Figure 1.2**). No matter the structural form, however, the photophysics that govern the reactivity of these catalysts remain broadly the same.

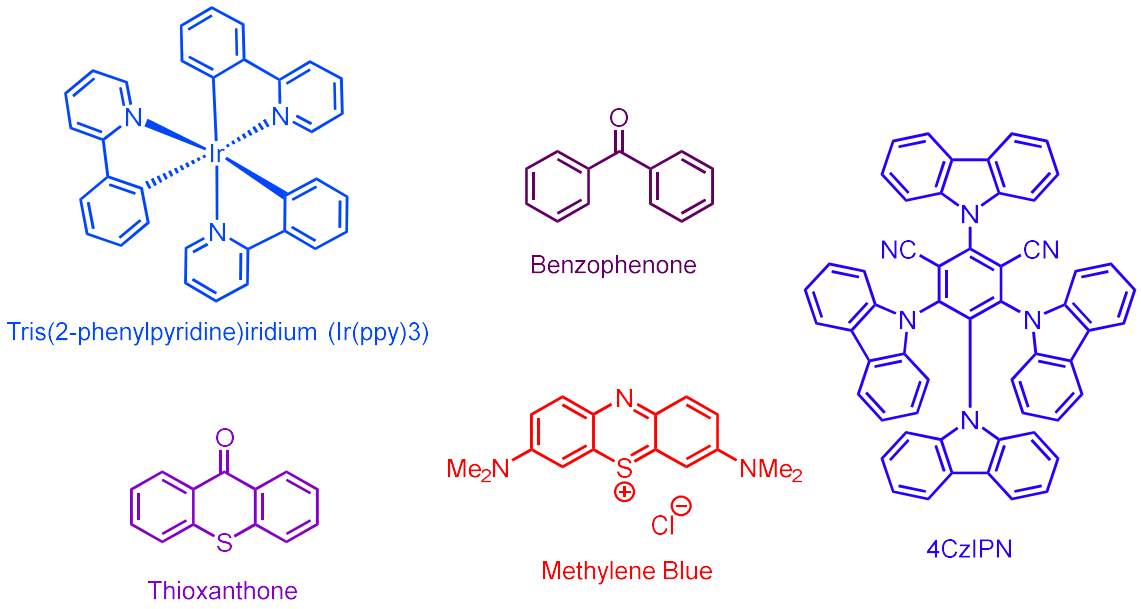

Figure 1.2: *Various photocatalysts that have, at varying times, been used in photocatalysis.*[4-6]

A simplified Jablonski diagram highlighting key photophysical processes is shown in **Figure 1.3**. By absorbing light of an appropriate wavelength, a photocatalyst becomes electronically excited: an electron is promoted from its electronic ground singlet state, $\mathbf{S_0}$, to the Franck-Condon region[7] of a high-lying singlet energy level, $\mathbf{S_n}$. The system then relaxes to its lowest lying singlet excited state, $\mathbf{S_1}$, through vibrational relaxation and internal conversion. This

occurs quickly; on the order of picoseconds. From here, the molecule is able to decay radiatively (fluorescence) or nonradiatively (via solvent collisions) back to its ground state. It is also possible for a catalyst to be quenched from this S_1 state via interaction with another chemical species, occasionally at a synthetically useful rate,[8] although this is rare. Another possibility, is for intersystem crossing (ISC) to occur — a nonradiative decay process that includes a change in spin, enabling the molecule to enter a triplet state T_n (which is lower in energy than its S_1 state). As with $S_1 \rightarrow S_0$ decay, $T_1 \rightarrow S_0$ transitions are possible both radiatively (phosphorescence) and nonradiatively, but conversion of the T_1 state back down to S_0 is spin-forbidden (Pauli's exclusion principle precludes two electrons from occupying the same orbital while having the same spin). As a consequence, excited triplet states are relatively long-lived (on the order of micro- to milliseconds) and it is primarily this characteristic that is exploited in photocatalysis: the longer an excited state persists, the greater the possibility for it to interact with another molecule.

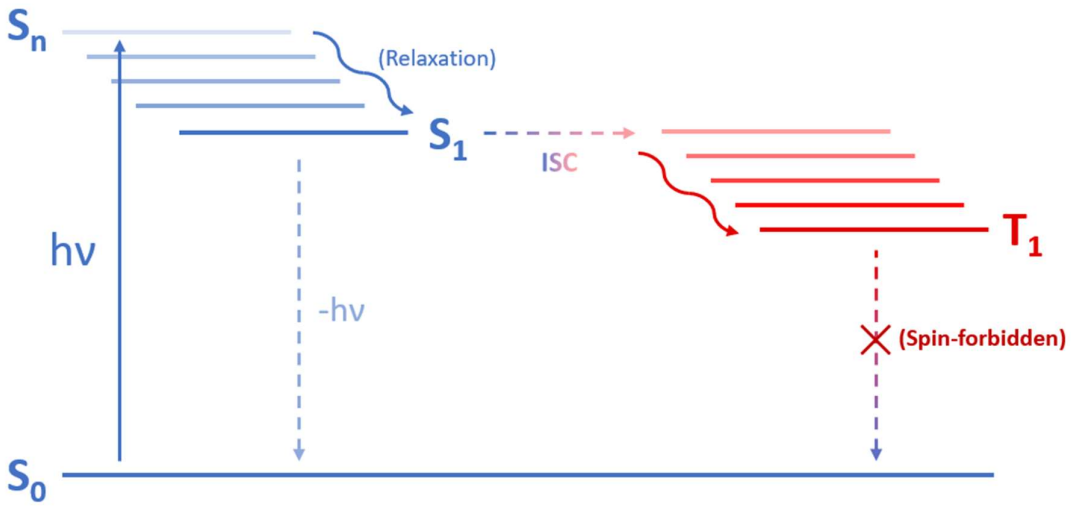

Figure 1.3: *A simplified Jablonski diagram, showing the possible electronic transitions of a photocatalyst.*

Early photochemists made use of sunlight to cause chemical transformations, sometimes with the aid of a photocatalyst. In particular, the Italian chemist Giacomo Ciamician, during the late 1800s and early 1900s, found ways to reduce/dimerise ketones and nitro compounds,

oxidise double bonds, and perform various inter and intramolecular [2+2] cycloadditions using the light that could be easily collected on a balcony at his university in Bologna.[9]

A small increase in activity was seen around the 1980s and 1990s, where some of the first photoredox catalysed reactions were explored. These chemists discovered and made use of various metal-based photocatalysts (normally complexes of ruthenium or iridium) to effect redox transformations of their substrates. Such discoveries were made by the likes of Kellogg,[10] Deronzier,[11, 12] and Okada.[13] The latter chemist is of special interest as the first person to explore the use of N-acyloxyphthalimides (**Scheme 1.1**) as precursors to various carbon-centered radical species, the utility of which is directly relevant to this thesis (*vide infra* section 6).

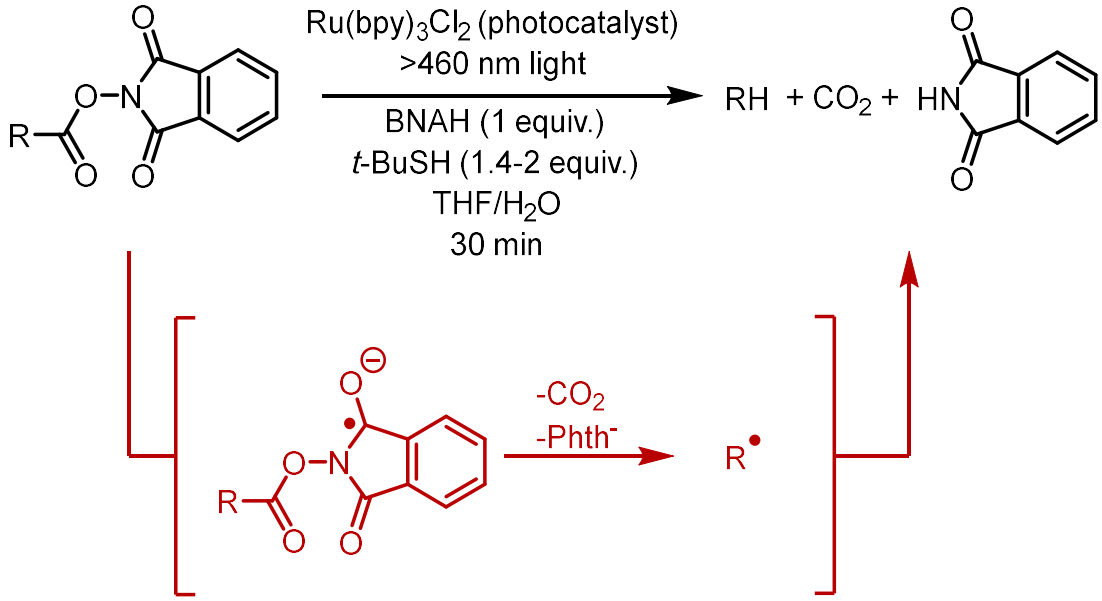

Scheme 1.1: *Photocatalytic reduction of N-acyloxyphthalimides leading to the generation of alkyl radicals, as described by Okada.*

Activation Modes in Photocatalysis

The activation of organic molecules by photocatalysts occurs primarily through several pathways: 1) single electron transfer; 2) hydrogen atom transfer; 3) proton-coupled electron transfer; and 4) triplet energy transfer. [4, 14]

1) Single electron transfer (SET) is the most relevant activation mode for this thesis: the photocatalyst either donates to or receives an electron from the substrate. Because the excited state of a photocatalyst features two singly occupied molecular orbitals (**Figure 1.4**), photocatalysts are generally able to operate as both strong single electron reductants (i.e., donating an electron to the organic substrate acting as an acceptor A → $A^{\cdot -}$), due to a high energy promoted electron, or as strong oxidisers (receiving an electron from the substrate acting as a donor D → $D^{\cdot +}$) due to the relatively low energy electron hole that remains after excitation. The former is defined as an oxidative quenching cycle, and the latter, a reductive quenching cycle (**Figure 1.5**).

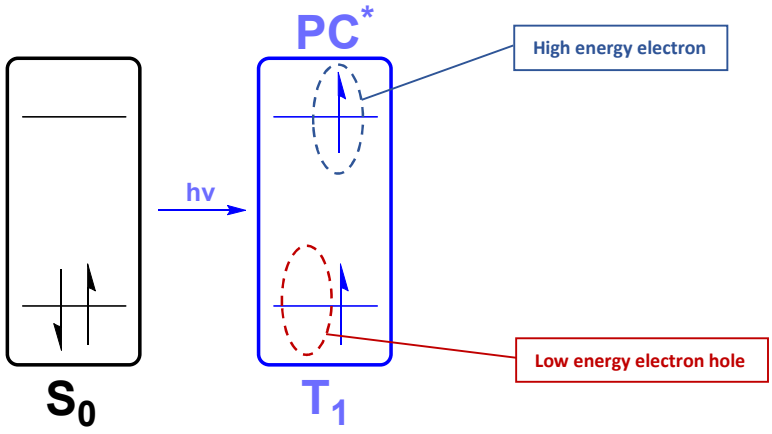

Figure 1.4: *Exciting a photocatalyst to its triplet state makes it both a better reductant and oxidant.*

Of course, to regenerate the photocatalyst (PC – see **Figure 1.5**), it must retrieve (or be relieved of) its lost (or gained) electron. This is achieved by a terminal oxidant/reductant, Ox or Red, which must either be present as a sacrificial component in a stoichiometric amount, or it can be done by the substrate itself, after it has undergone some initial molecular change and is ready to return to its original oxidation state. This latter process (i.e., when the terminal oxidant/reductant is an *in situ* generated intermediate) thus enables "redox neutral" transformations and is an important feature of photoredox catalysis.

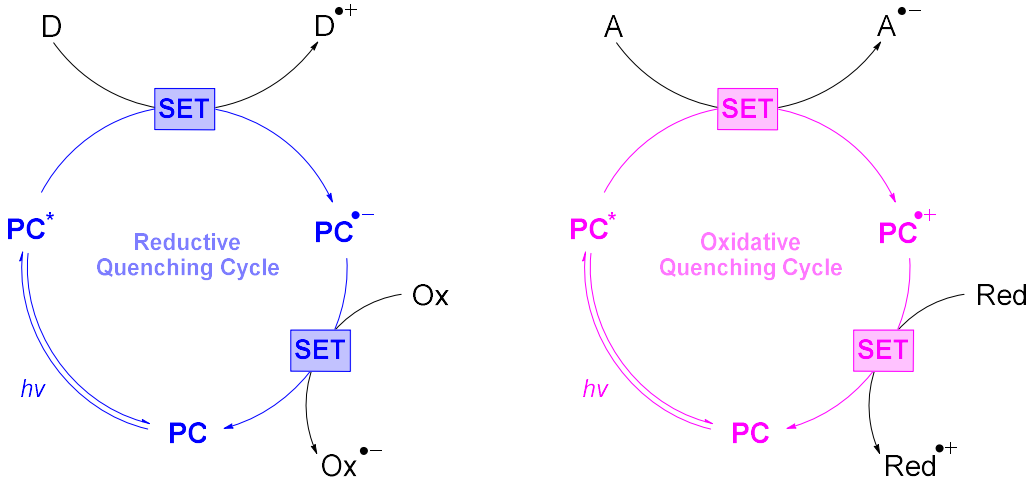

Figure 1.5: *The two possible quenching cycles a photocatalyst can circumnavigate when undergoing an SET process (PC = photocatalyst; D and A refer to the reactant as donor and acceptor respectively).*

2) In a hydrogen atom transfer (HAT) process, the photocatalyst effects the transfer of an electron along with a proton – having the effect of transferring atomic hydrogen. This involves the homolytic cleavage of a hydrogen bond, meaning that the proton and electron originate from the same place on the species donating the hydrogen atom. The HAT step either happens one step removed from the photocatalytic cycle (see path B in **Figure 1.6**), via a radical intermediate that is produced by the photocatalyst, or else the photocatalyst must be able to accommodate the extra proton itself (path A). The photocatalyst must then undergo reverse HAT or PCET (discussed next) to return to its initial state, either by interaction with a progressed reaction intermediate, or some sacrificial hydrogen atom abstractor.

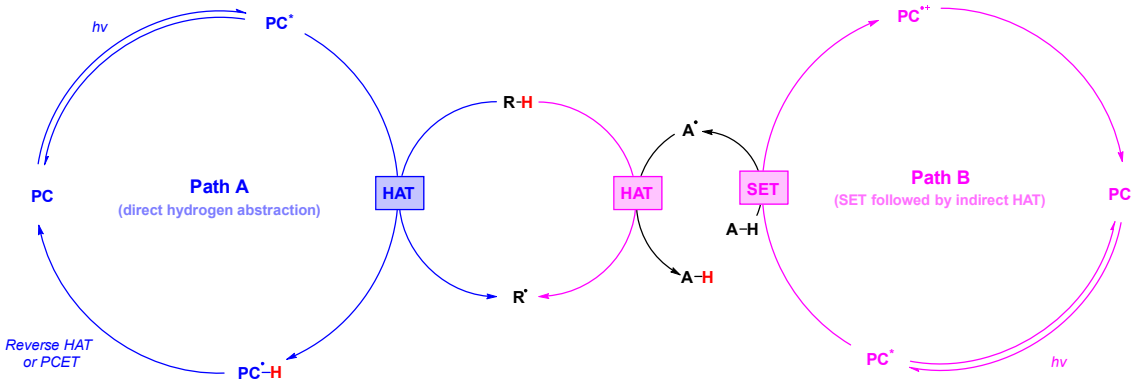

Figure 1.6: *The two generalised paths a photocatalyst undergoes when inducing an HAT process.*

3) Proton-coupled electron transfer (PCET), on the other hand, also involves the *net* transfer of a hydrogen atom, but the electron and proton do not originate from the same bond and so PCET occurs by a concomitant SET and deprotonation pathway. HAT is therefore a special case of PCET, in a sense. HAT and PCET are of no particular relevance to this thesis and will not be mentioned again; they are simply included here to show the breadth of synthetic scope photoredox catalysis can provide.

4) The final mode of activation for photocatalysts (and one which *is* relevant to the later parts of this thesis) is triplet energy transfer (EnT). In a EnT process, the excited photocatalyst ostensibly transfers its newly received energy directly to the substrate, following which it immediately returns to its initial state. The mechanism by which it achieves this transferal is known as Dexter electron transfer: the photocatalyst in its triplet excited state (PC^* in **Figure 1.7**) donates its energetically promoted electron to the substrate's LUMO while *simultaneously* receiving an electron from the substrates HOMO, thereby bringing the substrate to its triplet excited state and quenching the photocatalyst.

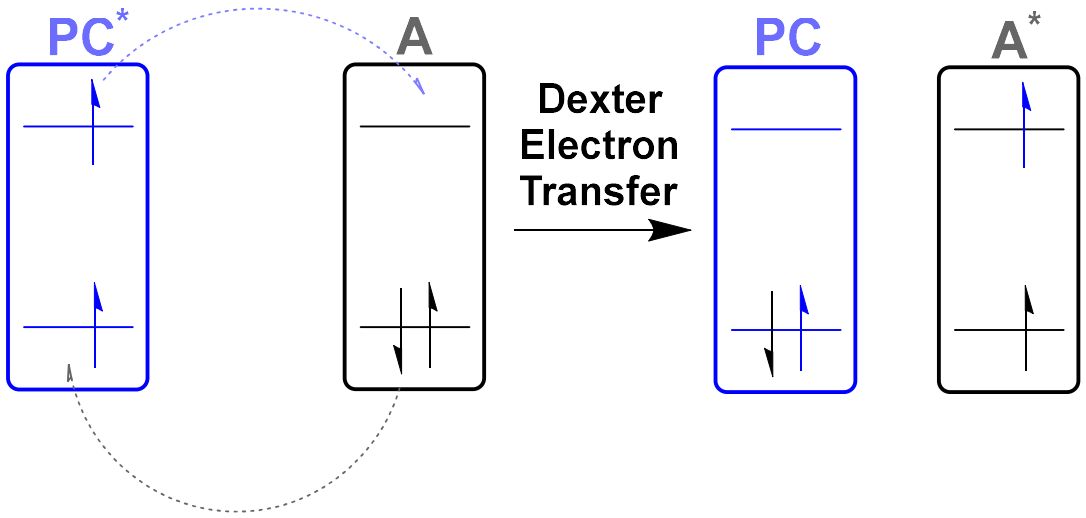

Figure 1.7: *A simple schematic depicting the process of Dexter electron transfer.*

After a lull in activity at the turn of the century, the field of photoredox catalysis saw a sudden explosion in publications during the late 2000s and early 2010s, following initial breakthroughs from the groups of MacMillan,[15] Stephenson[16] and Yoon.[17] The transition metal-based photocatalysts used decades prior found renewed use at the hands of these researchers, who utilised them to explore exciting reactions (such as double-bond

sensitisation for efficient, diastereoselective [2+2]-cycloadditions), as well coupling photocatalytic cycles with organocatalytic cycles (*vide infra*).

Since these initial publications, researchers have worked on expanding the breadth of photoredox chemistry. In part, this has been done by combining it with other catalysis modes. By using a photocatalytic cycle to turn over a metal-based catalytic cycle (often Ni or Cu), one can induce various coupling reactions: arylations,[18] trifluoromethylations,[19] etherifications,[20] and acylations,[21] to name a few.

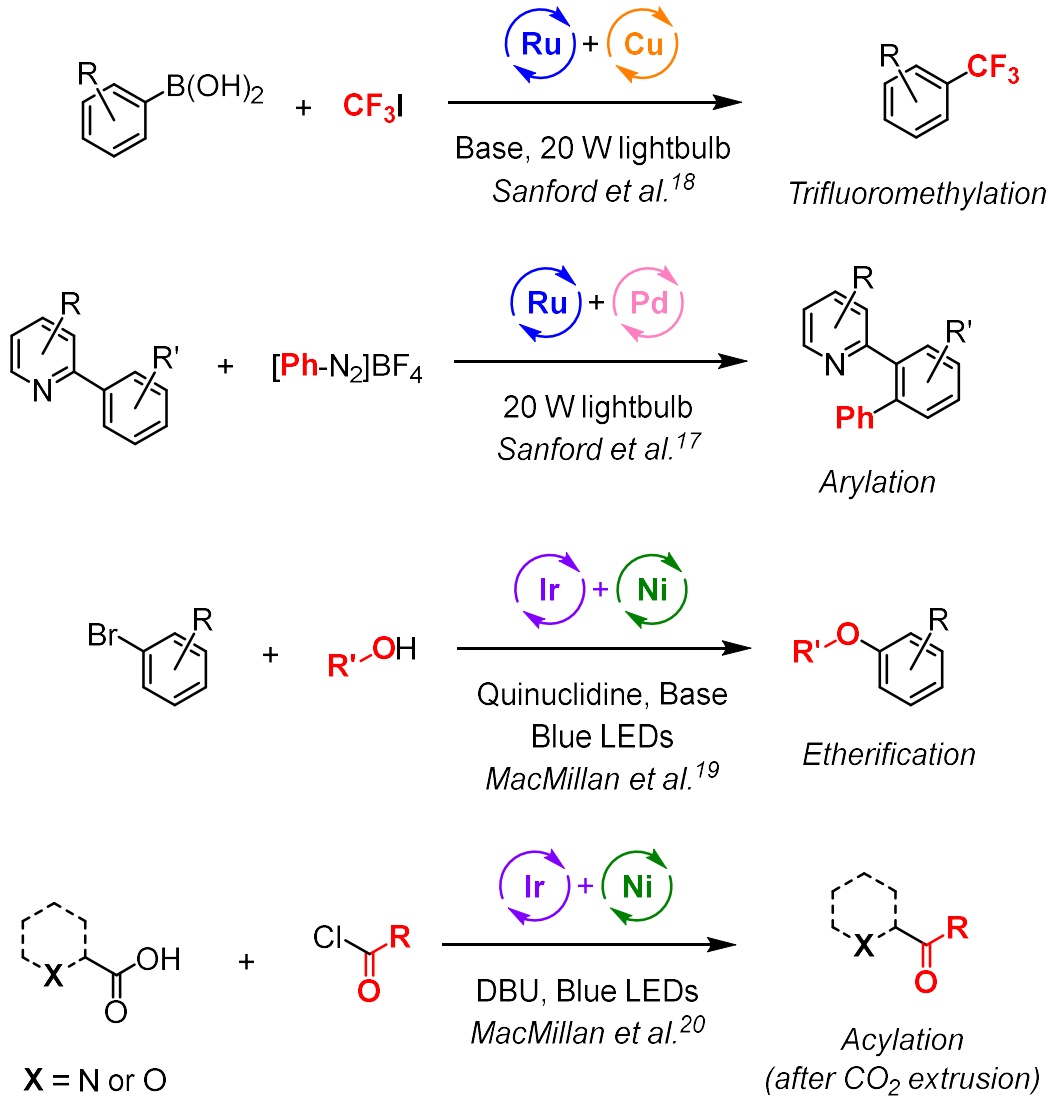

Figure 1.8: *Several methods that merge photoredox catalysis with metal catalysis.*

Numerous groups have also experimented with organic photocatalysts in an attempt to limit our reliance on expensive platinum-group-based photocatalysts. Here possible redox-active

organic compounds are numerous, with some examples being cyanoarenes,[6, 22] xanthones,[23, 24] and methylene blue[25] (*vide supra*, **Figure 1.2**). Further research has been dedicated to adapting photoredox catalysis to an industrial setting, with efforts being made in improving flow reactor technology[26] (which would improve the yield and throughput of photochemical transformations in larger scale contexts) as well as the utilization of photochemical methods in drug discovery and synthesis.[27, 28]

Photocatalysis remains an enticing field for many chemists, not only for its synthetic utility (as described above), but also for its sustainability: with the advent of modern LEDs that can stretch to the higher-frequency end of the visible spectrum, wavelengths can be fine-tuned to supply photons with energy perfectly suited to a specific reaction's requirements, instead of having to overload the reagents using damaging UV light. LEDs are often electrically cheaper to operate, allowing them to run by stored battery power during long power cuts (a pertinent problem in South Africa at this time).[29] Photocatalysis is also, of course, greener than traditional chemistry, seeing as radicals are formed catalytically, reducing the stoichiometric waste generated by traditional radical-forming reagents, such as tin hydrides .

Despite these benefits, photocatalysis still has numerous problems to overcome. Many of the metal-based photocatalysts use metals that are rare and prohibitively expensive for industries outside of research - platinum group metals are some of the rarest metals in our crust.[30] Furthermore, the energy efficiency of photocatalysis still has some way to go before it is efficient enough for use in industry. Because photon intensity is attenuated as a function of path length (via the Beer-Lambert law), photochemistry often suffers from scale-up issues when performed in large batch reactors.[31] Additionally, the quantum yields (the number of desired reactions divided by the total number of absorbed photons) for many photochemical reactions is often low (below 0.4). These problems, along with issues such as the prevalent use of DMF as a solvent[32] represent the current frontier in photocatalysis research.

2. Indoline Alkaloids

Indolines and indoles are extremely common in natural products as structural elements (**Figure 2.1**). Thousands of alkaloids contain indoles,[33] and there are numerous naturally occurring pyrolloindoline compounds.[34] Many pyrolloindoline-containing compounds exhibit a range of biological effects. A notable example of this is (–)-physostigmine, which has been found to be potent at inhibiting cholinesterase,[35] a property that lends its use in the treatment of glaucoma, and therefore at reducing the build-up of β-amyloid plaque in the brain. This mode of action also has relevance in the study of Alzheimer's disease.[36]

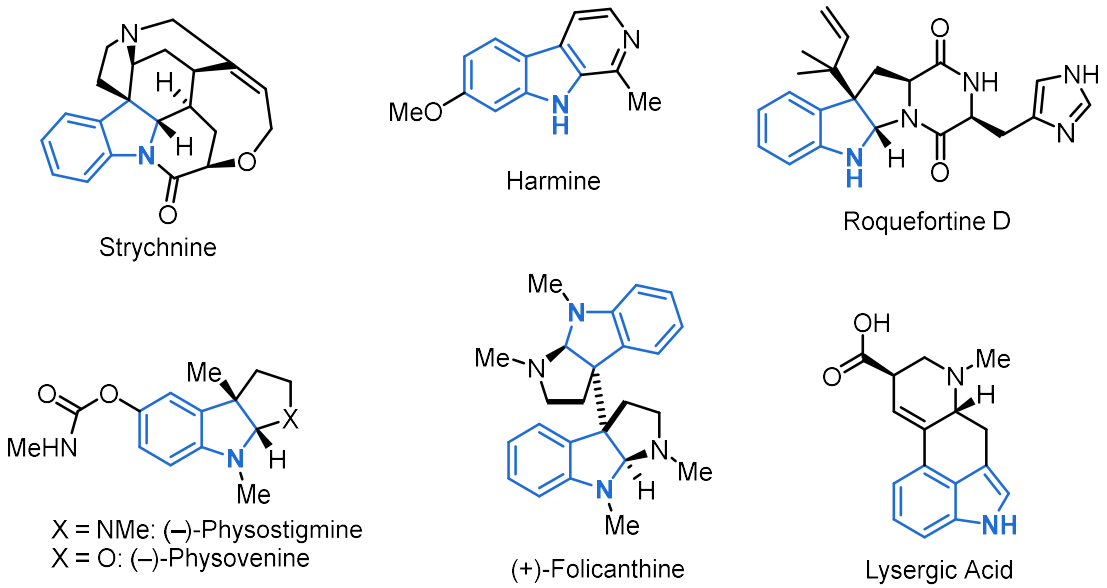

Figure 2.1: *Various natural products that contain either indoline or indole.*

Taking (–)-physostigmine as an example, we were interested in finding quick access to compounds containing that same fused tricyclic system: hexahydro[2,3-*b*]pyrroloindoles (HPIs) or hexahydro[2,3-*b*]furanoindoles (HFIs) – not only because of the known biological activity of similar compounds,[37, 38] but also because of the synthetic challenges inherent to forming all-carbon quaternary centres.[39]

There are several ways of approaching the synthesis of these HPIs/HFIs,[40] broadly covered by the two disconnection strategies shown in **Figure 2.2**.

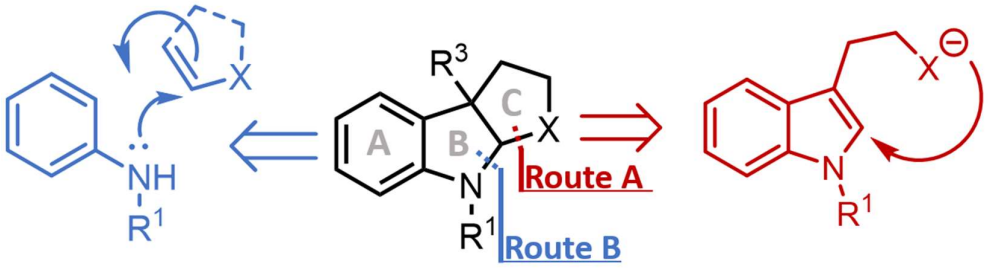

Figure 2.2: *Two common disconnection points for the retrosynthesis of HPIs/HFIs.*

The bond disconnection via route A involves forming the C ring last and is often achieved by intramolecular cyclisation of an indole such as by interrupting a classic Fischer indole synthesis at the indolenine via an intramolecular attack from a pendant heteroatomic nucleophile,[41] or by some other addition-cyclisation cascade.[42, 43] This route is biomimetic in a sense, as naturally occurring pyrroloindoline-containing compounds are thought to be derived from tryptamine,[34] which contains indole. Synthesis instead via route B forms the B ring last, and protocols taking this route involve anilines and can take the form of intramolecular carboaminations[44] and cascade cyclisations by reacting Michael acceptors with isocyanoacetates[45] (for example).

Related to route A is the use of oxindoles (instead of indoles) to facilitate cyclisation; this makes the C2 carbon electrophilic, rather than nucleophilic, allowing for a more natural cyclisation via a nucleophilic amine to form the C ring, not to mention that oxindoles are important features of many natural products as well,[46] making methods of synthesising them desirable in their own right. Ashimori *et al*.,[47] for example, outline a route to (±)-esermethole (a known precursor to (±)-physostigmine)[48] that features the reductive aminocyclisation of a 3,3-disubstituted oxindole featuring an aldehyde moiety (**Scheme 2.1**).

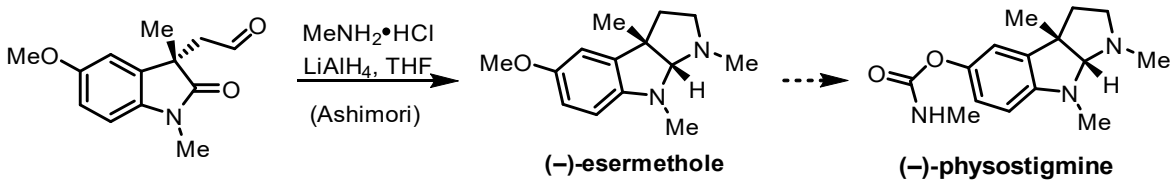

Scheme 2.1: *Route to (–)-physostigmine from the oxindole aldehyde.*

Oxindoles were an appealing option to us. The virtue of this intermediate, as we saw it, is that it can be prepared using an *N*-arylacrylamide system by way of a radical addition-cyclisation, a process to which photochemistry can readily be applied (**Scheme 2.2**). This affords the quaternary centre at C3 with ease, and *N*-arylacrylamides are simple to produce; indeed, forming 3,3-disubstituted oxindoles in this way is quite a common procedure, and numerous radical species have been used.[49] The stereochemical outcome of such radical cyclisations are difficult to control, however, as the radical is prone to attack both faces of the alkene. As such, our approach would also have to find a way of conveying enantioselectivity to the oxindole-producing step, as well as retaining the enantiopurity of substrates in the following steps, one of the key objectives for this research.

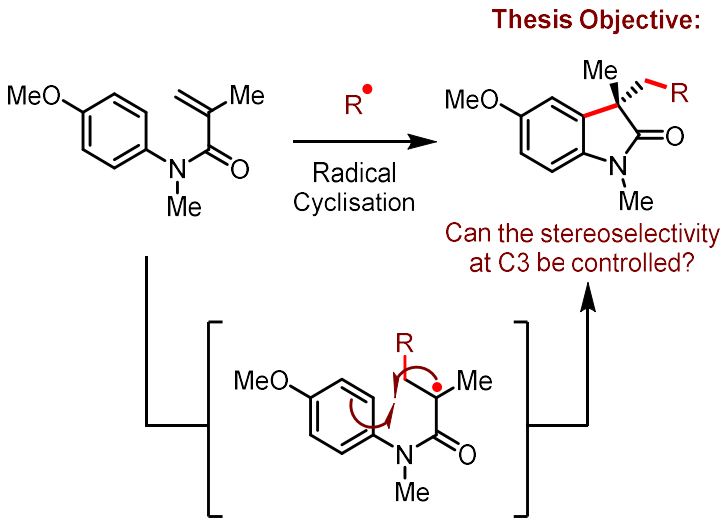

Scheme 2.2: *The route to 3,3-disubstituted oxindoles featuring N-arylacrylimides and acyl radicals.*

3. Stereoselectivity in Radical Chemistry

Historically, radicals in chemistry have been understood as unstable, transient species that can be difficult to control. Their reactive nature often leads to a broad range of possible side reactions, including self-dimerisation and hydrogen atom abstractions. This, along with their roughly flat geometry,[50] makes designing a stereoselective synthesis involving radical species difficult to envision. Nevertheless, researchers have found ways of producing highly enantioselective reactions that employ radicals.

Organometallic catalysts have been employed for this purpose. Notably, research from Meggers has explored the use of chiral-at-metal rhodium[51] and iridium[52] complexes which can be used in conjunction with a photocatalyst (or not, in the case of the iridium complexes) to effect highly enantioselective α- and β-functionalisations of certain ketones with attached pyrazoles and imidazoles (**Figure 3.1**). In these reactions, a ketone substrate binds to the metal via two sites vacated by the labile acetonitrile ligands. The ketone then finds itself locked in an environment made chiral by the very particular arrangement of the phenyl benzothiazole/benzoxazole ligands around the metal centre. This differentiates the faces for an oncoming radical, leading to high enantioselection.

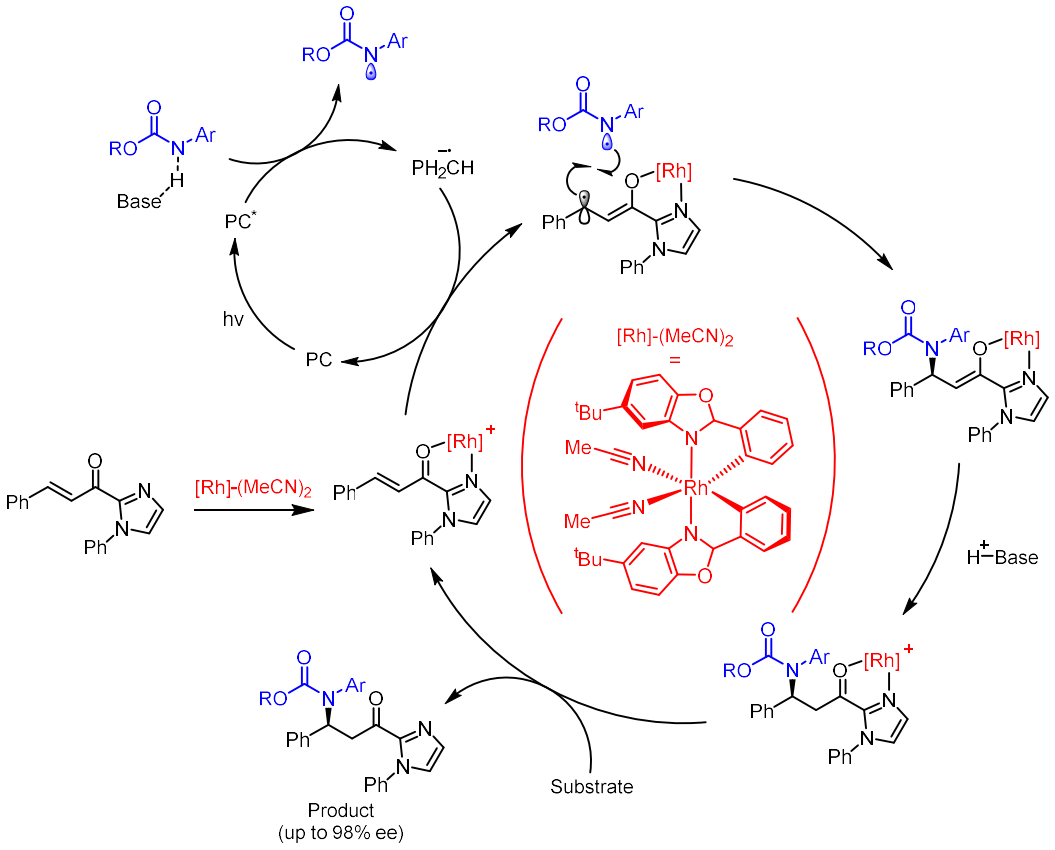

Scheme 3.1: *Mechanism for an enantioselective β-amination using a chiral-at-centre rhodium catalyst (depicted here in red) to direct the amide radical.*

Another common method to induce stereoselectivity in radical chemistry is by way of asymmetric organocatalysis. This can be done by introducing a chiral catalyst which may bind to the substrate and thereby enable stereodifferentiation. An example of this is seen in the work by MacMillan involving chiral enamine species as radical acceptors (**Figure 3.2**).[15] It was

found that the faces of an aldehyde/ketone substrate can be differentiated by employing a catalytic amount of chiral secondary amine. This amine and the substrate form an iminium species **i** *in situ*, which is in equilibrium with its enamine counterpart, **ii**. This enamine can then react with a radical by way of its double bond to form radical **iii**. Density functional theory calculations revealed that **ii** would take the shown conformation, with the alkene in the (*E*)-configuration to minimise non-bonding interactions with the ring, the methyl group shielding the *Re* face, and the alkene facing away from the bulky *tert*-butyl group. The overall effect is a radical addition that is highly selective for the desired face of the alkene. After this, **iii** is oxidised to reform the iminium in **iv**, thereby allowing the formation of the product aldehyde with regeneration of the chiral amine.

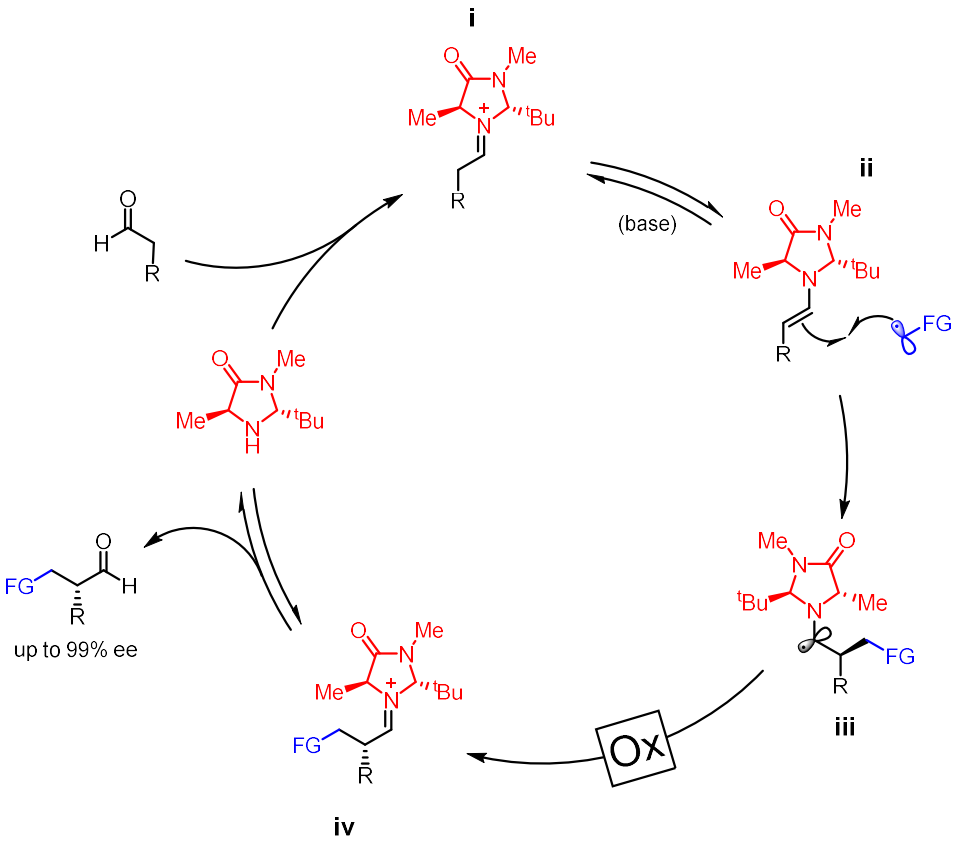

Scheme 3.2: *An example of the aminocatalytic cycle developed by MacMillan. Here, the radical favours a single side of the enamine due to the steric environment enforced by the organocatalyst.*

Enamine/iminium organocatalysis has been used in a variety of asymmetric radical additions[53-55] and has the added benefit of being able to be coupled with photocatalysis to improve the breadth of possible combinations (as has been mentioned already). Other chiral

organocatalysts have been used, such as thiols[56] and carbenes.[57] This prefunctionalisation strategy was of interest to us, especially because of MacMillan's use of this tactic to arylate aldehydes in the α-position (**Scheme 3.3**).[58] Here, by forming the imidazolidinone enamine and subsequently oxidising it to the radical cation, the researchers found that a pendant aromatic ring would rapidly add into the 3π-system. By modulating the size of the aryl moiety of the imidazolidinone catalyst (**Ar**), bond formation would occur preferentially from the *Si* face of the enamine intermediate, delivering the desired isomer with high levels of enantioselectivity.

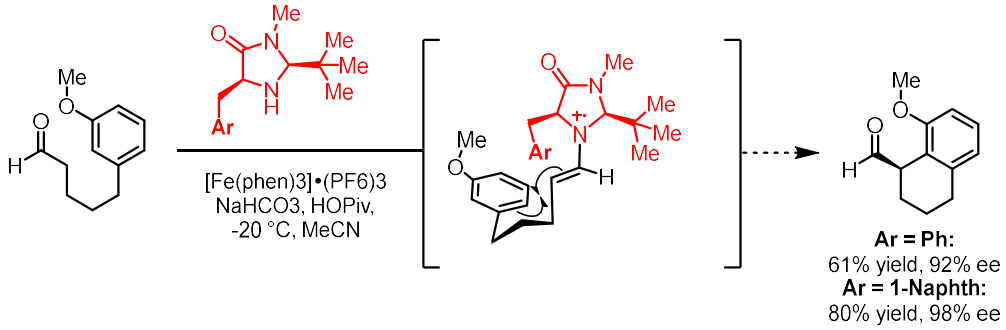

Scheme 3.3: *Enantioselective radical cyclisation using organocatalysis.*

This stereoselective radical cyclisation onto an aromatic ring enforced by some pre-installed chiral group spurred us to think of some similar way we could affect the stereochemical outcome of the arylation step of radical addition-cyclisation approaches to 3,3-disubstituted oxindoles. Thus, we envisioned that the use of a C1 radical synthon (acyl radical) with a chiral attachment $\mathbf{X_c}$ would direct the arylation ring closure step and provide an enantio-enriched 3,3-disubstituted oxindole which could be telescoped to accessing HPIs and HFIs such as (–)-physostigmine and (–)-physovenine, respectively, following auxiliary removal and cyclisation (**Scheme 3.4**).

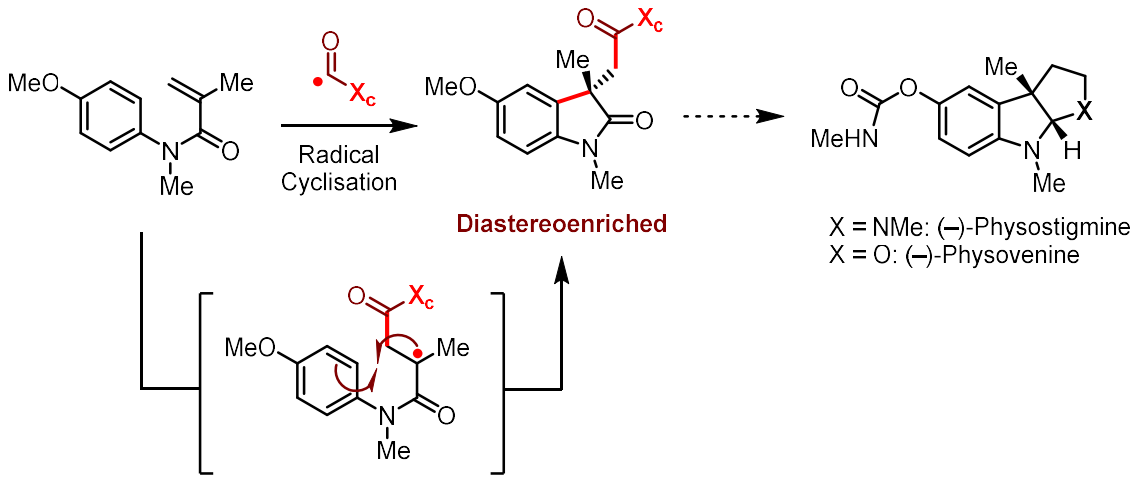

Scheme 3.4: *Updating* ***Scheme 2.2*** *to feature a chiral radical synthon envisaged to provide stereocontrol.*

Additionally, this would be an example of an arylation to produce an all-carbon quaternary centre — a challenging bond connection due to its the steric demands.[59] All of this would come into consideration when designing the central reaction for this thesis.

4. Designing a Chiral Acyl Radical

To achieve the acyl radical shown in **Scheme 3.4**, a suitable precursor (**Scheme 4.1**) would have to be designed to form it *in situ*, with two important design criteria to consider in this design. Firstly, formation of the radical should occur through photochemically-induced fragmentation of the precursor, either by homolytic cleavage via the excited state of the precursor, or by mesolytic cleavage via formation of the radical cation/anion of the precursor. Either way, an appropriate leaving group (**LG**) would need to be chosen. Secondly, the chiral auxiliary itself ($\mathbf{X_c}$) would need to be considered. $\mathbf{X_c}$ would need to have the requisite stereo directing properties in addition to being easy to remove after the cyclisation has occurred. Out of a large pool of potential options, this choice would also be motivated by access to starting material for the auxiliary in question.

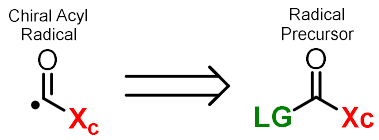

Scheme 4.1: *Forming the desired radical would require a precursor with an appropriate auxiliary and leaving group.*

4.1 Precursors to Acyl Radicals

There are numerous documented methods for generating acyl radicals. One method utilises a carbonylation approach and involves the addition of pre-generated alkyl radicals but comes at the cost of having to use poisonous carbon monoxide gas (**Figure 4.1.A**). furthermore, the method of generating the alkyl radical needs to be considered, eg: via photocatalysis.[60]

In perhaps the simplest case conceptually, acyl radicals can be generated from the corresponding aldehyde by abstracting the aldehydic hydrogen (**Figure 4.1.B**). While this is appealing from an atom-economy perspective, this is often achieved using a radical initiator (often peroxides, which can be sensitive to heat, light and mechanical shock)[61, 62] — although there do exist some photocatalytic methods to achieve this type of radical, such as by using decatungstate.[63]

Alternatively, the H atom can be replaced with heavy atoms with the goal being to lower the bond-dissociation energy between the carbonyl carbon and the substituent to greater encourage homolytic cleavage via radical initiation, heat, or high-frequency radiation. Examples in this vein include thioesters,[64] acyl selenides[65] and even acyl tellurides (**Figure 4.1.C**).[66]

On the other hand, acyl radicals can be generated photocatalytically through the use of visible light in conjunction with fragmenting groups which are susceptible to single electron oxidation and reduction (and subsequent mesolytic cleavage); α-keto acids can be decarboxylated after a SET to yield acyl radicals,[67] and, if the R group is attached via an acyl group (recall **Figure 1.4**), the N-acyloxyphthalimides of Okada seem like they would fit this description as well (**Figure 4.1.D**).

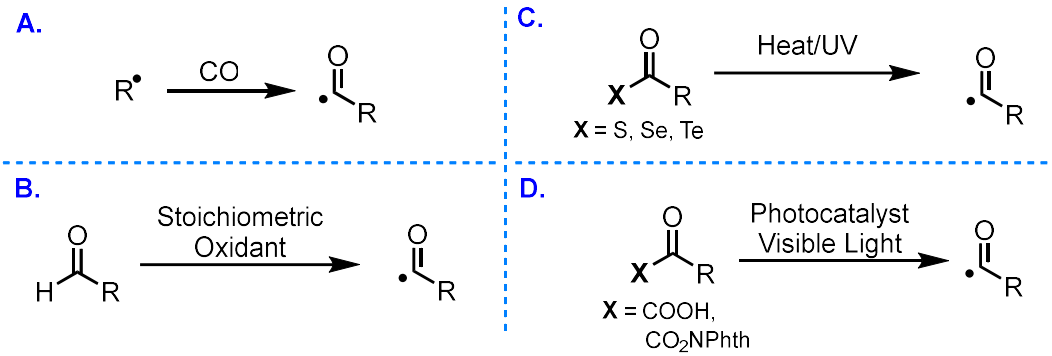

Figure 4.1: *Various routes to acyl radicals.*

Indeed, Overman *et al.* accomplished the formation and subsequent trapping of methoxycarbonyl radicals using N-acyloxyphthalimides as precursors,[68] and research within our group outlined similar chemistry using phthalimido oxamides to generate carbamoyl radicals.[69] Because of its established efficacy and history within the group, we decided to opt for this method of carbamoyl radical generation as the source of our acyl moiety.

4.2 Options for the Chiral Auxiliary

Since our radical design is predicated on the use of an acyl radical, we thought it sensible to make use of well-established chiral acyl auxiliaries such as the oxazolidinones devised by Evans[70, 71] as well as the imidazolidinone variant that featured significantly in work by our colleagues in the Hunter group (**Figure 4.2**).[63,64]

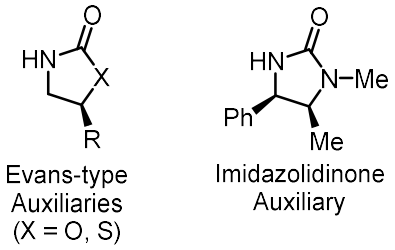

Figure 4.2: *Options for auxiliaries that could be linked via a nitrogen.*

Once again, our choice was largely guided by previous success and experience within the Hunter research group just mentioned (although in the context of 1,3-dicarbonyls)[72] and we therefore opted for the imidazolidinone auxiliary.

Aims & Objectives

With both aspects of the precursor design covered, we proposed the synthetic route shown in **Scheme 4.2.** We posited that compound **1** would lead to our desired acyl radical intermediate, and that this could be achieved using the mild conditions inherent to photocatalysis. Our hopes were that: 1) this proposed radical species would be stable and not decompose too readily *in situ* (acyl radicals have a tendency to decarbonylate into the corresponding alkyl radical); 2) that the chiral component of this species would direct the approach of the radical in some way (via radical species **A**) to produce diastereo enriched oxindole products and ultimately to HPI and HFI motifs, as shown in **Scheme 4.2**.

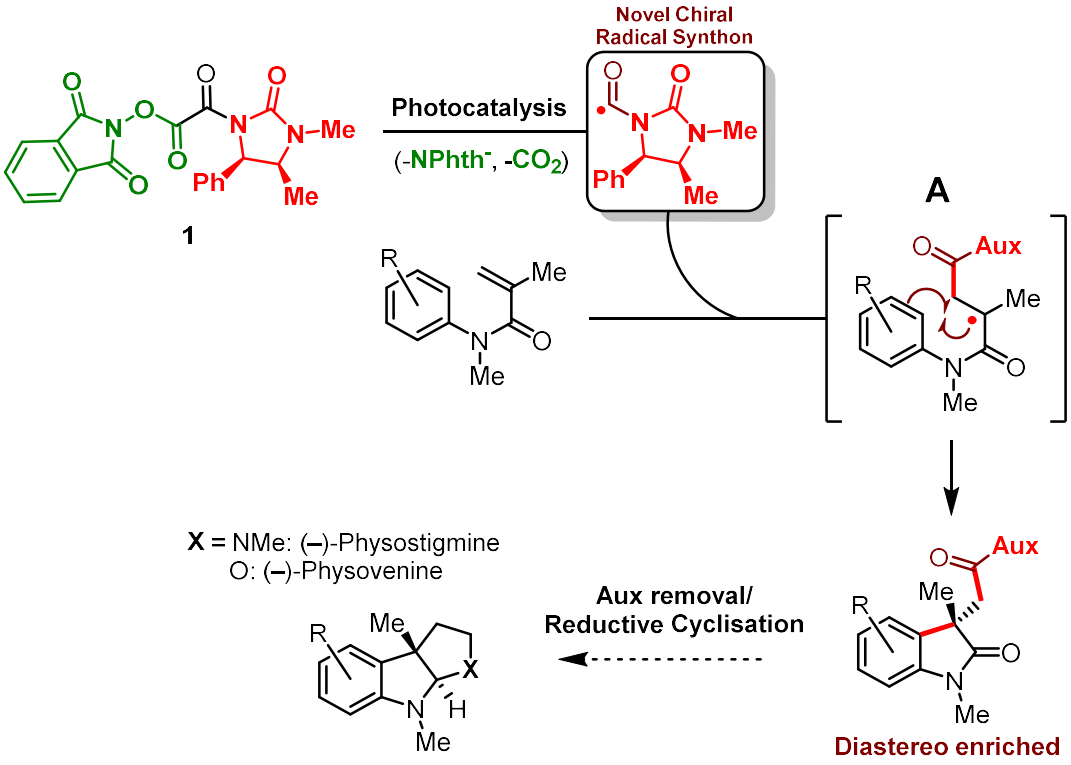

Scheme 4.2: *Using a chiral radical to achieve diastereoselectivity in the synthesis of oxindoles.*

It is worth noting that we were acutely aware that our system lacked conformational rigidity with respect to producing a conformationally well-defined transition-state, due to a low barrier of rotation about the carbonyl-auxiliary bond in the conjugate radical intermediate **A** — producing both the s-*cis* ($\mathbf{A}_{cis}$) and s-*trans* ($\mathbf{A}_{trans}$)— leading to the formation of two diastereomers (**Figure 4.3**).

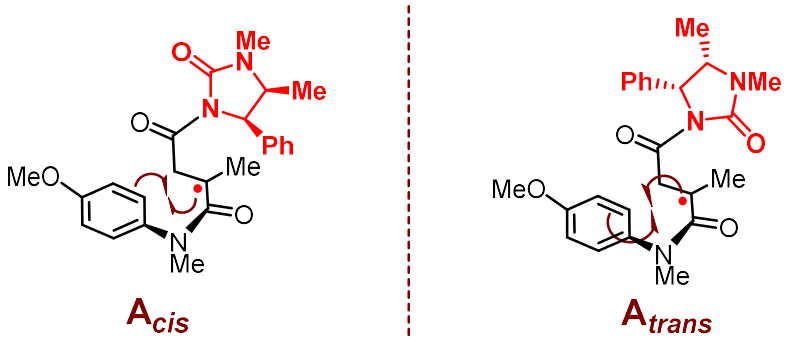

Figure 4.3: *A low barrier of rotation about the carbonyl-auxiliary bond leads to opposing steric conditions leading to an inverted stereoselectivity.*

Presumably, one of the conformations of intermediate **A** would be more sterically/electronically favourable than the other; the methyl and phenyl groups of the auxiliary point away from the rest of the molecule in $\mathbf{A}_{trans}$, potentially resulting in less steric strain than in $\mathbf{A}_{cis}$. Additionally, $\mathbf{A}_{trans}$ minimises the dipole-dipole repulsion of the two carbonyl moieties at the auxiliary amide bond, allowing them to face away from one another. In the event of imperfect selectivity, however, we hoped to explore chelation control using (chiral) Lewis acids as a potential solution, but we also saw the likelihood that the diastereomers would be separable by conventional chromatographic methods.[73] This latter point remains a significant advantage for traditional chiral auxiliary methods (i.e. diastereoselective methods) in contrast to enantioselective processes, which generally suffer from more expensive and complex enantiomer separation methods.[74] Additionally, the presence of the auxiliary might allow for crystalline products, which could be easily purified via recrystallisation.

Results and Discussion

5. Synthesis of Precursors

Our synthesis began with that of the chiral auxiliary. Our preference, as discussed, was for a chiral imidazolidinone (compound **2**) which could be synthesized on gram scale using (1*R*,2*S*)-(−)-ephedrine hydrochloride and urea (**Scheme 5.1**).

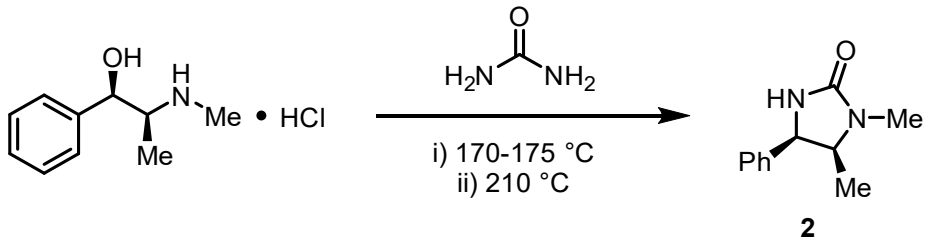

Scheme 5.1: *synthesis of imidazolidinone* ***2*** *using urea and* (1*R*,2*S*)-(−)-ephedrine hydrochloride.

While the yield for **2** was poor (37% after recrystallisation), it was in line with literature reports.[75] The protocol itself was quite convenient: only two reagents were required; the reaction could be done under air; the product could be easily recrystallised from EtOAc to form very pure crystalline product. The ^{1}H NMR of **2** (**Figure 5.1**) is shown below.

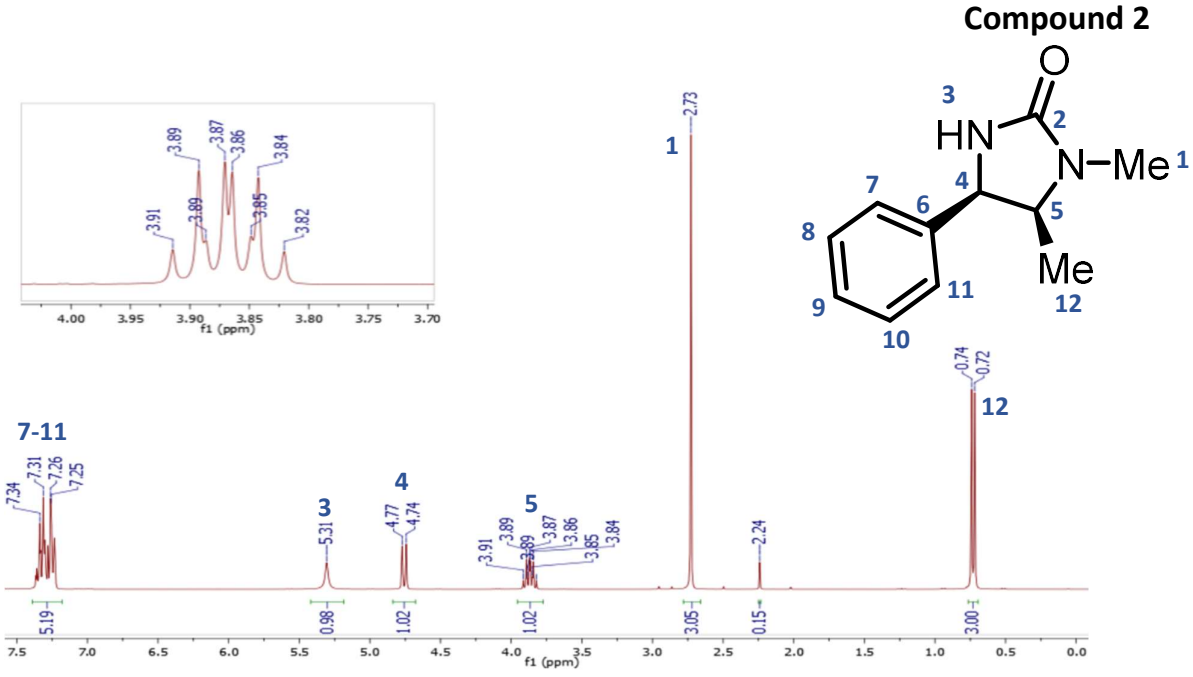

Figure 5.1: *^{1}H NMR (300 MHz, $CDCl_3$) spectrum of* ***2****.*

Exhibited are the requisite methyl, aromatic and amide proton signals, as well as the doublet at C4 (4.76 ppm) and characteristic quartet of doublets at C5 (3.87 ppm, J_1 = 8.4 Hz and J_2 = 6.6 Hz) — consistent with the conformationally restricted ring structure according to the Karplus equation. The ^{13}C NMR spectrum for **2** (**Figure 5.2**) shows the expected 9 signals, with one amide signal and 4 aromatic signals.

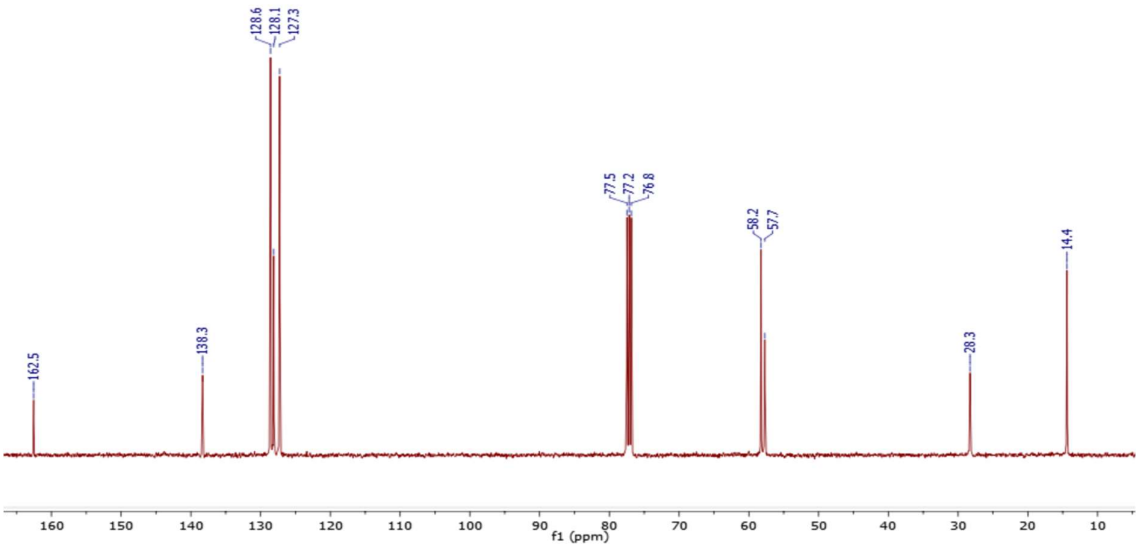

Figure 5.2: *^{13}C NMR (101 MHz, $CDCl_3$) spectrum of **2**.*

Mechanistically, the formation of this compound follows from an initial S_NAc at the carbonyl of the urea via the nitrogen of the ephedrine with the loss of ammonia (**Scheme 5.2**). This is partially catalysed by the acid (present in the ephedrine HCl salt that was used) but is also driven by the high temperature. The temperature must then be increased to effect the dehydration of the alcohol; this ablates the stereochemistry at C2, leaving a flat carbocation. Nevertheless, the methyl group at C1 directs nucleophilic attack of the remaining unsubstituted urea nitrogen towards the carbocation face opposite to the methyl, leaving the phenyl and methyl groups *cis* to one another in the final compound.

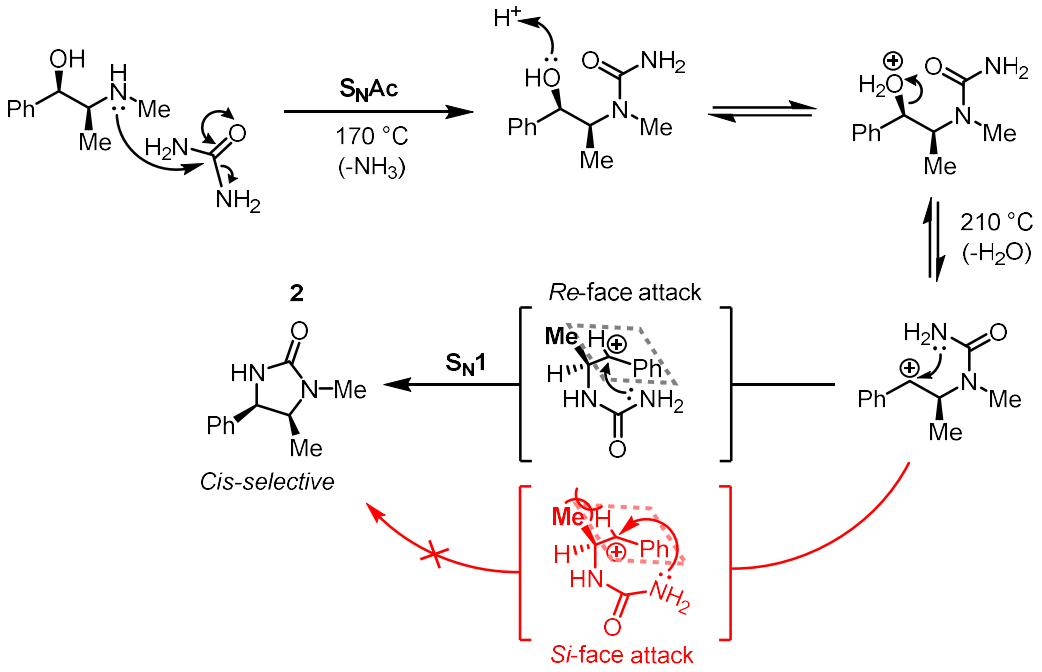

Scheme 5.2: *Mechanism for the formation of* ***2*** *showing the carbocation face selectivity in the final step; the methyl directs the amide nitrogen to attack from the Re face.*

Alternatively, it has been suggested[75] that the ephedrine undergoes an intramolecular S_N2 reaction (with the loss of water) to form a transient aziridinium ion (**Scheme 5.3**). This is then reopened in another S_N2 reaction with urea before a final S_NAc reaction closes the ring, forming the product with the loss of ammonia. The two S_N2 steps at C2 invert the stereochemistry twice, resulting in the net preservation of the *R*-configuration at this carbon.

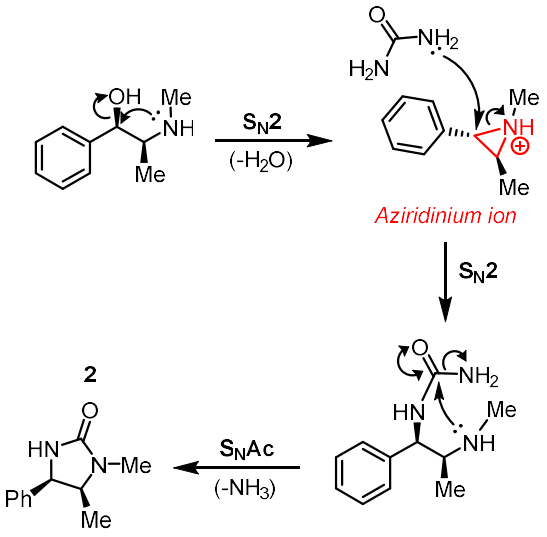

Scheme 5.3: *Alternative mechanism for the formation of* ***2****.*

The desired phthalimido oxamide **1** precursor for the desired chiral carbamoyl radical was synthesised in accordance with prior literature (**Scheme 5.4**);[68, 69] namely, via the double substitution of oxalyl chloride with *N*-hydroxyphthalimide and **2** (done sequentially). The need for the low temperature was two-fold: *1)* it prevented double substitution of the oxalyl chloride by the *N*-hydroxyphthalimide in step 1 (together with controlling the stoichiometry); *2)* it prevented over-substitution at the *N*-hydroxyphthalimide portion of **3**, by the incoming nucleophile.

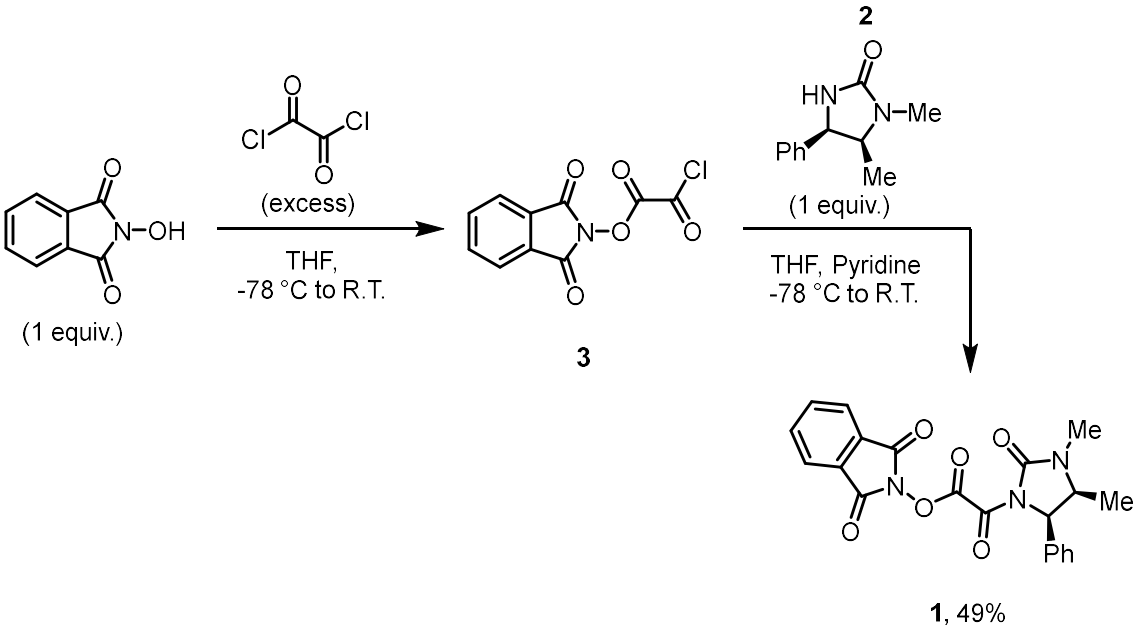

Scheme 5.4: *Synthesis of **1** from oxalyl chloride, N-hydroxyphthalimide and **2**.*

The ^{1}H NMR spectrum of **1** (**Figure 5.3**) depicts the familiar peaks of the auxiliary with the predictable addition of more aromatic signals from the added phthalimide fragment.

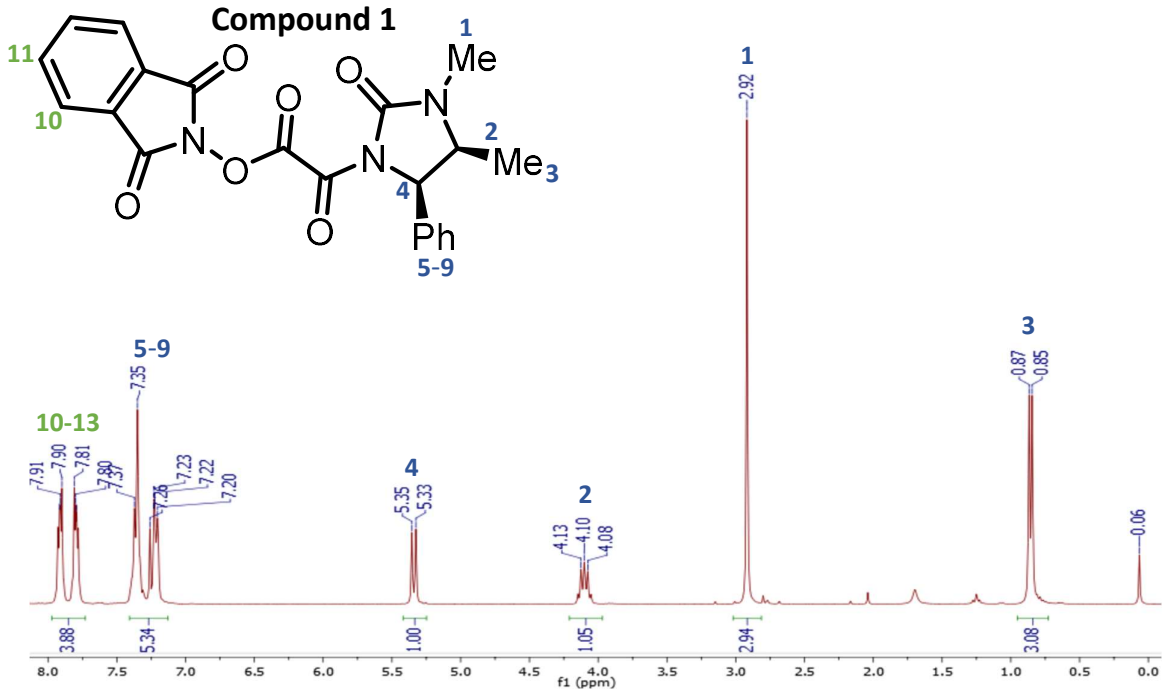

Figure 5.3: *^{1}H NMR (300 MHz in $CDCl_3$) spectrum of **1**.*

More telling, however, was the presence of 4 highly deshielded signals in the ^{13}C NMR spectrum (**Figure 5.4**) – at 161.1, 157.4, 155.7 and 153.8 ppm

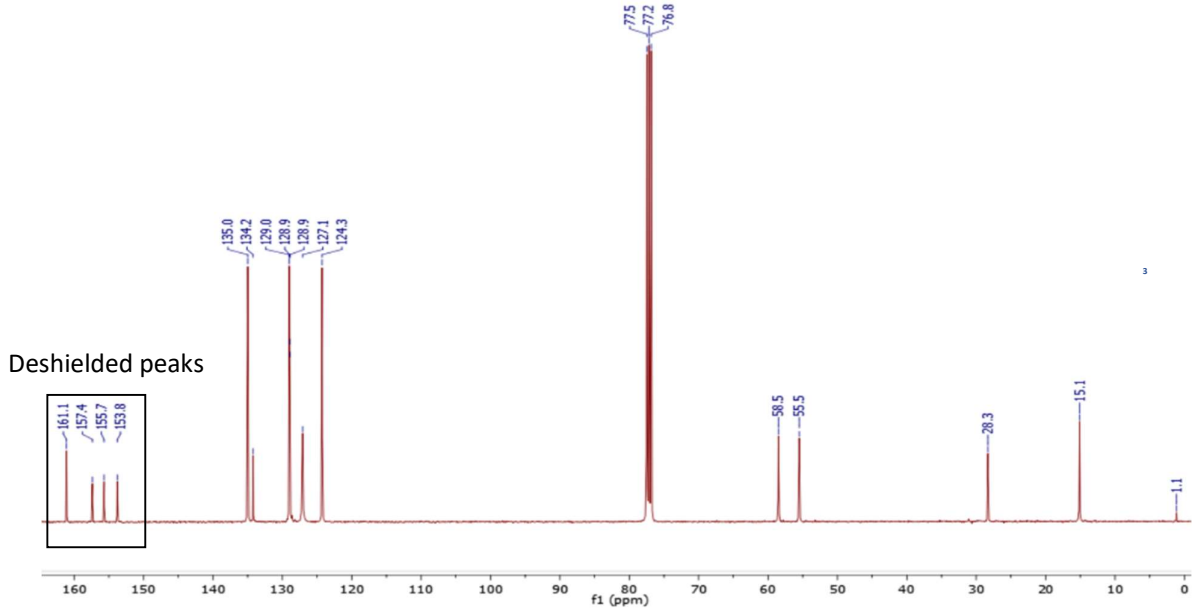

Figure 5.4: *^{13}C NMR (101 MHz in $CDCl_3$) spectrum of **1**.*

These correspond to the presence of the 5 carbonyls in the proposed structure, with the 2 magnetically equivalent carbonyls of the phthalimide moiety doubling up and increasing the intensity of the signal at 161.1 ppm.

With the precursor for the carbamoyl radical in hand, a small selection of aryl acrylamide Michael acceptors (**4**) was prepared. The synthesis of these were all achieved by coupling the relevant substituted *N*-methyl aniline with methacrylic acid using 2-chloro-1-methylpyridinium iodide (CMPI) as the peptide coupling reagent (**Scheme 5.5**).

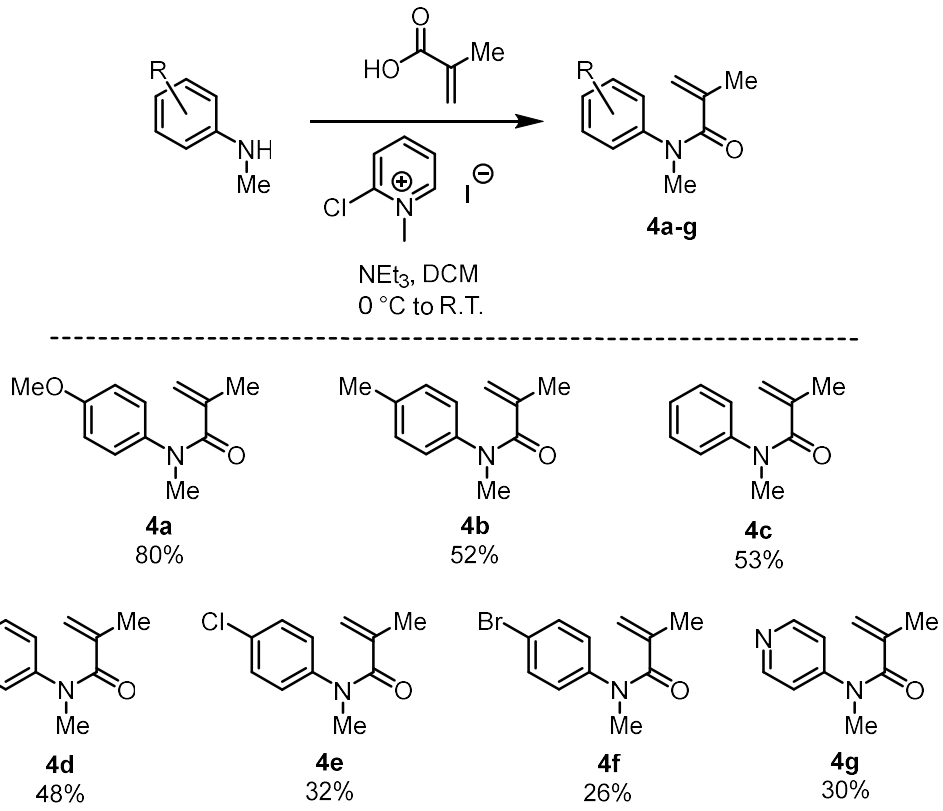

Scheme 5.5: *General synthesis for aryl acrylamide substrates.*

In total, 7 aryl acrylamides were made in this way, with a wide range of yields varying from an unoptimised 30-80% using CMPI (see experimental section, **4a**-**4g**).

6. Photoredox Reaction

6.1 Initial Observations

Initial studies of the radical addition-cyclisation were conducted using *N*-(4-methoxyphenyl)-*N*-methylmethacrylamide (**4a**) as the aryl acrylamide, since this is the substrate that ultimately leads to (–)-physostigmine. Subjecting compounds **1** and **4a** to photocatalytic conditions in accordance with previous work[69] pleasingly afforded **5a** in 81% yield after chromatography as a 2:1 mixture of diastereomers (**Scheme 6.1**).

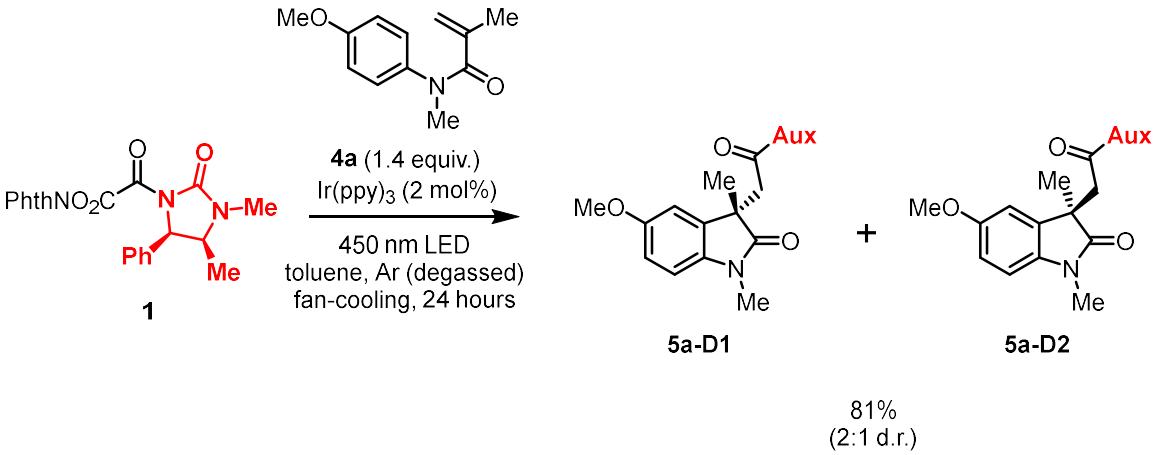

Scheme 6.1: *Photoredox catalysed radical cyclisation.*

It is worth noting that the diastereoselectivity was determined by isolating each diastereomer, as these were easily separable by standard column chromatography. By contrast, analysis of the crude reaction mixture, both by HPLC and ^{1}H-NMR, failed to give accurate data due to overlapping signals. Key signals in the ^{1}H-NMR of the major product **5a-D1** (**Figure 6.1** – stereochemistry was determined via X-ray crystallography, *vide infra*) were the set of diastereotopic methylene protons at C10, producing a characteristic geminal AB doublet system (4.07 and 3.49 ppm, with J = 17.4 Hz).

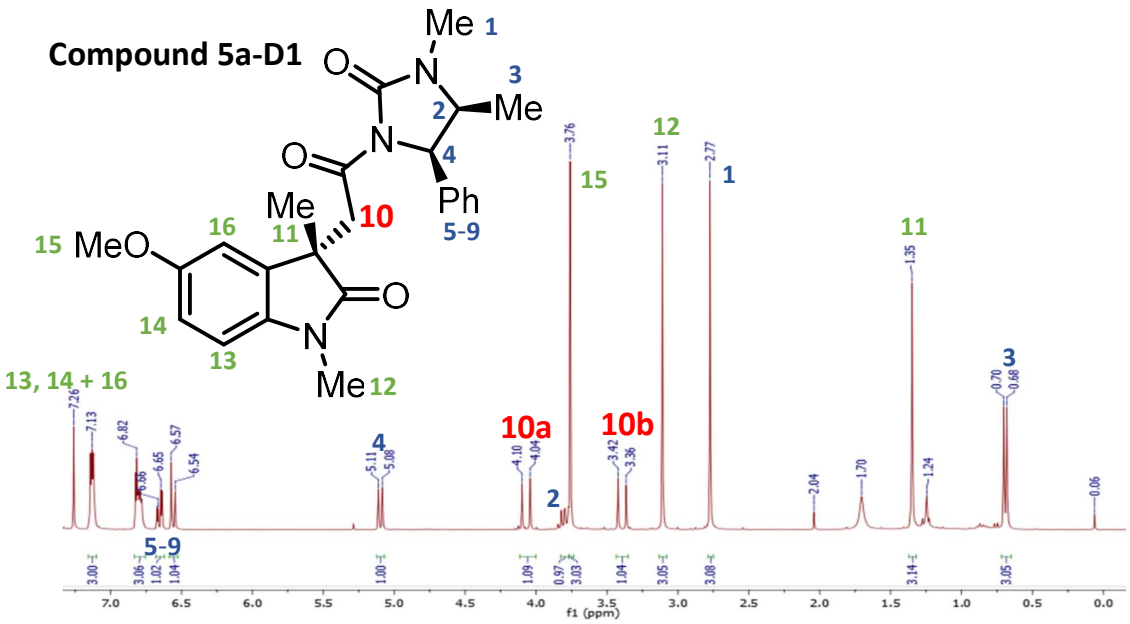

Figure 6.1: *^{1}H NMR (300 MHz, $CDCl_3$) spectrum of* ***5a-D1****.*

The ^{13}C NMR correctly revealed 22 resonances and HRMS analysis found the expected molecule mass, supporting its synthesis (see the experimental section). Conclusive evidence, however, was obtained via single crystal X-ray crystallography (**Figure 6.2**), which also revealed the relative configuration at the newly formed quaternary stereocentre (C3 of the oxindole) to be *S*. (–)-Physostigmine shares this configuration at the relevant carbon, and so we were pleased that our major isomer (albeit in modest selectivity) was consistent with the natural product. Unfortunately, attempts to improve the 2:1 selectivity, by reducing the temperature (-50 °C) did not affect the observed selectivity in either direction.

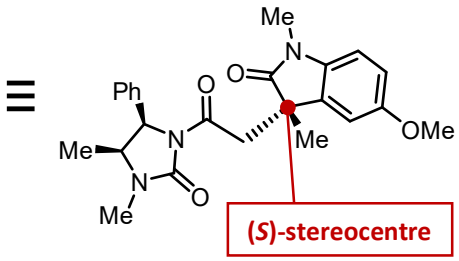

Figure 6.2: *Crystal structure of* ***5a-D1*** *(major diastereomer).*

The proposed mechanism for this reaction, using **4a** as a representative example, is shown in **Scheme 6.2**. The $Ir(ppy)_3$ catalyst absorbs a photon of 450 nm light, and the resulting excited species ($\mathbf{Ir^{III*}}$) reduces the phthalimido oxamide precursor **2** (for $Ir(ppy)_3$, $E_{1/2(IV/III*)}$ = -1.73 V vs SCE; similar phthalimido oxalates have been reported with an $E_{1/2}$ between -1.2 and -1.3 V vs SCE).[76] The resulting radical anion fragments, losing phthalimide anion and CO_2 to produce the desired chiral carbamoyl radical **i**. A Giese[77] addition to acrylamide **4a** produces the tertiary radical **ii**, in opposition to the less stable primary radical that could be formed on the adjacent carbon, that subsequently cyclises forming cyclohexenyl radical **iii**. The stability of radical **ii** arises from the radical's position α to the existing carbonyl, where there exists a SOMO→p* carbonyl interaction. Furthermore, The LUMO coefficient on an α,β-unsaturated carbonyl is largest on the β-position (in this case, the terminal end) of the alkene, and so radicals will attack at that position preferentially. Oxidation of **iii** by the now highly oxidizing Ir^{IV} species results in the cation **iv**, which is then deprotonated by the leftover phthalimide anion from the fragmentation of **2,** yielding the final product **5a**, as well as regenerating the ground state photocatalyst.

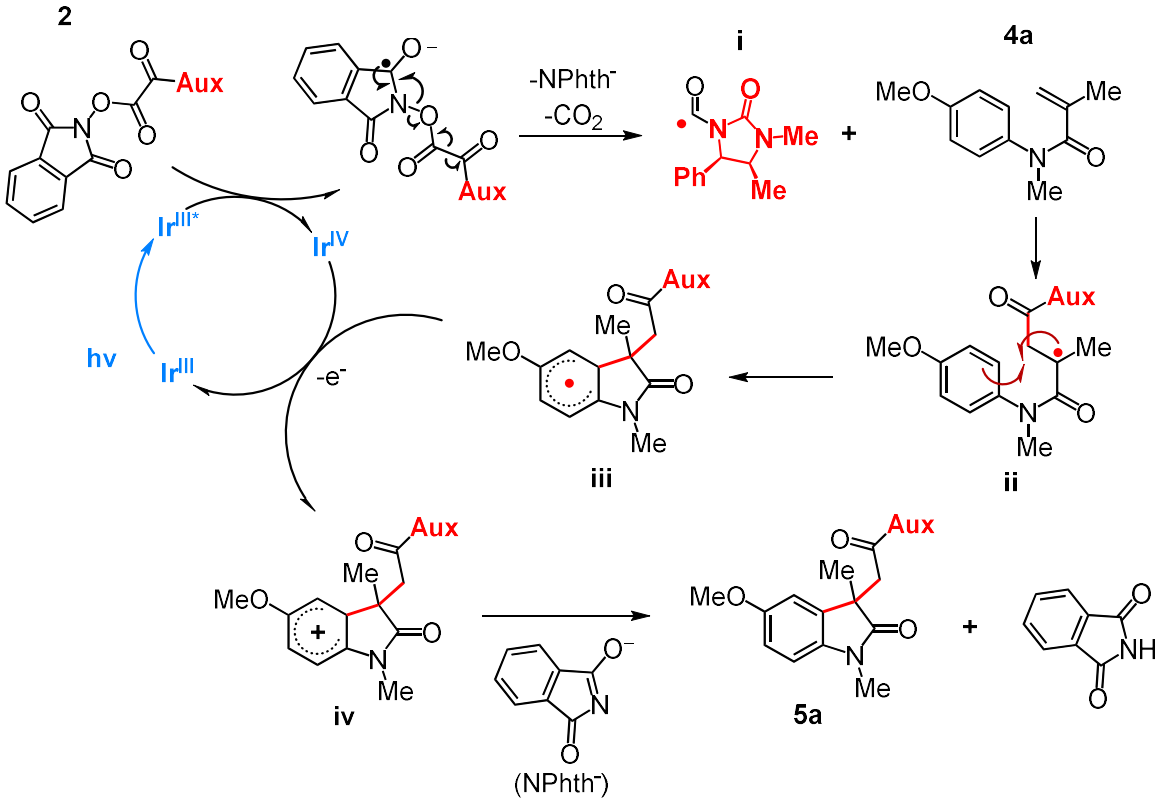

Scheme 6.2: *Proposed reaction mechanism for the photoredox-catalysed radical addition-cyclisation.*

Carrying out the reaction in the presence of TEMPO, modified with NEt_3 to serve as a sacrificial reductant to turn over the $Ir(ppy)_3$ catalyst), produced TEMPO-adduct **6** in 48% yield — providing some support for chiral radical **I** — while the product **5a** was not observed (**Scheme 6.3**). Admittedly, there is a possibility that the excited $\mathbf{Ir^{III*}}$ species could reduce the TEMPO to the $TEMPO^-$ anion, in which case the anion could attack **2** via a polar mechanism, giving **6** without the formation of any radical.

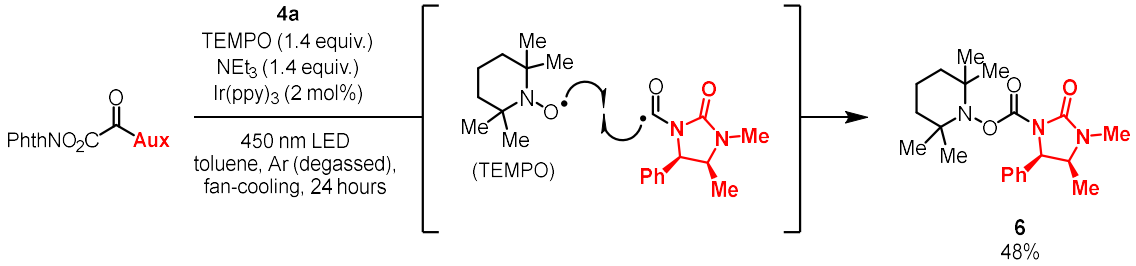

Scheme 6.3: *Trapping the carbomoyl radical using TEMPO.*

6.2 Optimisation and Scope

A small optimization study was subsequently carried out to investigate the effect of solvents on the yield and/or selectivity of the oxindole synthesis (**Table 6.1**). In the event, however, it was found that neither THF, acetonitrile nor ethyl acetate provided a better overall yield (entries 1–3), while toluene provided a slight improvement, providing **5a** in 88% yield (entry 4). The cheaper copper-based catalyst $[Cu(dap)_2]Cl$ was also attempted (For $[Cu(dap)_2]Cl$, $E_{1/2(II/I^*)}$ = -1.43 V vs SCE, while for $Ir(ppy)_3$, $E_{1/2(IV/III^*)}$ = -1.73 V, as previously mentioned), but this gave no product formation (entry 5).

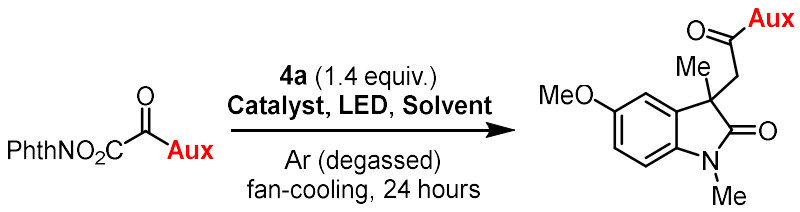

Entry	Light	Catalyst (2 mol%)	Solvent	Yield*
1	450 nm	$Ir(ppy)_3$	THF	82%
2	450 nm	$Ir(ppy)_3$	Acetonitrile	72%
3	450 nm	$Ir(ppy)_3$	Ethyl Acetate	83%
4	**450 nm**	**$Ir(ppy)_3$**	**Toluene**	**88%**
5	450 nm	$[Cu(dap)_2]Cl$	Toluene	0%
6	none	$Ir(ppy)_3$	Toluene	0%
7	450 nm	none	Toluene	0%

* *Yields determined by ^1H NMR (1,3,5*-trimethoxybenzene as the internal standard).

Table 6.1: *Some optimisations to the photoredox cyclisation.*

As expected, running the reaction without either the photocatalyst or the light source gave no reaction, confirming the necessity of the photocatalytic conditions (entries 6–7).

As was previously discussed, six additional aryl acrylamides **5a-g** were prepared; these were now used to probe the scope of this reaction (**Scheme 6.3**). Exchanging the methoxy group on the aromatic ring with a methyl group produced **5b** in 85% yield but with no significant stereoselectivity, while removing the aromatic substituent afforded **5c** in 76% yield and a 1.3:1 dr. Halogen substitution was also possible, producing **5d**–**5f** in 68–76% yield and a 1.5:1–2.1:1 dr. Modification of the aromatic ring to a pyridine was also tolerated, affording **5g** in 55% yield and a 1:1.3 dr (unusually, in favour of the less polar isomer). Given the chromatographic separability, these yields (in light of the modest selectivity) would prove useful for detailed structure-activity relationship studies of such indoline alkaloids, particularly at the initial drug development phases.

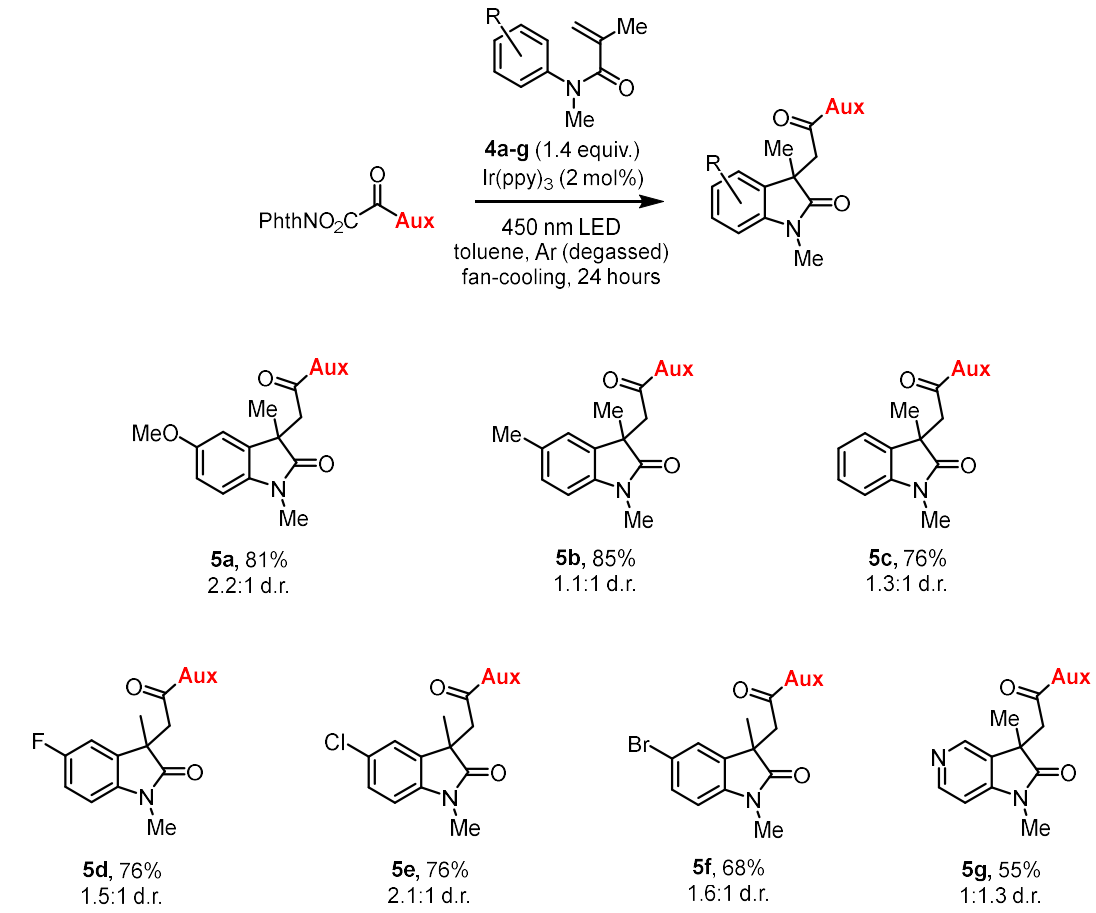

Figure 6.3: *Substrate scope.*

7. Towards Pyrroloindoline Alkaloids

We next turned to the challenge of converting our stereochemically pure oxindoles to indoline alkaloids.

With diastereopure **5a** in-hand, we recognised an opportunity to complete the total synthesis of (–)-esermethole and proposed a 3-step route (**Scheme 7.1**). This involved chemoselective reductive auxiliary removal to produce alcohol **7**, subsequent oxidation to aldehyde **8**, and finally a reductive amination-cyclisation sequence to the natural product retaining the (*S*)-stereocentre.

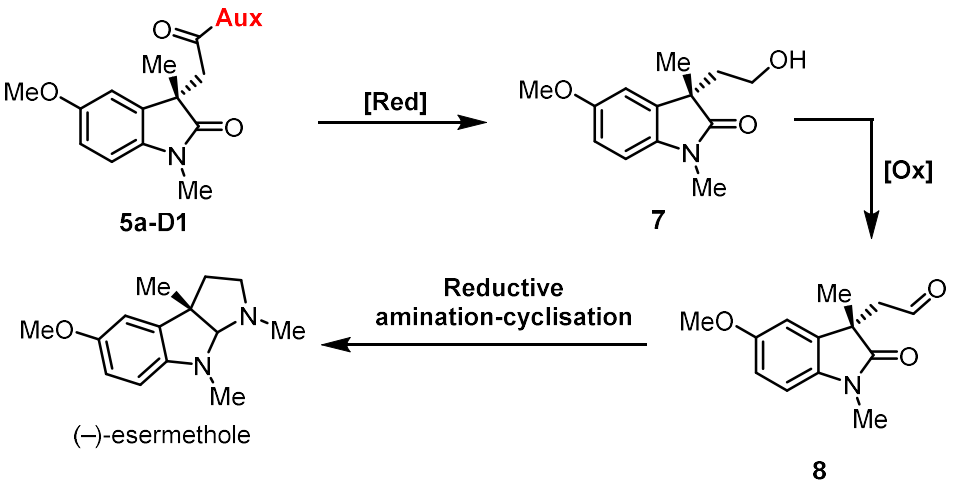

Scheme 7.1: *Envisaged strategy towards (–)-esermethole.*

With this in mind, we started probing possible reduction methods by subjecting **5a-D1** to $LiBH_4$ in THF. This was a tentative choice, but one chosen to differentiate the two "amides", noting that $NaBH_4$ was not reactive enough, while $LiAlH_4$ was deemed to be too strong a reductant. The chemoselectivity differentiation was based on the superior electrophilicity of the auxiliary *N*-acylamide (albeit as an *N*-acyl urea) carbon anticipated over that of the lactam carbonyl carbon. In the event, TLC showed complete conversion of starting material, and a significantly less polar product could be isolated from the reaction. The ^{1}H-NMR for this compound (**Figure 7.1**) was consistent with alcohol **7**: No signals pertaining to the auxiliary were observed, while a multiplet that could be assigned to the diastereotopic methylene protons Ha and Ha' appeared at approximately 3.46 and 3.95 ppm. Ostensibly, a strong alcohol proton signal was revealed around 5 ppm and the ^{13}C NMR spectrum revealed the expected 13 signals.

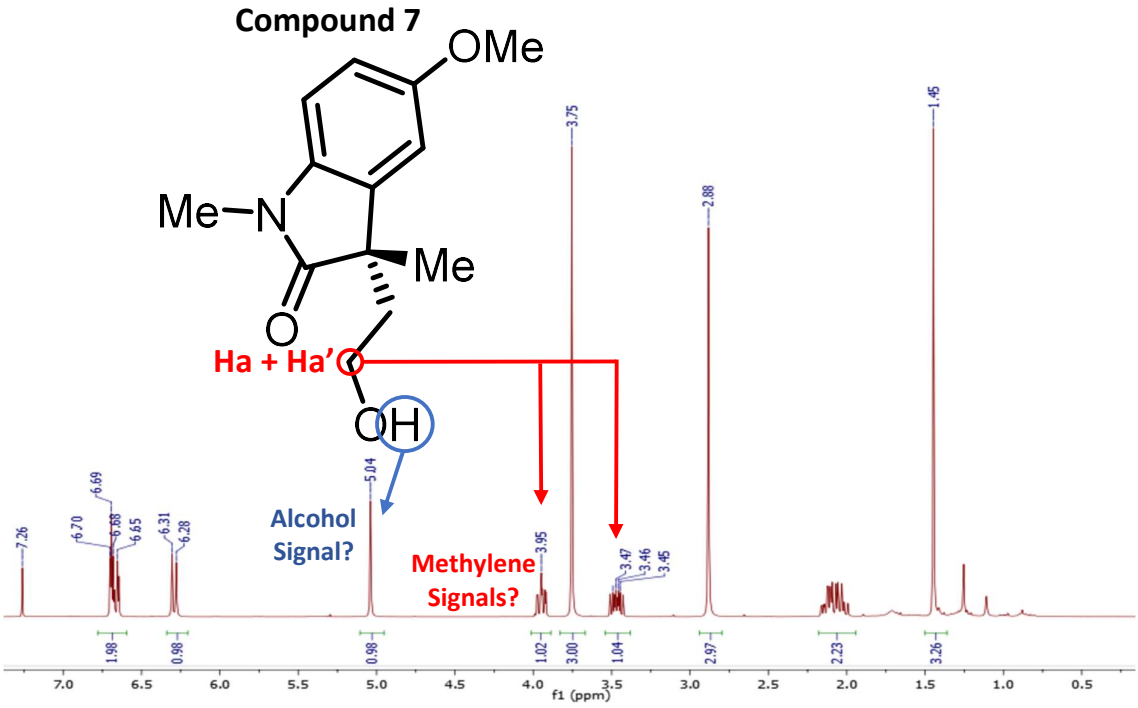

Figure 7.1: *Some evidence (from the ^{1}H-NMR) suggesting formation of the desired alcohol product* ***7****.*

Continuing with the envisaged sequence, however, led to significant doubts in this hypothesis: attempts at oxidation failed to produce **8**: the starting material was resistant to both Dess-Martin periodinane as well as Swern conditions, resulting in complete recovery of the starting material. Additionally, performing a D_2O wash did not exchange and thus remove the proposed alcohol signal. Our suspicions reached a peak upon closer scrutiny of the ^{13}C NMR spectrum when when identifying that a significant upfield shift existed for the assigned C=O carbon, relative to the related products **5a** and the methyl ester **11** (the synthesis and relevance of which is covered later). Looking at the oxindole starting material, **5a,** it was noted that there were three carbonyl moieties, each contributing a signal between 180 and 155 ppm (**Figure 7.2**: top). These carbonyl signals remain >155 ppm even when the chiral auxiliary is replaced by a methyl ester (**Figure 7.2**: middle - *vide infra*, compound **11**). By contrast, the most downfield ^{13}C NMR signal for the alleged **7** was at 153 ppm (**Figure 7.2**: bottom). This led us to consider other potential transformations **5a** could have undergone under the $LiBH_4$ conditions, and, after some review of the literature, we found that the NMR data corresponded exactly to the HFI (hexahydrofuroloindole) **9** shown in **Scheme 7.2**,[78] implying that the $LiBH_4$ had not only effected reduction of the auxiliary amide, but had pre-emptively cyclised the resulting alkoxide into the oxindole amide with concomitant reduction as well. The structure was thus reassigned to HFI **9**.

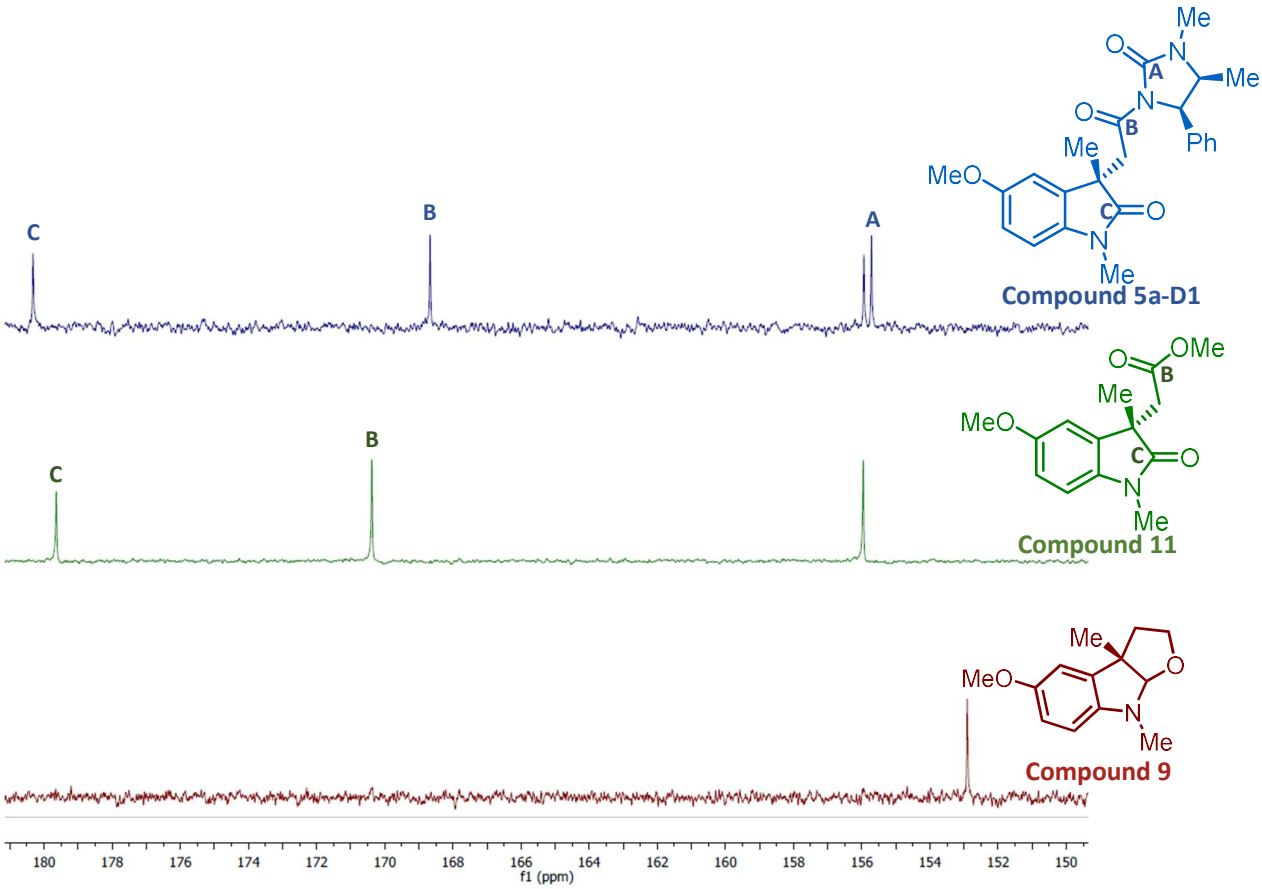

Figure 7.2: *When comparing **9** with the auxiliary amide and methyl ester analogues, the ^{13}C NMR signals for the carbonyl carbons at **B** and **C** disappear – all that remains is the single aromatic methoxy-bearing carbon signal around at 153 ppm.*

The lack of a carbonyl carbon was now accounted for, since **9** lacks a carbonyl group, and with the peak at 152 ppm assigned to the methoxy-bearing carbon as with ester **11**.; likewise, the ineffectiveness of the D_2O wash and the oxidation attempts were caused by the lack of a hydroxyl group in **9**. With this new perspective, the data could be reinterpreted (**Figure 7.3**).

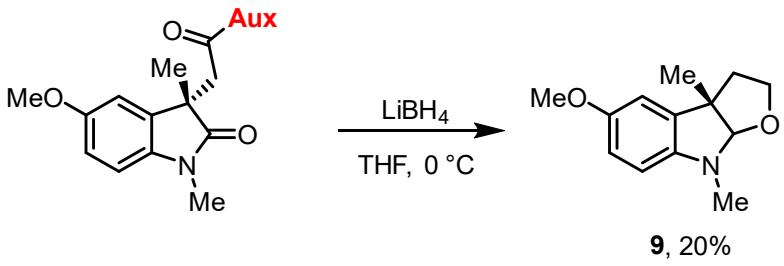

Scheme 7.2: *Treatment of **5a** with $LiBH_4$ led to the unexpected formation of HFI **9**.*

Compound 9

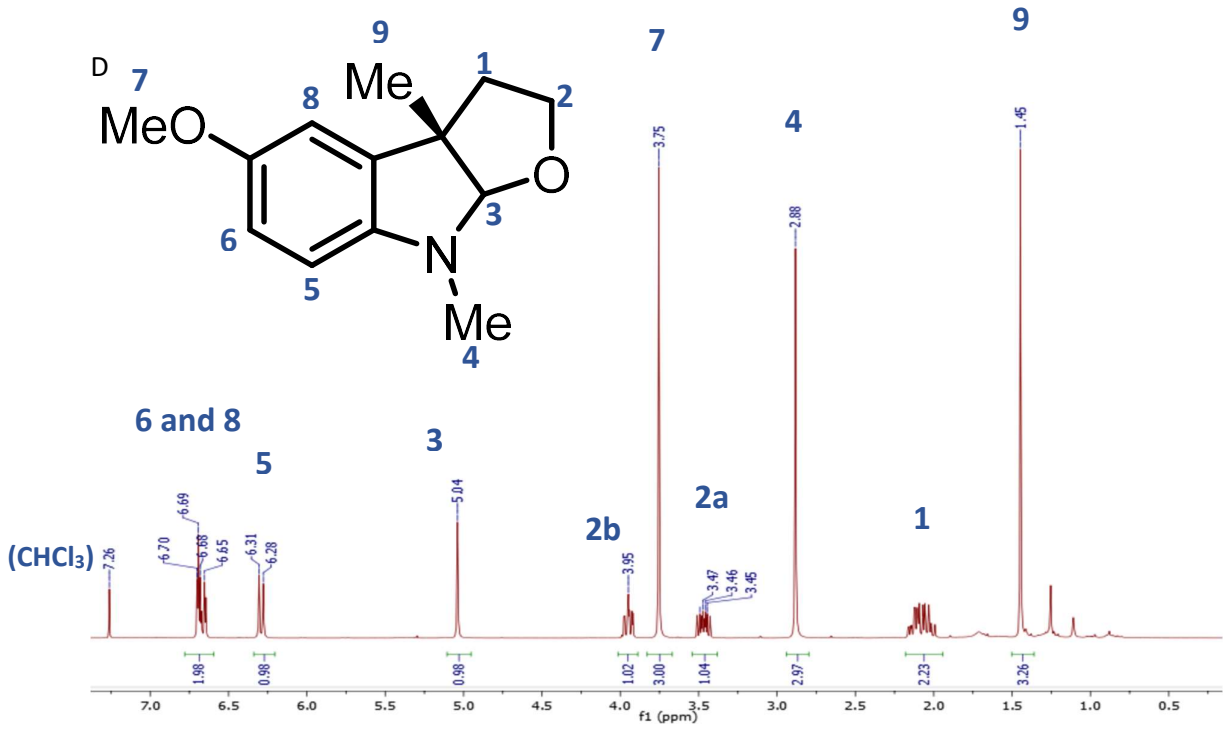

Figure 7.3: *Revised assignment for the ^{1}H NMR (300 MHz, $CDCl_3$) spectrum of* ***9****.*

While this compound was not the desired product, this compound *is* a valid precursor to the related natural product (–)-physovenine which exhibits similar effects *in vitro* (**Figure 7.4**);[79] **9** can be demethylated with BBr_3 and then reacted with methyl isocyanate to form (–)-physovenine.[80] Thus we had successfully completed, albeit somewhat serendipitously, the formal synthesis of (–)-physovenine.

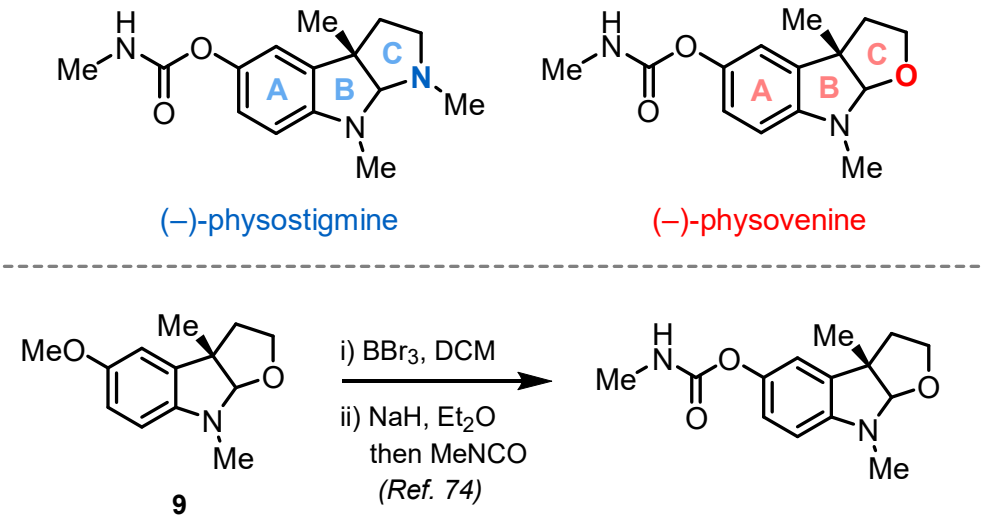

Figure 7.4: *(–)-Physovenine is similar to (–)-physostigmine in both biological activity and structure, bearing a tetrahydrofuran as its C ring compared to the tetrahydropyrrole of (–)-physostigmine.*

Given this novel way of accessing this structure, we screened a few different reducing agents to optimise for the best one (**Table 7.1**). The initial yield when using $LiBH_4$ was poor at 20%. This could have been due to a reduction at the auxiliary amide that was too sluggish, or a reduction rate at the oxindole that was too great, preventing subsequent cyclisation by removing the carbonyl handle too early. To assess both options, we started by looking at $NaBH_4$, a weaker reducing agent than its lithium counterpart since the sodium cation is worse at activating the carbonyl to electrophilic attack - this reduced the yield to 13%. Attempted reduction with the more sterically hindered reagent $LiAl(O^tBu)_3H$ yielded nothing, and so we eventually settled on the harsher reducing agent $LiAlH_4$, which afforded our best result at a yield of 40%.

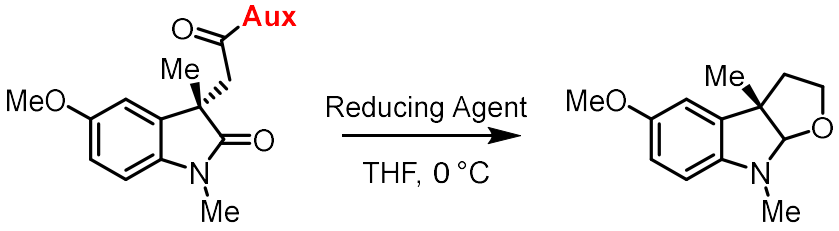

5a-D1 **9**

Entry	Reducing Agent	Yield of 9
1	$LiBH_4$	20%
2	$NaBH_4$	13%
3	$LiAl(O^tBu)_3H$	0%
4	**$LiAlH_4$**	**40%**

Table 7.1: *Various reducing agents used to produce **9**, and the yields thereby.*

After reduction of **5a-D1** with $LiAlH_4$, auxiliary **2** could also be recovered from the column in an amount equivalent to 60% of the starting material. Two things were important to note here: the fact that auxiliary could be recovered in this reaction spoke to the efficiency of this method, as the same auxiliary could theoretically be used to perform the same transformation multiple times. Additionally, the higher yield of **2**, compared to that of **9**, implied the formation of some side product in addition to **9** that also featured the loss of **2**.

Indeed, in many of these reductions, the over-reduced and pre-cyclised side product **10** could be isolated; its ^1H NMR spectrum is shown in **Figure 7.5**. Like the spectrum for **9**, this one featured no signals pertaining to the auxiliary, but there were also two more aliphatic doublets as an AB system, which it seemed reasonable to assign as α- to nitrogen of an indoline. This byproduct was therefore seen as the result of poor selectivity on the part of the reducing agent, with the oxindole amide being fully reduced before cyclisation could occur.

Compound 10

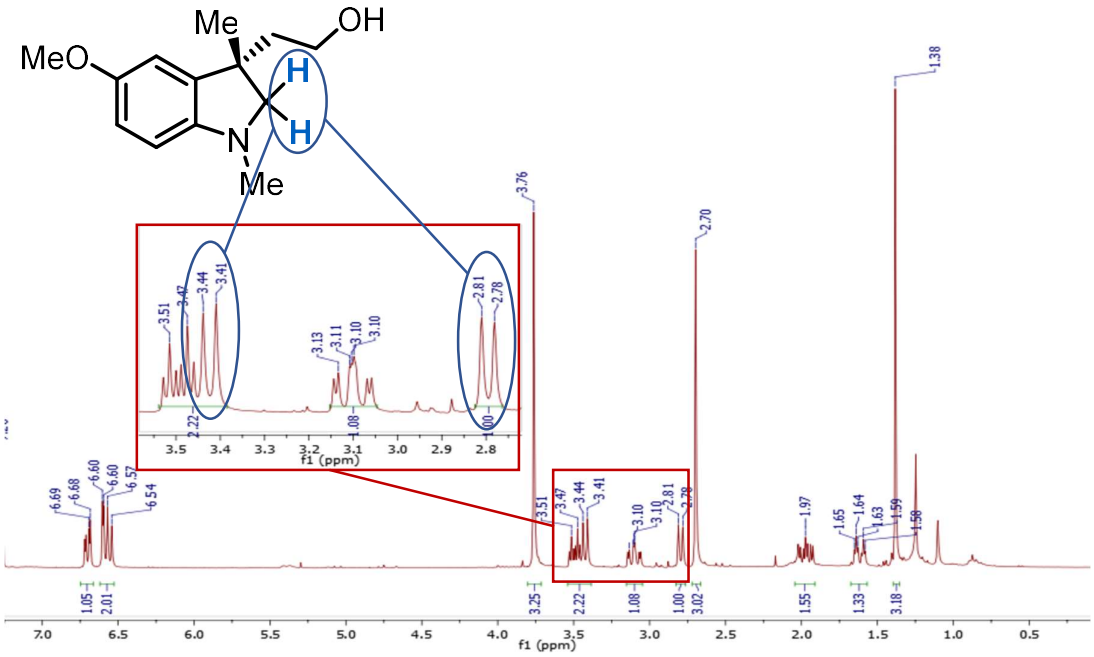

Figure 7.5: *^{1}H NMR spectrum of **10** (minor product obtained in the reduction of **5a-D1**).*

A possible mechanism for the formation of **9** is proposed in **Scheme 7.3**. Initial hydride reduction from $LiAlH_4$ eliminates the auxiliary to yield an aldehyde (**i**-**ii**), which subsequently reacts with another equivalent of $LiAlH_4$, leaving the hydroxyl aluminate **iii**. This moiety would normally result in the alcohol following the aqueous quenching that completes the reaction, but *in situ* it remains charged and therefore nucleophilic. The oxindole amide can then also be reduced, producing a similar species, **iv**, as a hemiaminal. Nearby electrons on the nitrogen may now migrate to form the iminium **v**, which rapidly reacts with the more persistent hydroxyl aluminate that remains, closing the tetrahydrofuran ring and completing **9**. Furthermore, over-reduction of the hemiaminal to the indoline, **10**, could be accommodated by this mechanism.

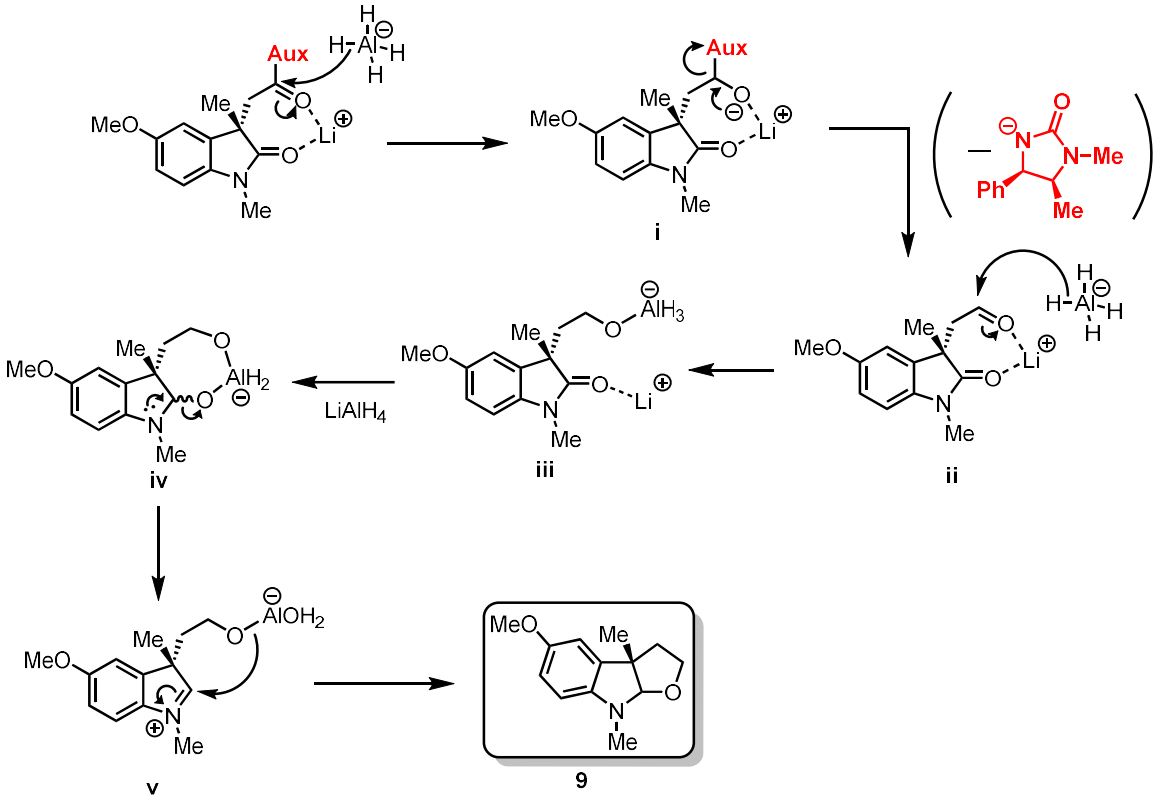

Scheme 7.3: *Proposed mechanism for the formation of **9***

With the aim of increasing the selectivity of the reduction, and ultimately the overall yield of **9**, we investigated a route that first deprotected the auxiliary to produce the methyl ester **11**, and then performed the reductive cyclisation (**Scheme 7.4**). The methyl ester offered better chemodifferentiation over the oxindole amide. In the event, deprotection with NaOMe in

MeOH successfully afforded **11** in 71% yield, and subsequent reduction with $LiBH_4$ (returning to the milder reductant to improve selectivity) provided **9** in 70% yield. This represented a 50% yield over the two steps, which was a modest improvement in yield vs the direct $LiAlH_4$ reduction (40% yield). More importantly, however, this second approach does provide one with more synthesis options for downstream functionalisation.

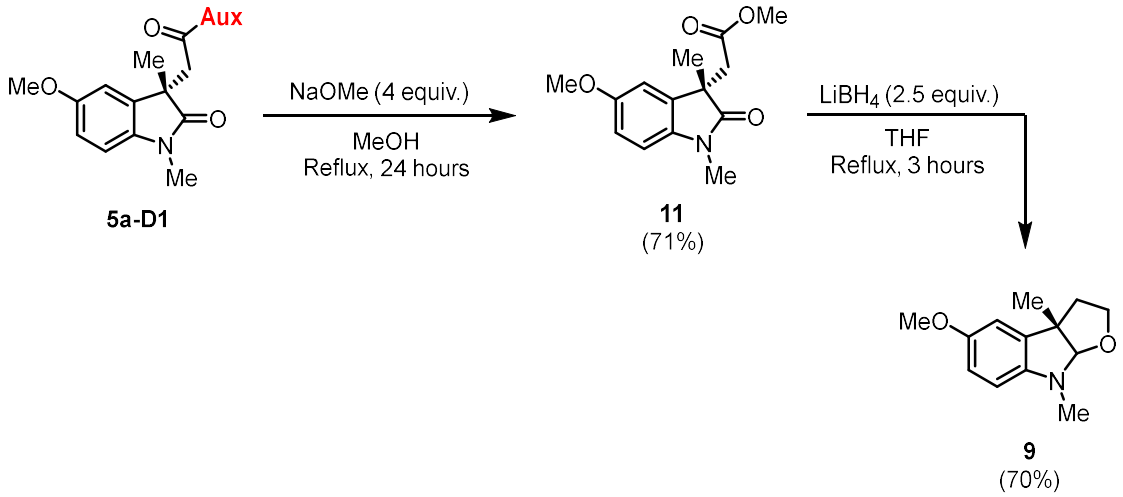

Scheme 7.4: *Altered route to **9** via an inserted esterification.*

8. Explorations to Improve Diastereoselectivity and Atom Efficiency

With the aim of improving diastereoselectivity, we also experimented with using an Evans-type chiral auxiliary (in place of **2**). Compound **12** (the Evans-type analogue of **1**) was synthesized in much the same way as **1**, except that pyridine was replaced with the much stronger base *n*-BuLi in the second step (see the Experimental section), owing to the lower nucleophilicity of the oxazolidinone when compared to **2**. When **12** was reacted with **4c** to produce **13** (**Scheme 8.1**), however, the yield was slightly lower than when **1** was used instead, and any diastereoselectivity was imperceptible. Considering this we opted not to continue exploration of the Evans variation as part of this thesis.

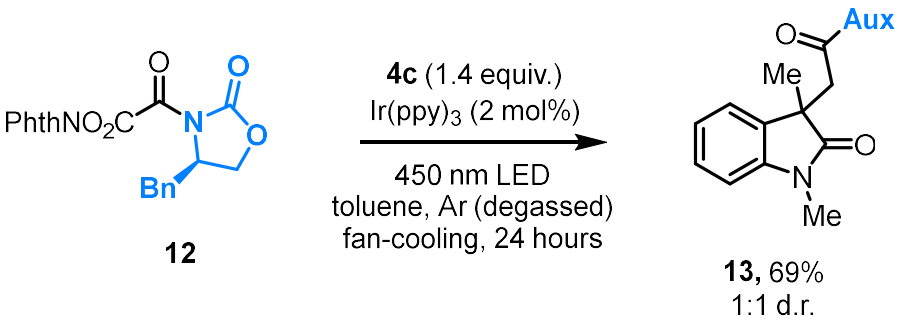

Scheme 8.1: *Comparison between using an Evans-type and imidazolidinone chiral auxiliary.*

In addition to varying the auxiliary, we also sought to improve the atom efficiency of the precursor; the phthalimido fragment, in particular, is quite significant in terms of mass, and is simply lost over the course of the reaction. Previous work in the group showed that carbamoyl radicals could be formed from oxamic acids using an oxidative decarboxylative process.[81] This method involves the use of $AgNO_3$ and the organic photocatalyst 4CzIPN as catalysts, as well as a stoichiometric amount of $K_2S_2O_8$ to act as the terminal oxidant. Another benefit to using this method (apart from being able to use a lighter radical precursor) was that it eschewed the use of an expensive platinum-group metal photocatalyst in favour of the far greener 4CzIPN. With these improvements in mind, we synthesized oxamic acid **14** to be used in the reaction shown in **Scheme 8.2**. However, after 48 hours we only recorded a 35% yield of **5a**. Starting material **14** was judged to have been used up at this point; however, this was difficult to judge via TLC as the acid tended to stick to the plate and therefore mingle with baseline spots. Even if the reaction had not yet reached completion, when compared to the earlier method using $Ir(ppy)_3$ (which generated **5a** in an 81% yield after just 24 hours) this new approach was inferior.

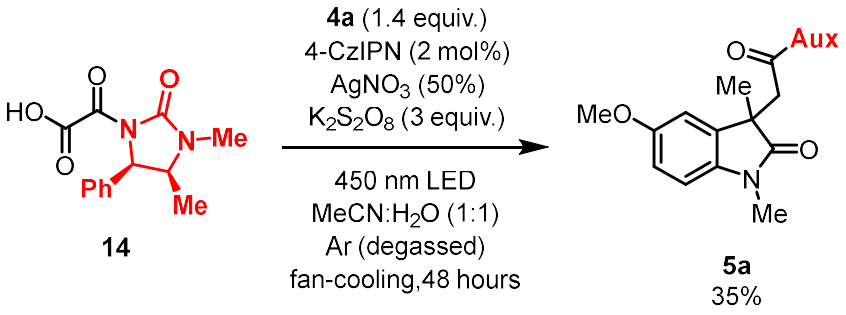

Scheme 8.2: *Using oxamic acid **14** as the radical precursor to form **5a**.*

The proposed mechanism for this process is shown in **Scheme 8.3** and it likely proceeds as per the literature report, featuring a dual metal/photocatalytic cycle. Oxidation of **14** by Ag(II) produces **i** which decarboxylates to produce the chiral acyl radical **ii**. The addition-cyclisation cascade proceeds as before, but the second oxidation — to the cyclohexadienyl cation — is now facilitated by the highly oxidizing 4CzIPN$^{\bullet+}$, generated by $K_2S_2O_8$ oxidation. Finally, the $SO_4^{\bullet-}$ regenerates the active Ag(II) catalyst species. The advantage of this dual cycle is the thermal activation energy required for $K_2S_2O_8$ homolysis to produce the oxidizing $SO_4^{\bullet-}$ (100 °C) can be circumvented through the use of a tandem photocatalytic cycle.

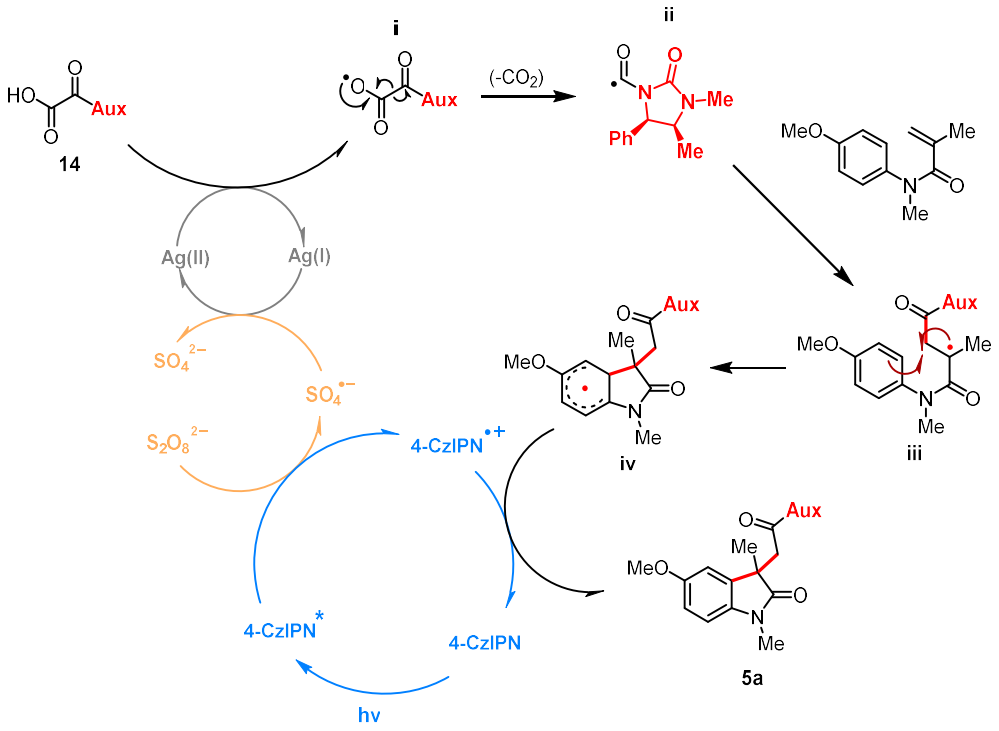

Scheme 8.3: *Proposed mechanism for radical addition-cyclisation starting with oxamic acid* ***14****.*

Conclusions and Future Work

9. Conclusions

Stereochemical control in synthetic procedures featuring radicals is largely thought to be difficult to achieve.[82] By making use of a radical species that has a chiral auxiliary attached, we were able to afford some level of diastereoenrichment in the formation of various oxindoles; additionally, by opting for a diastereomer-forming method (instead of one that forms the desired enantiomers directly) we were able to easily isolate a compound with the desired quaternary carbon chirality, without needing to settle for some loss of enantiopurity or having to use expensive chromatographic techniques. Finally, synthesis of these oxindoles was achieved using photoredox catalysis, further showcasing the practicality of this field of chemistry. We then showed that the diastereomer of interest could be taken to a known precursor of the natural product (–)-physovenine through a reductive cascade, indicating the applicability of the process. The results shown in this thesis have since been published in *Synthesis*.[83]

The diastereoselectivity of the photoredox cyclisation was admittedly moderate to low, at a maximum of around 2:1. The lack of efficiency in this aspect is probably due to a lack of rigidity in the chiral auxiliary attachment; intermediate **ii** in **Figure 6.2** features a fully rotatable C-C bond (highlighted in red). It is also important to note that while separation of enantiomers can be costly/time consuming in an industrial setting, there can be relatively simple ways purify such mixtures. For example, if a given compound is crystalline, recrystallisation can improve purity, even of enantiomeric mixtures, and if a compound is not crystalline, it can sometimes be made to be by attaching certain compounds to it (such as by esterifying a carboxylic acid with menthol). With this in mind, one could envision using a different chiral auxiliary to the one used in this research, with the final product being more readily recrystallised.

10. Future Work

More optimal diastereoselectivity for the oxindole-forming reaction may result from further modification of the chiral auxiliary. This could mean finding the right part of the auxiliary to load with more steric bulk, by replacing the phenyl ring with a benzyl or naphthyl group, for example, or by modifying the N-Me moiety. Alternatively, reducing conformational flexibility in the transition state by employing some sort of chelating agent might improve stereoselectivity.

Further experimentation with oxazolidinone auxiliaries is still warranted. While the imidazolidinone auxiliary is convenient to synthesize, the starting material ((*1R, 2S*)-(-)-ephedrine hydrochloride) is a controlled substance that is difficult to procure. Oxazolidinone auxiliaries, while potentially less convenient to synthesise and install, can be derived from readily available amino acids. Furthermore, they are typically more labile and thus could offer some downstream functionalisation advantages.

The improved atom economy credentials of the method involving 4CzIPN was not enough, in our minds, to outweigh the significant reduction in yield compared to our initial conditions, and so further optimisations continued with renewed use of **1** and $Ir(ppy)_3$. The fact that such a transformation is possible using an organic photocatalyst is nevertheless exciting; the conditions employed were identical to the reported procedure and were thus not optimized to our specific reagents. Perhaps further investigations into this route would lead to a method producing the desired oxindoles in a yield that is competitive with the more expensive, platinum group metal-catalysed reaction.

Further work could be done converting various oxindole derivatives (such as the ones synthesised as part of this thesis) to the corresponding HFI or (–)-physovenine analogues and then testing their bioactivity in the form of an A-ring SAR. Hence, revisiting the route to reach the original target molecule, (–)-physostigmine: aminolysis of ester **11** (or perhaps even oxindole **5a-D1**) could be achieved by stirring with methylamine (or its lithium anion) to yield amide **15** - this has literature precedent in the case of the ester.[84] **15** could then be reductively cyclized to form (–)-esermethole, and then converted to (–)-physostigmine (as per a similar method to that shown in **Scheme 8.4**).[80]

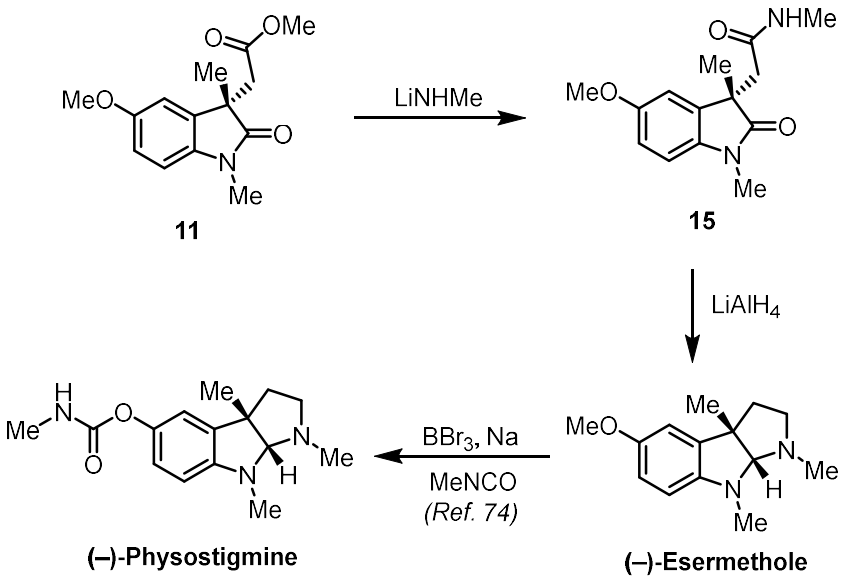

Scheme 8.4: *Alternative route to (–)-physostigmine via amide* ***15****.*

Experimental Section

11. General Information

Unless otherwise specified, all reagents and photoinitators were purchased from commercial sources and used without further purification. Anhydrous solvents were obtained using a solvent purification system drying over 3Å molecular sieves. Photochemical reactions were carried out using an EvoluChem™ PhotoRedOx Box under irradiation at 450 nm using an EvoluChem™ LED (30 W). Standard borosilicate glass vessels were used. Where required, reactions were heated using a standard stirrer/metal heating block combination fitted with a temperature probe. ^{1}H NMR and ^{13}C NMR spectra were recorded on Varian Mercury 300 MHz (75 MHz for ^{13}C), Bruker 400 MHz (101 MHz for ^{13}C), Bruker 600 MHz (151 MHz for ^{13}C) instruments. All spectral data were acquired at 295 K. Chemical shifts are reported in parts per million (ppm, δ), downfield from tetramethylsilane (TMS, δ = 0.00 ppm), and are referenced to residual solvent [$CDCl_3$, δ = 7.26 ppm (^{1}H) and 77.16 ppm (^{13}C)]. Coupling constants (*J*) are reported in Hertz (Hz). The multiplicity abbreviations used are br broad, s singlet, d doublet, t triplet, q quartet, m multiplet, app apparent. Infrared (IR) spectra were recorded on a PerkinElmer Spectrum 100 FT-IR spectrometer. High-resolution mass spectra were obtained from the University of Stellenbosch Mass Spectrometry Service and recorded in electrospray positive mode with a time-of-flight analyzer system on a Waters Synapt G2 machine. Melting points were determined using a Reichert-Jung Thermovar hot-stage microscope and are uncorrected. Thin-layer chromatography was carried out on silica gel 60F_{254} precoated aluminum foil sheets (unless otherwise stated) and were visualized using UV light (254 nm) or staining with acidic *p*-anisaldehyde, ninhydrin or $KMnO_4$ solutions. Flash column chromatography was carried out using silica gel 60 (unless otherwise stated), eluting with the specified solvent system.

11. Synthetic Procedures and Compound Characterisation

General Procedures

General Procedure A: Synthesis of *N*-hydroxyphthalimido Oxamides.

A solution of *N*-hydroxyphthalimide (1 equiv.) in anhydrous THF under argon was cooled to -78 °C and oxalyl chloride (5 equiv.) added dropwise. The reaction mixture was allowed to slowly reach room temperature and then stirred overnight. The resulting solution was then concentrated on the rotary evaporator and dried under vacuum (to remove excess oxalyl chloride). The residue was re-dissolved in anhydrous THF, cooled to -78 °C followed by the sequential addition of the relevant chiral auxiliary (1 equiv.) in THF and pyridine (1 equiv). The reaction mixture was once again allowed to reach room temperature and left to stir overnight. The organic solvent was removed in vacuo and the crude residue extracted using aqueous HCl (10%) and 3 washes of EtOAc. The combined organic extracts were then washed with sat. aqueous $NaHCO_3$ solution until the aqueous layer has changed from red to pale yellow. The combined organic extracts were then finally washed with sat. brine, dried over $MgSO_4$, filtered, and the organic solvent was removed in vacuo. The resulting crude colourless solid was then recrystallised from a minimum amount of hot EtOAc

General Procedure B: Synthesis of *N*-Aryl Acrylamides.

To a solution cooled 0 °C to of the relevant *N*-methylaniline (1 equiv.), acrylic acid (1.2 equiv.) and 2-Chloro-1-methylpyridinium iodide (1.2 equiv.) in anhydrous dichloromethane under argon, was added triethylamine (3 equiv.) dropwise. This solution was lifted out of the ice bath and allowed to stir overnight. Aqueous HCl (1.0 M) was then added, and the organic layer separated and washed with sat. aqueous $NaHCO_3$ solution, followed by brine. The organic layer was then dried over $MgSO_4$, concentrated in vacuo, and the crude residue purified by column chromatography.

General Procedure C. Photoredox Cyclisation.

A solution of *N*-aryl acrylamide (1.4 equiv.), phthalimido oxamide (1 equiv.) and $Ir(ppy)_3$ (2 mol%) in toluene was degassed with argon for 10 minutes. The vial was then sealed using parafilm to be irradiated at 450 nm for 24 hours. The reaction solvent was removed under vacuum, and the compounds of interest (diastereomers) were then separated and purified by flash column chromatography from the resulting residue.

11.1 Synthesis of Starting Materials

(*4R,5S*)-1,5-dimethyl-4-phenylimidazolidin-2-one, 2:

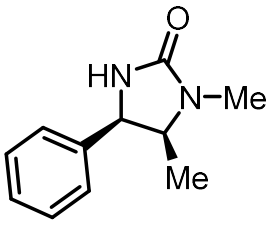

(*1R, 2S*)-(-)-ephedrine hydrochloride (53.84 g, 263.0 mmol, 1 equiv.) and urea (47.35 g, 788.0 mmol, 3 equiv.) were added to a round bottomed flask (250 mL) with a stirrer bar. The mixture was heated to 170 °C at which point the solids melted and the solution was then stirred at this temperature for 2 hours. The temperature was then raised to 210 °C and left to stir for another hour. After cooling (approx. 15 minutes), the mixture was extracted with EtOAc (500 mL) and washed with of water (4 x 50 mL), followed by sat. brine (50 mL). The organic layer was dried over $MgSO_4$ and, following filtration, the product was left to recrystallise out from the filtrate, yielding colourless needles of **2** (18.56 g, 37%).

R_f=0.11 (50% EtOAc/Hexane); **M.P.**: 177-179 °C, lit: 175[85]; **IR** (film, $\nu_{max/cm^{-1}}$): 3267, 2976, 2861, 1701, 1664, 1439, 763, 702 ; **^{1}H-NMR:** (300 MHz, $CDCl_3$), δ(ppm): 7.38–7.20 (m, 5H), 5.31 (brs, 1H), 4.76 (d, *J* = 8.4 Hz, 1H), 3.87 (qd, J_1 = 8.3, J_2 = 6.6 Hz, 1H), 2.73 (s, 3H), 0.73 (d, *J* = 6.6 Hz, 3H); **^{13}C-NMR:** (101 MHz, $CDCl_3$), δ(ppm): 162.5, 138.3, 128.6, 128.1, 127.3, 58.2, 57.7, 28.3, 14.4; **HRMS:** m/z Found: 191.1188, Calculated for $C_{11}H_{14}N_2O$ (M^+): 191.1184.

1,3-Dioxoisoindolin-2-yl 2-((*4S,5R*)-3,4-dimethyl-2-oxo-5-phenylimidazolidin-1-yl)-2-oxoacetate, 1

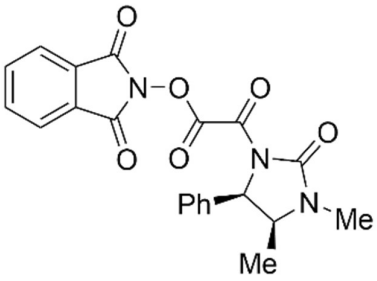

This synthesis followed general procedure A, using 1.50 g of *N*-hydroxyphthalimide (9.20 mmol) and with (*4R,5S*)-1,5-dimethyl-4-phenylimidazolidin-2-one as the relevant chiral auxiliary. Recrystallisation afforded **1** (1.85 g, 49%) as glittery colourless crystals.

R_f : 0.43 (70% EtOAc/Hexane); **M.P.** 231-233 °C; **IR** (film, ν_{max}/cm^{-1}): 1824, 1788, 1736, 1694, 1400, 1127, 972, 695; **^{1}H NMR** (300 MHz, $CDCl_3$) δ (ppm) 7.98–7.87 (m, 2H), 7.84–7.75 (m, 2H), 7.41–7.16 (m, 5H), 5.34 (d, *J* = 8.6 Hz, 1H), 4.18-4.02 (m, 1H), 2.92 (s, 3H), 0.86 (d, *J* = 6.6, 3H); **^{13}C NMR** (101 MHz, $CDCl_3$) δ (ppm) 161.1, 157.4, 155.7, 153.8, 135.0, 134.2, 129.0, 128.9, 128.9, 127.1, 124.3, 58.5, 55.5, 28.3, 15.1; **HRMS** (ESI^+) *m/z:* Calculated for $C_{21}H_{18}N_3O_6$ (M+H): 408.1190, Found: 408.1204.

1,3-dioxoisoindolin-2-yl (*R*)-2-(5-benzyl-3-methyl-2-oxoimidazolidin-1-yl)-2-oxoacetate, 12

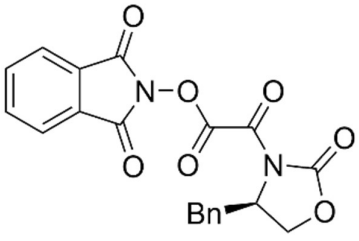

This synthesis followed general procedure A, using 500 mg of *N*-hydroxyphthalimide (3.07 mmol), with (*R*)-4-benzyloxazolidin-2-one as the relevant chiral auxiliary and with one addition to the procedure: following the dissolution of (*R*)-4-benzyloxazolidin-2-one in THF (30 mL), n-butyllithium (2.5 M in THF, 1.2 equiv.) was added and the auxiliary solution was left to stir for 30 minutes before being added dropwise to the reaction mixture. Recrystallisation afforded **12** (880 mg, 50%) as colourless crystals.

R_f = 0.73 (70% EtOAc/Hexane); colourless solid; **M.P.** 169-171 °C; **IR** (film, vmax/cm^{-1}): 1793, 1739, 1697, 1388, 1139, 1020; **^{1}H NMR** (300 MHz, $CDCl_3$) δ (ppm) 7.97–7.77 (m, 4H), 7.41–7.14 (m, 5H), 4.77 (m, 1H), 4.51–4.33 (m, 2H), 3.47–3.38 (m, 1H), 3.02–2.91 (m, 1H); **^{13}C-NMR** (101 MHz, $CDCl_3$) δ (ppm) 160.8, 156.7, 156.2, 152.4, 135.1, 134.0, 129.6, 129.4, 129.2, 128.9, 127.9, 124.4, 68.2, 54.3, 37.3.

2-((*4S,5R*)-3,4-dimethyl-2-oxo-5-phenylimidazolidin-1-yl)-2-oxoacetic acid, 14

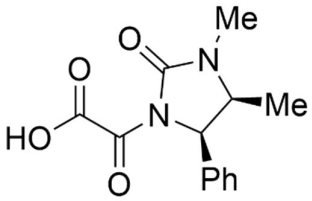

To a solution of (*4R,5S*)-1,5-Dimethyl-4-phenylimidazolidin-2-one[1] (300 mg, 1.58 mmol, 1 equiv.) in anhydrous THF (30 mL) cooled to -78 °C, was added oxalyl chloride (0.26 mL, 3.15 mmol, 2 equiv.) dropwise and the reaction mixture was allowed was allowed to slowly come to room temperature. The reaction was stirred for a further 3 hours, before adding 1M aqueous NaOH (4 mL, 4 mmol, 2.5 equiv.) dropwise. The solution was concentrated under vacuum, and the resulting yellow paste was extracted with sat. $NaHCO_3$ solution and EtOAc. The aqueous layer was acidified with 1 M HCl, and extracted with EtOAc, and the combined organic washings were dried over $MgSO_4$. The organic solution was then concentrated and dried under vacuum to yield **14** (336 mg, 81%) as a colourless solid.

R_f: 0.11 (10% MeOH/DCM); **M.P.** 185-188 °C; **IR** (film, $\nu_{max/cm^{-1}}$): 3069, 1758, 1692, 1432, 1335, 1177; **^{1}H NMR** (300 MHz, $CDCl_3$) δ (ppm) 7.42–7.29 (m, 3H), 7.24–7.17 (m, 2H), 5.35 (d, *J* = 6.5 Hz, 1H), 4.15–4.06 (m, 1H), 2.83 (s, 3H), 0.80 (d, *J* = 4.9 Hz, 3H); **^{13}C NMR** (101 MHz, $CDCl_3$) δ (ppm) 164.9, 162.4, 155.9, 136.9, 129.6, 129.4, 128.1, 59.3, 56.5, 28.2, 15.1 **HRMS** (ESI^+) *m/z*: Calculated for $C_{21}H_{18}N_3O_6$ $(M+H)^+$: 263.1026, Found: 263.1036.

N-(4-methoxyphenyl)-*N*-methylmethacrylamide, 4a[86]

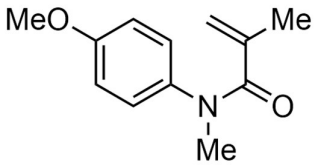

Prepared according to general procedure B, using 4-methoxy-*N*–methylaniline (1.00g, 7.28 mmol). Chromatography with EtOAc/hexane (10–30%) afforded **4a** (1.2 g, 80%) as an orange oil. **R_f**: 0.15 (20% EtOAc/Hexane); **IR** (film, $\nu_{max/cm^{-1}}$): 1650, 1623; **^{1}H NMR** (300 MHz, $CDCl_3$) δ (ppm) 7.04 (app. d, *J* = 8.9 Hz, 2H), 6.84 (app. d, *J* = 8.9 Hz, 2H), 5.01 (s, 1H), 4.98 (s, 1H), 3.80 (s, 3H), 3.29 (s, 3H), 1.73 (s, 3H); **^{13}C NMR** (101 MHz, $CDCl_3$) δ (ppm) 172.3, 158.5, 141.1, 137.6, 127.9, 119.0, 114.5, 55.6, 38.0, 20.5; **HRMS** (ESI^+) *m/z*: Calculated for $C_{12}H_{16}NO_2$ (M+H): 206.1176, Found: 206.1182

N-methyl-*N*-(p-tolyl)methacrylamide, 4b[86]

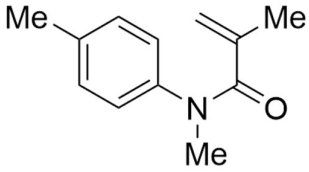

Prepared according to general procedure B, using *N*,4-dimethylaniline (0.50g, 4.13 mmol). Chromatography with EtOAc/hexane (10–30%) afforded **4b** (0.41 g, 52% yield), as an orange oil. $\mathbf{R_f}$: 0.46 (30% EtOAc/Hexane); **^{1}H NMR** (300 MHz, $CDCl_3$) δ (ppm) 7.13 (app. d, *J* = 8.1 Hz, 2H), 7.00 (app. d, *J* = 8.3 Hz, 2H), 5.01 (s, 1H), 4.98 (s, 1H), 3.31 (s, 3H), 2.34 (s, 3H), 1.74 (s, 3H); **^{13}C NMR** (101 MHz, $CDCl_3$) δ (ppm) 172.2, 142.1, 140.9, 136.9, 129.9, 126.4, 119.2, 37.8, 21.1, 20.5.

N-methyl-*N*-phenylmethacrylamide, 4c[87]

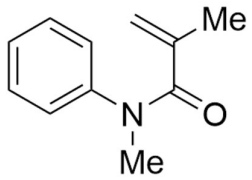

Prepared according to general procedure B, using *N*-methylaniline (1.00 g, 9.33 mmol). Chromatography with EtOAc/hexane (10–30%) afforded **4c** (0.87 g, 53%) as a yellow oil. $\mathbf{R_f}$: 0.32 (30% EtOAc/hexane); **^{1}H-NMR** (300 MHz, $CDCl_3$) δ (ppm) 7.40–7.06 (m, 5H), 5.03 (s, 1H), 5.00 (s, 1H), 3.34 (s, 3H), 1,73 (s, 3H); **^{13}C NMR** (101 MHz, $CDCl_3$) δ (ppm) 172.2, 144.5, 140.5, 129.3, 127.0, 126.5, 119.6, 37.8, 20.3

N-(4-fluorophenyl)-*N*-methylmethacrylamide, 4d[88]

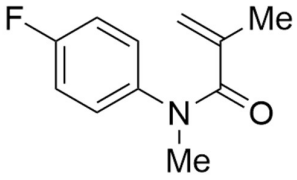

Prepared according to general procedure B, using 4-fluoro-*N*-methylaniline (0.50 g, 4.00 mmol). Chromatography with EtOAc/hexane (10–30%) afforded **4d** (0.40 g, 48%) as a purple oil. $\mathbf{R_f}$: 0.36 (30% EtOAc/Hexane); **^{1}H NMR** (300 MHz, $CDCl_3$) δ (ppm) 7.17–6.96 (m, 4H), 5.04 (s, 1H), 4.96 (s, 1H), 3.31 (s, 3H), 1.75 (s, 3H); **^{13}C NMR** (101 MHz, $CDCl_3$) δ (ppm) 172.1, 161.3 (d, *J* = 248.5 Hz), 140.7, 140.6, 128.3 (d, *J* = 8.1 Hz), 119.5, 116.2 (d, *J* = 23.2 Hz), 37.9, 20.4.

N-(4-chlorophenyl)-*N*-methylmethacrylamide, 4e[86]

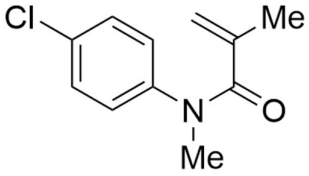

Prepared according to general procedure B, using 4-chloro-*N*-methylaniline (0.53 g, 3.72 mmol). Chromatography with EtOAc/hexane (10–30%) afforded **4e** (0.25 g, 32%) as an orange oil. $\mathbf{R_f}$: 0.35 (30% EtOAc/Hexane); **^{1}H NMR** (300 MHz, $CDCl_3$) δ (ppm) 7.30 (app. d, *J* = 8.8 Hz, 2H), 7.06 (app. d, *J* = 8.7 Hz, 2H), 5.06 (s, 1H), 4.97 (s, 1H), 3.31 (s, 3H), 1.76 (s, 3H); **^{13}C NMR** (101 MHz, $CDCl_3$) δ (ppm) 172.0, 143.2, 140.5, 132.7, 129.5, 127.8, 119.9, 37.8, 20.4.

N-(4-bromophenyl)-*N*-methylmethacrylamide, 4f[88]

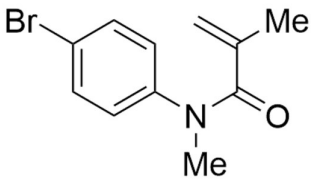

Prepared according to general procedure B, using 4-bromo-*N*-methylaniline (0.47 g, 2.51 mmol). Chromatography with EtOAc/hexane (10–30%) afforded **4f** (0.16 g, 26%) as a red oil. $\mathbf{R_f}$: 0.38 (30% EtOAc/Hexane); **^{1}H NMR** (300 MHz, $CDCl_3$) δ (ppm) 7.46 (app. d, *J* = 8.7 Hz, 2H), 7.01 (app. d, *J* = 8.7 Hz, 2H), 5.07 (s, 1H), 4.97 (s, 1H), 3.31 (s, 3H), 1.77 (s, 3H); **^{13}C NMR** (101 MHz, $CDCl_3$) δ (ppm) 172.0, 143.7, 140.4, 132.5, 128.2, 120.5, 119.9, 37.7, 20.4.

N-methyl-*N*-(pyridin-4-yl)methacrylamide, 4g[88]

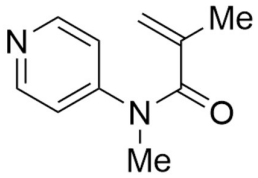

Prepared according to general procedure B, using *N*-methylpyridin-4-amine (250 mg, 2.31 mmol). Chromatography with EtOAc afforded **4g** (121 mg, 30%) as an amorphous white solid. $\mathbf{R_f}$: 0.37 (80% EtOAc/Hexane); **IR** (film, vmax/cm^{-1}): 1644, 1624, 1584, 1499, 1364, 1117; **^{1}H NMR** (300 MHz, $CDCl_3$) δ (ppm) 8.54 (m, 2H), 7.10 (m, 2H), 5.17 (s, 1H), 5.03 (s, 1H), 3.38 (s, 3H), 1.87 (s, 3H); **^{13}C NMR** (101 MHz, $CDCl_3$) δ (ppm) 172.0, 152.1, 150.5, 140.0, 120.8, 119.7, 36.9, 20.1.

9.3 Photocatalytic Syntheses:

3-(2-((*4S,5R*)-3,4-dimethyl-2-oxo-5-phenylimidazolidin-1-yl)-2-oxoethyl)-5-methoxy-1,3-dimethylindolin-2-one, 5a

Prepared according to general procedure C. Using 69.8 mg of **4a** (0.34 mmol), 100 mg of **1** (0.24 mmol) and 3.21 mg $Ir(ppy)_3$ (2 mol %) was obtained **5a** (82.1 mg, 81%; d.r.: 2.2:1 with **5a-D1** in excess)

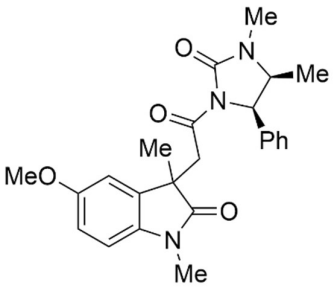

5a-D1: 56.5 mg; light yellow solid; R_f: 0.17 (70% EtOAc/Hexane); **M.P.** 163-167 °C; **IR** (film, $\nu_{max/cm^{-1}}$): 2933, 1713, 1690, 1386, 1035, 702; **^{1}H-NMR** (300 MHz, $CDCl_3$) δ(ppm) 7.15-7.10 (m, 3H), 6.85–6.75 (m, 3H), 6.70–6.5 (m, 2H), 5.10 (d, *J* = 8.5 Hz, 1H), 4.07 (d, *J* = 17.1 Hz, 1H), 3.80 (qd, J_1 = 8.4 Hz, J_2 = 6.6 Hz, 1H), 3.76 (s, 3H), 3.39 (d, *J* = 17.1), 3.11 (s, 3H), 2.77 (s, 3H), 1.35 (s, 3H), 0.69 (d, *J* = 6.6, 3H); **^{13}C-NMR** (101 MHz, $CDCl_3$) δ(ppm) 180.3, 168.7, 155.9, 155.7, 137.3, 136.0, 135.0, 128.3, 127.7, 126.6, 112.0, 109.7, 108.3, 59.1, 55.9, 54.1, 46.3, 42.2, 28.2, 26.5, 25.3, 15.0; **HRMS** (ESI^+) *m/z*: Calculated for $C_{24}H_{28}N_3O_4$ $(M+H)^+$: 422.2074, Found: 422.2083.

5a-D2: 25.6 mg; off-white amorphous solid; R_f: 0.41 (70% EtOAc/Hexane); **IR** (film, $\nu_{max/cm^{-1}}$): 2928, 1723, 1709, 1684, 1386, 1235, 697; **^{1}H NMR** (300 MHz, $CDCl_3$) δ (ppm) 7.30–7.20 (m, 2H), 7.05–6.95 (m, 2H), 6.80–6.65 (m, 3H), 5.02 (d, *J* = 8.5, 1H), 4.02 (d, *J* = 17.4 Hz), 3.74 (s, 3H), 3.74 (m, 1H), 3.38 (d, *J* = 17.4 Hz), 3.12 (s, 3H), 2.78 (s, 3H), 1.36 (s, 3H), 0.69 (d, *J* = 6.6, 3H); **^{13}C NMR** (101 MHz, $CDCl_3$) δ (ppm) 179.9, 168.6, 156.1, 155.6, 137.5, 136.1, 135.4, 128.5, 128.1, 126.9, 111.7, 109.9, 108.3, 59.0, 55.9, 54.1, 46.1, 42.6, 28.2, 26.6, 25.1, 15.0. **HRMS** (ESI^+) *m/z*: Calculated for $C_{24}H_{28}N_3O_4$ $(M+H)^+$: 422,2074, Found: 422.2082.

3-(2-((*4S,5R*)-3,4-dimethyl-2-oxo-5-phenylimidazolidin-1-yl)-2-oxoethyl)-1,3,5-trimethylindolin-2-one, 5b

Prepared according to general procedure C. Using 64.3 mg of **4b** (0.34 mmol), 100 mg of **1** (0.24 mmol) and 3.21 mg $Ir(ppy)_3$ (2 mol %) was obtained **5b** (83.0 mg, 85%; d.r.: 1.1:1 with **5b-D1** in slight excess)

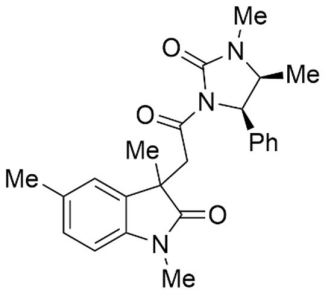

5b-D1: 43 mg; pale yellow solid; **M.P.** 183-193 °C ; **R_f**: 0.24 (70% EtOAc/Hexane); **IR:** 2965, 2915, 1706, 1607, 1380, 1236; **^{1}H-NMR** (300 MHz, $CDCl_3$) δ(ppm) 7.15–7.06 (m, 3H), 6.99 (s, 1H), 6.92 (d, *J* = 7.9 Hz, 1H), 6.83–6.73 (m, 2H), 6.54 (d, *J* = 7.8 Hz, 1H), 5.09 (d, *J* = 8.4 Hz, 1H), 4.08 (d, *J* = 17.2 Hz, 1H), 3.81 (m, 1H), 3.37 (d, *J* = 17.1 Hz, 1H), 3.10 (s, 3H), 2.77 (s, 3H), 2.29 (s, 3H), 1.34 (s, 3H), 0.68 (d, *J* = 6.5 Hz, 3H); **^{13}C-NMR** (101 MHz, $CDCl_3$) δ(ppm) 180.6, 168.7, 155.9, 141.3, 136.0, 133.7, 131.3, 128.2, 127.9, 127.6, 126.6, 122.8, 107.8, 59.1, 54.0, 45.9, 42.2, 28.2, 26.4, 25.2, 21.3, 15.0; **HRMS** (ESI^+) *m/z*: Calculated for $C_{24}H_{28}N_3O_3$ $(M+H)^+$: 406.2125, Found: 406.2144.

5b-D2: 40 mg; orange-yellow amorphous solid; **R_f**: 0.52 (70% EtOAc/Hexane); **IR** (film, ν_{max}/cm^{-1}): 2919, 2852, 1710, 1624, 1374, 1229; **^{1}H-NMR** (300 MHz, $CDCl_3$) δ(ppm) 7.30–7.20 (m, 3H), 7.05-6.65 (m, 5H), 5.03 (d, *J* = 8.4 Hz, 1H), 4.02 (d, *J* = 17.3 Hz, 1H), 3.72 (m, 1H), 3.38 (d, *J* = 17.3 Hz, 1H), 3.12 (s, 3H), 2.79 (s, 3H), 2.28 (s, 3H), 1.35 (s, 1H), 0.70 (d, *J* = 6.6 Hz, 3H); **^{13}C-NMR** (101 MHz, $CDCl_3$) δ(ppm) 180.2, 168.7, 156.1, 141.5, 136.1, 134.0, 131.3, 128.8, 128.5, 128.1, 126.9, 122.9, 107.8, 59.0, 54.1, 45.7, 42.6, 28.2, 26.5, 25.1, 21.3, 14.9; **HRMS** (ESI^+) *m/z*: Calculated for $C_{24}H_{28}N_3O_3$ $(M+H)^+$: 406.2125, Found: 406.2125.

3-(2-((4S,5R)-3,4-dimethyl-2-oxo-5-phenylimidazolidin-1-yl)-2-oxoethyl)-1,3-dimethylindolin-2-one, 5c

Prepared according to general procedure C. Using 59.6 mg of **4c** (0.34 mmol), 100 mg of **1** (0.24 mmol) and 3.21 mg $Ir(ppy)_3$ (2 mol %) was obtained **5c** (51.0 mg, 76%; d.r.: 1.3:1, with **5c-D1** in slight excess)

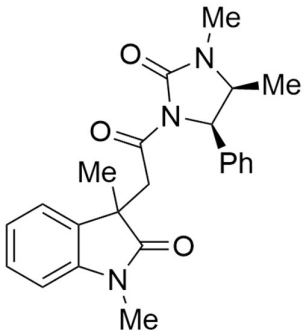

5c-D1: 28.8 mg; yellow amorphous solid; **R_f**: 0.21 (70% EtOAc/Hexane); **IR** (film, ν_{max}/cm^{-1}): 2975, 2924, 1708, 1613, 1380; **^{1}H-NMR** (300 MHz, $CDCl_3$) δ(ppm) 7.40–7.05 (m, 5H), 6.98–6.91 (m, 1H), 6.80–6.71 (m, 1H), 5.09 (d, *J* = 8.52, 1H), 4.13 (d, *J* = 16.9 Hz, 1H), 3.89 (dq, J_1 = 8.2 Hz, J_2 = 6.6 Hz, 1H), 3.37 (d, *J* = 16.8, 1H), 3.12 (s, 3H), 2.76 (s, 3H), 3.34 (s, 3H), 0.76 (d, *J* = 6.5, 3H); **^{13}C-NMR** (101 MHz, $CDCl_3$) δ(ppm) 180.6, 168.7, 155.9, 143.7, 136.0, 128.7, 128.3, 127.7, 127.6, 126.6, 122.1, 108.1, 59.1, 54.0, 45.9, 42.1, 28.3, 26.4, 25.1; **HRMS** (ESI^+) *m/z*: Calculated for $C_{23}H_{26}N_3O_3$ $(M+H)^+$: 392.1969, Found: 392.1979.

5c-D2: 22.1 mg; oil; R_f: 0.48 (70% EtOAc/Hexane); **IR** (film, $\nu_{max/cm^{-1}}$): 2923, 2854, 1707, 1611, 1379, 1235; **^{1}H-NMR** (300 MHz, $CDCl_3$) δ(ppm) 7.30–7.18 (m, 5H), 7.16–7.10 (m, 1H), 7.04–6.92 (m, 3H), 6.82–6.77 (m, 1H), 5.01 (d, *J* = 8.4 Hz, 1H), 4.06 (d, *J* = 17.1 Hz, 1H), 3.71 (dq, J_1 = 8.4 Hz, J_2 = 6.7 Hz, 1H), 3.37 (d, *J* = 17.0 Hz, 1H), 3.14 (s, 3H), 2.79 (s, 3H), 1.38 (s, 3H), 0.70 (d, *J* = 6.6 Hz, 3H); **^{13}C-NMR** (101 MHz, $CDCl_3$) δ(ppm) 180.3, 168.7, 156.1, 143.9, 136.1, 134.0, 128.6, 128.1, 127.9, 127.0, 122.0, 108.1, 59.1, 54.1, 45.8, 42.5, 28.2, 26.5, 25.0, ; **HRMS** (ESI^+) *m/z*: Calculated for $C_{23}H_{26}N_3O_3$ $(M+H)^+$: 392.1969, Found: 392.1974.

3-(2-((4S,5R)-3,4-dimethyl-2-oxo-5-phenylimidazolidin-1-yl)-2-oxoethyl)-5-fluoro-1,3-dimethylindolin-2-one, 5d

Prepared according to general procedure C. Using 65.7 mg of **4d** (0.34 mmol), 100 mg of **1** (0.24 mmol) and 3.21 mg $Ir(ppy)_3$ (2 mol %) was obtained **5d** (74.9 mg, 76%; d.r.: 1.5:1 with **5d-D1** in excess)

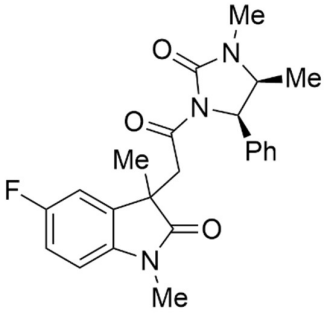

5d-D1: 45.4 mg; off-white Solid; R_f: 0.18 (70% EtOAc/Hexane); **IR** (film, $\nu_{max/cm^{-1}}$): 2920, 1711, 1621, 1382, 1070 ; **^{1}H-NMR** (300 MHz, $CDCl_3$) δ(ppm) 7.20–7.10 (m, 3H), 6.95–6.90 (m, 1H), 6.85–6.74 (m, 3H), 6.58–6.50 (m, 1H), 5.08 (d, *J* = 8.4 Hz, 1H), 4.08 (d, *J* = 17.2 Hz, 1H), 3.80 (m, 1H), 3.39 (d, *J* = 17.2 Hz, 1H), 3.11 (s, 3H), 2.78 (s, 3H), 1.34 (s, 3H), 0.70 (d, *J* = 6.4 Hz, 3H); **^{13}C-NMR** (101 MHz, $CDCl_3$) δ(ppm) 180.3, 168.5, 159.1 (d, *J* = 240.4 Hz), 155.8, 139.6, 135.9, 135.3 (d, *J* = 8.1 Hz), 128.3, 127.7, 126.6, 113.7 (d, *J* = 23.2 Hz), 110.2 (d, *J* = 25.2 Hz), 108.4 (d, *J* = 8.1 Hz), 59.1, 54.0, 46.3, 42.2, 28.2, 26.6, 25.0, 15.0; **HRMS** (ESI^+) *m/z*: Calculated for $C_{23}H_{25}FN_3O_3$ $(M+H)^+$: 410.1874, Found: 410.1888.

5d-D2: 29.5 mg; orange-yellow amorphous solid*;* **R_f**: 0.42 (70% EtOAc/Hexane)*;* **IR** (film, $\nu_{max/cm^{-1}}$): 2921, 1710, 1618, 1381, 1236, 1115 ; **^{1}H-NMR** (300 MHz, $CDCl_3$) δ(ppm) 7.40–7.20 (m, 3H), 7.04–6.96 (m, 2H), 6.92–6.85 (m, 2H), 6.73–6.65 (m, 1H), 5.02 (d, *J* = 8.5 Hz, 1H), 4.00 (d, *J* = 17.5 Hz, 1H), 3.76 (m, 1H), 3.43 (d, *J* = 17.5 Hz, 1H), 3.12 (s, 3H), 2.79 (s, 3H), 1.35 (s, 3H), 0.71 (d, *J* = 6.6 Hz, 3H); **^{13}C-NMR** (101 MHz, $CDCl_3$) δ(ppm) 45.4 mg; 179.9, 168.5, 159.1 (d, *J* = 240.4 Hz), 156.0, 139.8, 136.0, 135.6 (d, *J* = 7.1 Hz), 128.6, 128.1, 126.9, 113.8 (d, *J* = 23.2 Hz), 110.3 (d, *J* = 24.2 Hz), 108.4 (d, *J* = 8.1 Hz), 59.0, 54.1, 46.1, 42.5, 28.2, 26.6, 24.9, 15.0; **HRMS** (ESI^+) *m/z*: Calculated for $C_{23}H_{25}FN_3O_3$ $(M+H)^+$: 410.1874, Found: 410.1882.

5-chloro-3-(2-((4S,5R)-3,4-dimethyl-2-oxo-5-phenylimidazolidin-1-yl)-2-oxoethyl)-1,3-dimethylindolin-2-one, 5e

Prepared according to general procedure C. Using 71.3 mg of **4e** (0.34 mmol), 100 mg of **5** (0.24 mmol) and 3.21 mg $Ir(ppy)_3$ (2 mol %) was obtained **5e** (78.2 mg, 76% yield; d.r.: 2.1:1 with **5e-D1** in excess).

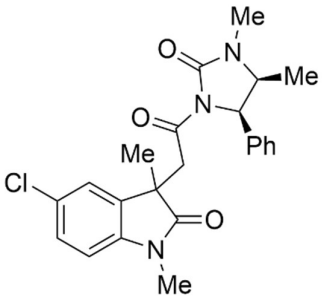

5e-D1: 52.8 mg, yellow amorphous solid; R_f: 0.14 (70% EtOAc/Hexane); **IR** (film, $\nu_{max/cm^{-1}}$): 2922, 1709, 1609, 1381, 1235; **^{1}H-NMR** (300 MHz, $CDCl_3$) δ(ppm) 7.21–7.10 (m, 4H), 7.09–7.02 (m, 1H), 6.85–6.75 (m, 2H), 6.57–6.50 (m, 1H), 5.08 (d, *J* = 8.5 Hz, 1H), 4.11 (d, *J* = 17.2 Hz, 1H), 3.81 (dq, J_1 = 8.4 Hz, J_2 = 6.7 Hz, 1H), 3.38 (d, *J* = 17.2 Hz, 1H), 3.10 (s, 3H), 2.78 (s, 3H), 1.34 (s, 3H), 0.70 (d, *J* = 6.6 Hz, 3H); **^{13}C-NMR** (101 MHz, $CDCl_3$) δ(ppm) 179.8, 168.4, 156.0, 142.5, 136.0, 135.7, 128.6, 128.1, 127.7, 127.2, 126.9, 122.5, 109.0, 59.0, 54.2, 45.9, 42.6, 28.3, 26.6, 25.0, 14.9, **HRMS** (ESI^+) *m/z*: Calculated for $C_{23}H_{25}{}^{35}ClN_3O_3$ $(M+H)^+$: 426.1579, Found: 426.1586.

5e-D2: 25.4 mg, yellow amorphous solid; R_f: 0.47 (70% EtOAc/Hexane); **IR** (film, $\nu_{max/cm^{-1}}$): 2923, 1716, 1686, 1382, 1234; **^{1}H-NMR** (300 MHz, $CDCl_3$) δ(ppm) 7.30–7.22 (m, 3H), 7.21–7.16 (m, 1H), 7.11–7.08 (m, 1H), 7.03–6.96 (m, 2H), 6.73–6.72 (m, 1H), 5.00 (d, *J* = 8.46 Hz, 1H), 4.03 (d, *J* = 17.5 Hz, 1H), 3.77 (dq, J_1 = 8.4 Hz, J_2 = 6.6 Hz, 1H), 3.42 (d, *J* = 17.5 Hz, 1H), 3.11 (s, 3H), 2.80 (s, 3H), 1.35 (s, 3H), 0.71 (d, *J* = 6.6 Hz, 3H); **^{13}C-NMR** (101 MHz, $CDCl_3$) δ(ppm) 180.2, 168.6, 155.8, 142.4, 135.9, 135.4, 128.4, 127.8, 127.6, 127.3, 126.6, 122.5, 109.0, 59.1, 54.0, 46.1, 42.2, 28.3, 26.6, 25.0, 15.0, **HRMS** (ESI^+) *m/z*: Calculated for $C_{23}H_{25}{}^{35}ClN_3O_3$ $(M+H)^+$: 426.1579, Found: 426.1583.

5-bromo-3-(2-((4S,5R)-3,4-dimethyl-2-oxo-5-phenylimidazolidin-1-yl)-2-oxoethyl)-1,3-dimethylindolin-2-one, 5f

Prepared according to general procedure C. Using 85.4 mg of **4f** (0.34 mmol), 100 mg of **1** (0.24 mmol) and 3.21 mg $Ir(ppy)_3$ (2 mol %) was obtained **5f** (76.6 mg, 68%; d.r.: 1.6:1 with **5f-D1** in excess)

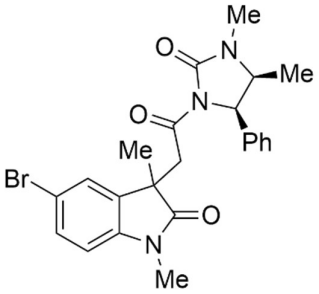

5f-D1: 46.7 mg; orange amorphous solid; R_f: 0.18 (70% EtOAc/Hexane); **IR** (film, $\nu_{max/cm^{-1}}$): 2963, 1711, 1607, 1382, 1258, 1076; **^{1}H-NMR** (300 MHz, $CDCl_3$) δ(ppm) 7.40–7.10 (m, 5H), 6.85–6.75 (m, 2H), 6.53–6.44 (m, 1H), 5.08 (d, *J* = 8.5 Hz, 1H), 4.10 (d, J = 17.2 Hz, 1H), 3.80 (m, 1H), 3.37 (d, 17.2 Hz, 1H), 3.09 (s, 3H), 2.78 (s, 3H), 1.33 (s, 3H), 0.69 (d, J = 6.5 Hz, 3H); **^{13}C-NMR** (101 MHz, $CDCl_3$) δ(ppm) 180.0, 168.5, 155.7, 142.8, 135.8, 135.7, 130.5, 128.3, 127.7, 126.5, 125.1, 114.6, 109.5, 59.1, 54.0, 46.0, 42.1, 28.2, 26.5, 24.9, 15.0 ; **HRMS** (ESI^+) *m/z*: Calculated for $C_{23}H_{25}{}^{79}BrN_3O_3$ $(M+H)^+$: 470.1074, Found: 470.1078,.

5f-D2: 29.9 mg; yellow oil**;** R_f: 0.51 (70% EtOAc/Hexane); **IR** (film, $\nu_{max/cm^{-1}}$): 2963, 1712, 1607, 1382, 1258, 1075; **^{1}H-NMR** (300 MHz, $CDCl_3$) δ(ppm) 7.41–7.20 (m, 5H), 7.04-6.94 (m, 2H), 6.70–6.63 (m, 1H), 4.99 (d, *J* = 8.4 Hz, 1H), 4.03 (d, *J* = 17.5 Hz, 1H), 3.77 (m, 1H), 3.42, (d, *J* = 17.5 Hz, 1H), 3.11 (s, 3H), 2.81 (s, 3H), 1.35 (s, 3H), 0.71 (d, *J* = 6.6, 3H); **^{13}C-NMR** (101 MHz, $CDCl_3$) δ(ppm) 179.6, 168.4, 155.9, 143.0, 136,0, 136.0, 130.6, 128.6, 128.1, 126.8, 125.2, 114.5, 109.6, 59.0, 54.1, 45.8, 42.7, 28.2, 26.6, 25.0, 14.9; **HRMS** (ESI^+) *m/z*: Calculated for $C_{23}H_{25}{}^{79}BrN_3O_3$ $(M+H)^+$: 470.1074, Found: 470.1078.

3-(2-((4S,5R)-3,4-dimethyl-2-oxo-5-phenylimidazolidin-1-yl)-2-oxoethyl)-1,3-dimethyl-1,3-dihydro-2H-pyrrolo[3,2-c]57yridine-2-one, 5g

Prepared according to general procedure C. Using 55.2mg of **4g** (0.31 mmol), 91.1 mg of **1** (0.22 mmol) and 2.9 mg $Ir(ppy)_3$ (2 mol %) was obtained **5g** (55.5 mg, 55%; d.r.: 1:1.3 with the **5g-D2** in slight excess)

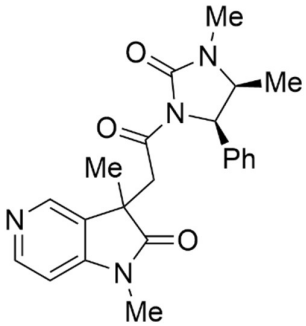

5g-D1: 24.1 mg; white amorphous solid; R_f: 0.31 (70% EtOAc/Hexane - Alumina plate); **IR** (film, $\nu_{max/cm^{-1}}$): 2922, 1704, 1607, 1386, 1234, 1117, 1025; **^{1}H-NMR** (300 MHz, $CDCl_3$) δ(ppm) 8.47–8.20 (m, 2H), 7.04–6.85 (m, 3H), 4.97 (d, *J* = 8.5 Hz, 1H), 4.10 (d, *J* = 18.1 Hz, 1H), 3.85 (m, 1H), 3.57 (d, *J* = 18.2 Hz, 1H), 3.18 (s, 3H), 2.81 (s, 3H), 1.41 (s, 3H), 0.71 (d, *J* = 6.6 Hz, 3H); **^{13}C-NMR** 101 MHz, $CDCl_3$) δ(ppm) 179.6, 168.0, 155.7, 144.7, 135.8, 131.5, 128.7, 128.3, 126.8, 104.4, 59.0, 54.3, 44.1, 43.4, 28.3, 27.1, 24.4, 14.9; **HRMS** (ESI^+) *m/z*: Calculated for $C_{22}H_{25}N_4O_3$ $(M+H)^+$: 393.1921, Found: 393.1933.

5g-D2: 31.37 mg; white amorphous solid; R_f: 0.40 (70% EtOAc/Hexane – Alumina plate); **IR** (film, $\nu_{max/cm^{-1}}$): 2922, 1721, 1381, 1259, 1020; **^{1}H-NMR** (300 MHz, $CDCl_3$) δ(ppm) 8.35–8.22 (m, 2H), 7.20-7.06 (m, 3H), 6.85–6.72 (m, 2H), 6.65–6.58 (m, 1H), 5.06 (d, *J* = 8.5 Hz, 1H), 4.16 (d, *J* = 17.5 Hz, 1H), 3.81 (m, 1H), 3.44 (d, *J* = 17.4 Hz, 1H), 3.12 (s, 3H), 2.77 (s, 3H), 1.38 (s, 3H), 0.68 (d, *J* = 6.6 Hz, 3H); **^{13}C-NMR** (101 MHz, $CDCl_3$) δ(ppm) 180.2, 168.4, 155.5, 152.6, 147.8, 139.8, 135.7, 129.9, 128.5, 127.9, 126.4, 104.0, 59.1, 54.0, 44.5, 42.6, 28.2, 26.6, 24.5, 15.0; **HRMS** (ESI^+) *m/z*: Calculated for $C_{22}H_{25}N_4O_3$ $(M+H)^+$: 393.1921, Found: 393.1939.

2,2,6,6-tetramethylpiperidin-1-yl (4S,5R)-3,4-dimethyl-2-oxo-5-phenylimidazolidine-1-carboxylate, 6

This reaction follows the same protocol as that of general procedure C, except that in place of the aryl acrylamide, 53.1 mg of TEMPO (0.34 mmol, 1.4 equiv.) and 0.05 mL of NEt_3 (0.34 mmol, 1.4 equiv.) are used. Using 69.8 mg of **4a** (0.34 mmol), 100 mg of **1** (0.24 mmol) and 3.2 mg $Ir(ppy)_3$ (2 mol %) was obtained **6** (43.6 mg, 48%) as a white solid.

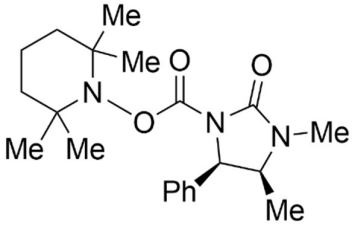

R_f: 0.50 (EtOAc); **M.P.** 197-210 °C; **IR** (film, $\nu_{max/cm^{-1}}$): 1777, 1697, 1330, 1223; **^{1}H-NMR** (300 MHz, $CDCl_3$) δ(ppm) 7.36–7.14 (m, 5H), 5.14 (d, *J* = 8.5 Hz, 1H), 3.91 (m, 1H), 2.81 (s, 3H), 1.68–1.21 (m, 6H), 1.17 (s, 3H), 0.98 (s, 3H), 0.90 (s, 3H), 0.79 (d, *J* = 6.6 Hz, 3H), 0.76 (s, 3H); **^{13}C-NMR** (101 MHz, $CDCl_3$) δ(ppm) 155.1, 152.5, 137.0, 128.6, 128.3, 127.1, 60.7, 60.5, 60.4, 54.4, 39.2, 39.1, 31.8, 31.7, 28.4, 21.3, 20.5, 17.0, 15.2; **HRMS** (ESI^+) *m/z*: Calculated for $(M+H)^+$: 374,2438, Found: 374.2452.

9.4 Towards HFIs

Methyl 2-(5-methoxy-1,3-dimethyl-2-oxoindolin-3-yl)acetate, 11

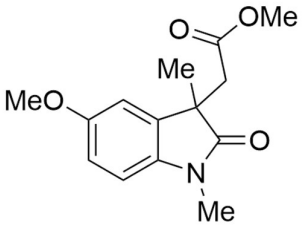

50 mg (0.12 mmol, 1 equiv.) of **5a** was added to a 25 mL round-bottomed flask, followed by a stir bar. The reaction flask was purged with argon for 10 minutes, after which the compound was dissolved in approximately 4 mL of anhydrous methanol. With stirring on, 2.7 mL of 0.175 M (0.47 mmol, 4 equiv.) sodium methoxide in methanol was added, and the reaction was refluxed for 24 hours (under argon). The reaction was then quenched with 2 mL of concentrated ammonium chloride solution for 15 min. Methanol was removed via rotary evaporation, and the aqueous layer was extracted with 3x5 mL EtOAc. The combined organic washings were washed with 7 mL of concentrated ammonium chloride solution, followed by 10 mL of brine before being dried over $MgSO_4$ and concentrated under vacuum. The resulting residue was purified by flash column chromatography (50% EtOAc/Hexane) to yield **11** (22.1 mg, 71%) as a viscous yellow oil.

R_f: 0.57 (70% EtOAc/Hexane); **IR** (film, $\nu_{max/cm^{-1}}$): 2958, 2925, 1703, 1260; **^{1}H-NMR** (300 MHz, $CDCl_3$) δ(ppm) 6.85–6.7 (m, 3H), 3.78 (s, 3H), 3.46 (s, 3H), 3.22 (s, 3H), 2.99 (d, *J* = 16.5 Hz, 1H), 2.82 (d, *J* = 16.5 Hz, 1H), 1.35 (s, 1H); **^{13}C-NMR** (101 MHz, $CDCl_3$) δ(ppm) 179.6, 170.4, 156.0, 137.2, 134.4, 112.0, 110.3, 108.4, 55.9, 51.7, 45.9, 41.4, 26.6, 24.4; **HRMS** (ESI^+) *m/z*: Calculated for $C_{14}H_{18}NO_4$ $(M+H)^+$: 264.1230, Found: 264.1247.

3-(2-hydroxyethyl)-5-methoxy-1,3-dimethylindolin-2-one, 9 (via 11)

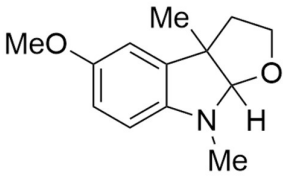

4 mL of anhydrous THF was added to a 50 mL round-bottomed flask containing 46.7 mg (0.18 mmol, 1 equiv.) of **11**. After purging the flask with argon and with stirring, 2 M (0.22 mL, 0.44 mmol, 2.5 equiv.) $LiBH_4$ in THF was added, and the reaction was heated under reflux for 3 hours. The reaction was quenched with approximately 5 mL of concentrated ammonium chloride solution for 15 minutes. The reaction was diluted with 20 mL of EtOAc and 10 mL of distilled water, and the aqueous layer was washed with 3x10 mL of EtOAc. The combined EtOAc washings were washed with a further 15 mL of distilled water, followed by 15 mL of brine, before being dried over $MgSO_4$. This solution was concentrated under vacuum

and the residue was purified by column chromatography (10% EtOAc/Hexane) to yield **9** (29.6 mg, 70%) as a colourless oil.

R_f: 0.9 (70% EtOAc/Hexane); **IR** (film, $\nu_{max/cm^{-1}}$): 2924, 1500, 1217, 756; **^{1}H-NMR** (300 MHz, $CDCl_3$) δ(ppm) 6.72–6.62 (m, 2H), 6.29 (d, *J* = 8.5 Hz, 1H), 5.04 (s, 1H), 3.95 (m, 1H), 3.75 (s, 3H), 3.47 (m, 1H), 2.88 (s, 3H), 2.08 (m, 2H), 1.45 (s, 3H); **^{13}C-NMR** (101 MHz, $CDCl_3$) δ(ppm) 152.9, 145.0, 136.2, 112.3, 110.6, 105.8, 105.5, 67.5, 56.2, 52.6, 41.6, 31.8, 24.6; **HRMS** (ESI^+) *m/z*: Calculated for $C_{13}H_{18}NO_2$ $(M+H)^+$: 220.1332, Found: 220.1341; **(*R*)-12a:** α_D^{20} +31.2 (c 0.74, CH_2Cl_2), **(*S*)-12a:** α_D^{20} -48.2 (c 1.00, CH_2Cl_2).

3-(2-hydroxyethyl)-5-methoxy-1,3-dimethylindolin-2-one, 9 (via 5a)

43.5 mg (1.15 mmol, 4 equiv.) of $LiAlH_4$ was added to a 50 mL round-bottomed flask which had been previously purged with argon. 2 mL of anhydrous THF was added, and the flask was cooled to -40 °C in an acetonitrile/liquid nitrogen bath. Separately, a solution of 10 mL THF and 120.8 mg (0.29 mmol, 1 equiv.) of **5a** was prepared in another 50 mL round-bottomed flask that had been purged with argon, and this solution was added dropwise to the $LiAlH_4$ solution with stirring. This mixture was allowed to stir for 10 minutes, before bringing up to 0 °C in an ice bath, adding approximately 10 mL of diethyl ether, followed by 50 µL of water, 50 µL of 10% aqueous NaOH solution, and then 150 µL of water to quench for 15 minutes. $MgSO_4$ was added, and the mixture was left to stir for a further 15 minutes, before filtering through celite. The resulting organic solution was concentrated under vacuum, and the residue that was left was subjected to purification via flash column chromatography (10% EtOAc/Hexane), yielding 25.5 mg (40%) of **9**.

References

1. M. Leslie, *Science*, 2009, **323**, 1286-1287.
2. G. S. Singhal, G. Renger, S. K. Sopory, K. D. Irrgang and Govindjee, in *Concepts in Photobiology: Photosynthesis and Photomorphogenesis*, Kluwer Academic Publishers, Boston, 1999, pp. 11-51.
3. S. Banu and P. P. Yadav, *Org. Biomol. Chem.*, 2022, **20**, 8584-8598.
4. N. A. Romero and D. A. Nicewicz, *Chem. Rev.*, 2016, **116**, 10075-10166.
5. R. Bevernaegie, S. A. M. Wehlin, B. Elias and L. Troian-Gautier, *ChemPhotoChem*, 2021, **5**, 217-234.
6. E. Speckmeier, T. G. Fischer and K. Zeitler, *J. Am. Chem. Soc.*, 2018, **140**, 15353-15365.
7. H. Mustroph, *ChemPhysChem*, 2016, **17**, 2616-2629.
8. M. Sneha, G. L. Thornton, L. Lewis-Borrell, A. S. H. Ryder, S. G. Espley, I. P. Clark, A. J. Cresswell, M. N. Grayson and A. J. Orr-Ewing, *ACS Catal.*, 2023, **13**, 8004-8013.
9. A. Albini and M. Fagnoni, *ChemSusChem*, 2008, **1**, 63-66.
10. T. J. Van Bergen, D. M. Hedstrand, W. H. Kruizinga and R. M. Kellogg, *J. Org. Chem.*, 1979, **44**, 4953-4962.
11. H. Cano-Yelo and A. Deronzier, *Tetrahedron Lett.*, 1984, **25**, 5517-5520.
12. H. Cano-Yelo and A. Deronzier, *J. Chem. Soc., Perkin Trans. 2*, 1984, DOI: 10.1039/p29840001093, 1093-1098.
13. K. Okada, K. Okubo, N. Morita and M. Oda, *Tetrahedron Lett.*, 1992, **33**, 7377-7380.
14. M. H. Shaw, J. Twilton and D. W. C. MacMillan, *J. Org. Chem.*, 2016, **81**, 6898-6926.
15. D. A. Nicewicz and D. W. C. MacMillan, *Science*, 2008, **322**, 77-80.
16. J. M. R. Narayanam, J. W. Tucker and C. R. J. Stephenson, *J. Am. Chem. Soc.*, 2009, **131**, 8756-8757.
17. M. A. Ischay, M. E. Anzovino, J. Du and T. P. Yoon, *J. Am. Chem. Soc.*, 2008, **130**, 12886-12887.
18. D. Kalyani, K. B. McMurtrey, S. R. Neufeldt and M. S. Sanford, *J. Am. Chem. Soc.*, 2011, **133**, 18566-18569.
19. Y. Ye and M. S. Sanford, *J. Am. Chem. Soc.*, 2012, **134**, 9034-9037.
20. J. A. Terrett, J. D. Cuthbertson, V. W. Shurtleff and D. W. C. MacMillan, *Nature*, 2015, **524**, 330-334.
21. C. C. Le and D. W. C. MacMillan, *J. Am. Chem. Soc.*, 2015, **137**, 11938-11941.
22. G. Pandey and R. Laha, *Angew. Chem. Int. Ed.*, 2015, **54**, 14875-14879.
23. N. F. Nikitas, P. L. Gkizis and C. G. Kokotos, *Org. Biomol. Chem.*, 2021, **19**, 5237-5253.
24. J.-B. Xia, C. Zhu and C. Chen, *J. Am. Chem. Soc.*, 2013, **135**, 17494-17500.
25. S. P. Pitre, C. D. McTiernan, H. Ismaili and J. C. Scaiano, *J. Am. Chem. Soc.*, 2013, **135**, 13286-13289.
26. D. Cambié, C. Bottecchia, N. J. W. Straathof, V. Hessel and T. Noël, *Chem. Rev.*, 2016, **116**, 10276-10341.
27. D. A. Dirocco, K. Dykstra, S. Krska, P. Vachal, D. V. Conway and M. Tudge, *Angew. Chem. Int. Ed.*, 2014, **53**, 4802-4806.
28. J. J. Douglas, M. J. Sevrin and C. R. J. Stephenson, *Org. Proc. Res. Dev.*, 2016, **20**, 1134-1147.
29. Z. Merrington, Some level of load shedding stability only expected end of March 2025: Eskom, https://www.sabcnews.com/sabcnews/some-level-of-load-shedding-stability-only-expected-end-of-march-2025-eskom/, (accessed 4/26/2023).
30. A. A. Yaroshevsky, *Geochem. Int.*, 2006, **44**, 48-55.
31. E. E. Callard-Langdon, A. Steven and R. J. Kahan, *ChemCatChem*, 2023, **15**, e202300537.

32. Z. Y. Hu, J. Chang, F. F. Guo, H. Y. Deng, G. T. Pan, B. Y. Li and Z. L. Zhang, *Medicine (Baltimore)*, 2020, **99**, e20749.
33. S. M. Umer, M. Solangi, K. M. Khan and R. S. Z. Saleem, *Molecules*, 2022, **27**, 7586.
34. C. Sun, W. Tian, Z. Lin and X. Qu, *Nat. Prod. Rep.*, 2022, **39**, 1721-1765.
35. M. Hallak and E. Giacobini, *Neurochem. Res.*, 1986, **11**, 1037-1048.
36. T. G. Beach, Y.-M. Kuo, C. Schwab, D. G. Walker and A. E. Roher, *Neurosci. Lett.*, 2001, **310**, 21-24.
37. D. Doens, M. E. Valdés-Tresanco, V. Vasquez, M. B. Carreira, Y. De La Guardia, D. E. Stephens, V. D. Nguyen, V. T. Nguyen, J. Gu, M. L. Hegde, O. V. Larionov, P. A. Valiente, R. Lleonart and P. L. Fernández, *ACS Chem. Neurosci.*, 2019, **10**, 4250-4263.
38. P. Ruiz-Sanchis, S. A. Savina, F. Albericio and M. Álvarez, *Chem. – Eur. J.*, 2011, **17**, 1388-1408.
39. C. J. Douglas and L. E. Overman, *Proc. Natl. Acad. Sci. U. S. A.*, 2004, **101**, 5363-5367.
40. G.-J. Mei, W. L. Koay, C. X. A. Tan and Y. Lu, *Chem. Soc. Rev.*, 2021, **50**, 5985-6012.
41. B. W. Boal, A. W. Schammel and N. K. Garg, *Org. Lett.*, 2009, **11**, 3458-3461.
42. X. Zhang, L. Han and S.-L. You, *Chem. Sci.*, 2014, **5**, 1059.
43. C. Ma, T. Zhang, J.-Y. Zhou, G.-J. Mei and F. Shi, *Chem. Commun.*, 2017, **53**, 12124-12127.
44. V. Bizet, G. M. Borrajo-Calleja, C. Besnard and C. Mazet, *ACS Catal.*, 2016, **6**, 7183-7187.
45. J. R. Wolstenhulme, A. Cavell, M. Gredičak, R. W. Driver and M. D. Smith, *Chem. Commun.*, 2014, **50**, 13585-13588.
46. Z.-Y. Cao, F. Zhou and J. Zhou, *Acc. Chem. Res.*, 2018, **51**, 1443-1454.
47. A. Ashimori, B. Bachand, M. A. Calter, S. P. Govek, L. E. Overman and D. J. Poon, *J. Am. Chem. Soc.*, 1998, **120**, 6488-6499.
48. M. G. Kulkarni, A. P. Dhondge, A. S. Borhade, D. D. Gaikwad, S. W. Chavhan, Y. B. Shaikh, V. B. Ningdale, M. P. Desai, D. R. Birhade and M. P. Shinde, *Tetrahedron Lett.*, 2009, **50**, 2411-2413.
49. J.-R. Chen, W.-J. Xiao and X.-Y. Yu, *Synthesis*, 2014, **47**, 604-629.
50. M. N. Paddon-Row and K. N. Houk, *J. Phys. Chem.*, 1985, **89**, 3771-3774.
51. Z. Zhou, Y. Li, B. Han, L. Gong and E. Meggers, *Chem. Sci.*, 2017, **8**, 5757-5763.
52. H. Huo, X. Shen, C. Wang, L. Zhang, P. Röse, L.-A. Chen, K. Harms, M. Marsch, G. Hilt and E. Meggers, *Nature*, 2014, **515**, 100-103.
53. G. Cecere, C. M. König, J. L. Alleva and D. W. C. MacMillan, *J. Am. Chem. Soc.*, 2013, **135**, 11521-11524.
54. H.-W. Shih, M. N. Vander Wal, R. L. Grange and D. W. C. MacMillan, *J. Am. Chem. Soc.*, 2010, **132**, 13600-13603.
55. Y.-Q. Zou, F. M. Hörmann and T. Bach, *Chem. Soc. Rev.*, 2018, **47**, 278-290.
56. T. Hashimoto, Y. Kawamata and K. Maruoka, *Nat. Chem.*, 2014, **6**, 702-705.
57. Q. Chen, T. Zhu, P. K. Majhi, C. Mou, H. Chai, J. Zhang, S. Zhuo and Y. R. Chi, *Chem. Sci.*, 2018, **9**, 8711-8715.
58. J. C. Conrad, J. Kong, B. N. Laforteza and D. W. C. MacMillan, *J. Am. Chem. Soc.*, 2009, **131**, 11640-11641.
59. K. W. Quasdorf and L. E. Overman, *Nature*, 2014, **516**, 181-191.
60. A. Cartier, E. Levernier, V. Corcé, T. Fukuyama, A. L. Dhimane, C. Ollivier, I. Ryu and L. Fensterbank, *Angew. Chem. Int. Ed.*, 2019, **58**, 1789-1793.
61. X.-H. Yang, W.-T. Wei, H.-B. Li, R.-J. Song and J.-H. Li, *Chem. Commun.*, 2014, **50**, 12867-12869.
62. J.-W. Yuan, Q.-Y. Yin, L.-R. Yang, W.-P. Mai, P. Mao, Y.-M. Xiao and L.-B. Qu, *RSC Adv.*, 2015, **5**, 88258-88265.
63. S. Esposti, D. Dondi, M. Fagnoni and A. Albini, *Angew. Chem. Int. Ed.*, 2007, **46**, 2531-2534.
64. D. Crich and Q. Yao, *The Journal of Organic Chemistry*, 1996, **61**, 3566-3570.
65. D. L. Boger and R. J. Mathvink, *J. Org. Chem.*, 1989, **54**, 1777-1779.

66. C. Chen and D. Crich, *Tetrahedron Lett.*, 1993, **34**, 1545-1548.
67. H.-L. Zhu, F.-L. Zeng, X.-L. Chen, K. Sun, H.-C. Li, X.-Y. Yuan, L.-B. Qu and B. Yu, *Org. Lett.*, 2021, **23**, 2976-2980.
68. C. R. Jamison and L. E. Overman, *Acc. Chem. Res.*, 2016, **49**, 1578-1586.
69. W. F. Petersen, R. J. K. Taylor and J. R. Donald, *Org. Lett.*, 2017, **19**, 874-877.
70. D. A. Evans, *Aldrichimica Acta*, 1982, **15**, 23-32.
71. D. A. Evans, J. Bartroli and T. L. Shih, *J. Am. Chem. Soc.*, 1981, **103**, 2127-2129.
72. M. R. Gokada, R. Hunter, A. Andrijevic, W. F. Petersen, S. Samanta, G. Venter and S. Rees-Jones, *J. Org. Chem.*, 2017, **82**, 10650-10658.
73. Y. Gnas and F. Glorius, *Synthesis*, 2006, DOI: 10.1055/s-2006-942399, 1899-1930.
74. M. Ciriani, R. Oliveira and C. A. M. Afonso, *Green Chem.*, 2022, **24**, 4328-4362.
75. K. Jenkins, Doctor of Philosphy, University of Sussex, 1998.
76. Y. Slutskyy and L. E. Overman, *Org. Lett.*, 2016, **18**, 2564-2567.
77. B. Giese, J. A. González-Gómez and T. Witzel, *Angew. Chem. Int. Ed.*, 1984, **23**, 69-70.
78. M. G. Kulkarni, A. P. Dhondge, A. S. Borhade, D. D. Gaikwad, S. W. Chavhan, Y. B. Shaikh, V. B. Nigdale, M. P. Desai, D. R. Birhade and M. P. Shinde, *Eur. J. Org. Chem.*, 2009, **2009**, 3875-3877.
79. Q.-s. Yu, C. Liu, M. Brzostowska, L. Chrisey, A. Brossi, N. H. Greig, J. R. Atack, T. T. Soncrant, S. I. Rapoport and H.-E. Radunz, *Helv. Chim. Acta*, 1991, **74**, 761-766.
80. T. Matsuura, L. E. Overman and D. J. Poon, *J. Am. Chem. Soc.*, 1998, **120**, 6500-6503.
81. C. M. Mazodze and W. F. Petersen, *Org. Biomol. Chem.*, 2022, **20**, 3469-3474.
82. G. Bar and A. F. Parsons, *Chem. Soc. Rev.*, 2003, **32**, 251.
83. W. F. Petersen, J. Späth, M. J. Oddy and R. Hunter, *Synthesis*, 2023, **55**, 1736-1743.
84. T. Ren, R. Qu and L. Song, *Org. Biomol. Chem.*, 2023, **21**, 8089-8093.
85. G. Cardillo, A. D'Amico, M. Orena and S. Sandri, *J. Org. Chem.*, 1988, **53**, 2354-2356.
86. D. C. Fabry, M. Stodulski, S. Hoerner and T. Gulder, *Chem. - Eur. J.*, 2012, **18**, 10834-10838.
87. T. Wu, X. Mu and G. Liu, *Angew. Chem. Int. Ed.*, 2011, **50**, 12578-12581.
88. P. Biswas, S. Paul and J. Guin, *Angew. Chem.*, 2016, **128**, 7887-7891.

Appendix (^{1}H and ^{13}C Spectra)

Compound 2:

^{1}H-NMR, $CDCl_3$, 300 MHz

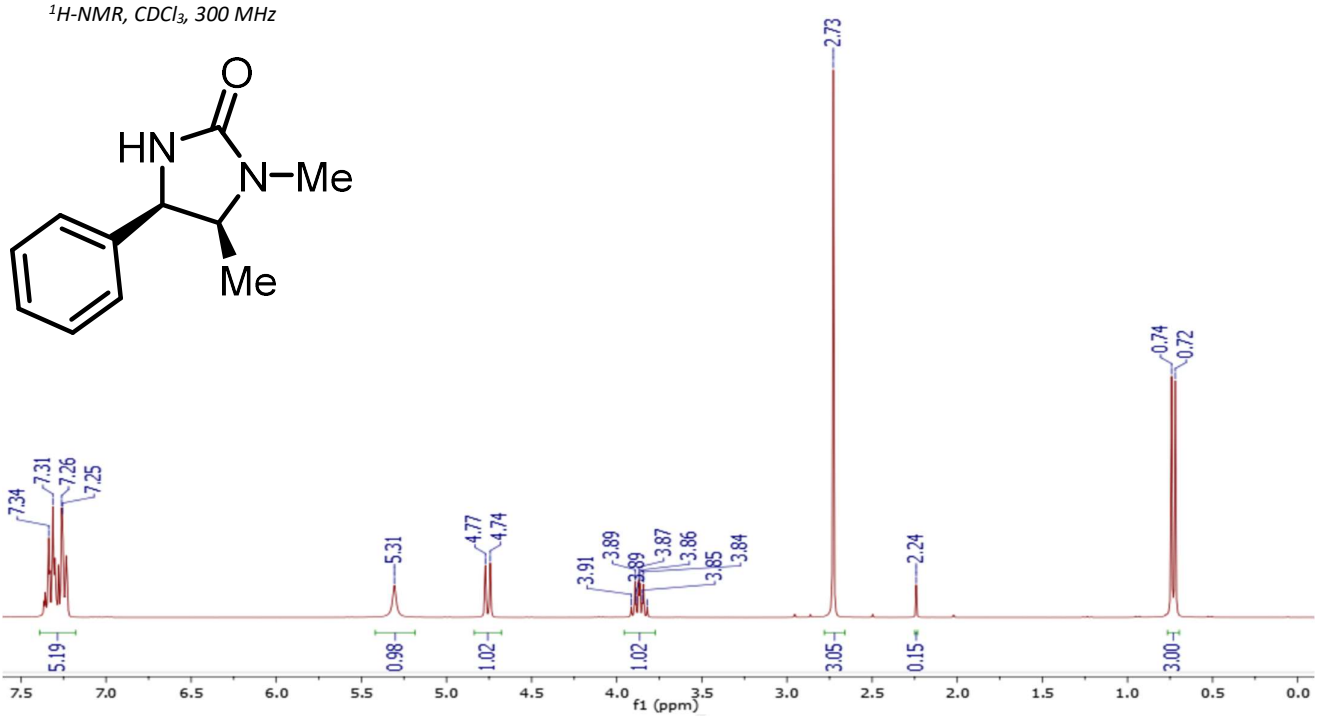

^{13}C-NMR, $CDCl_3$, 101 MHz

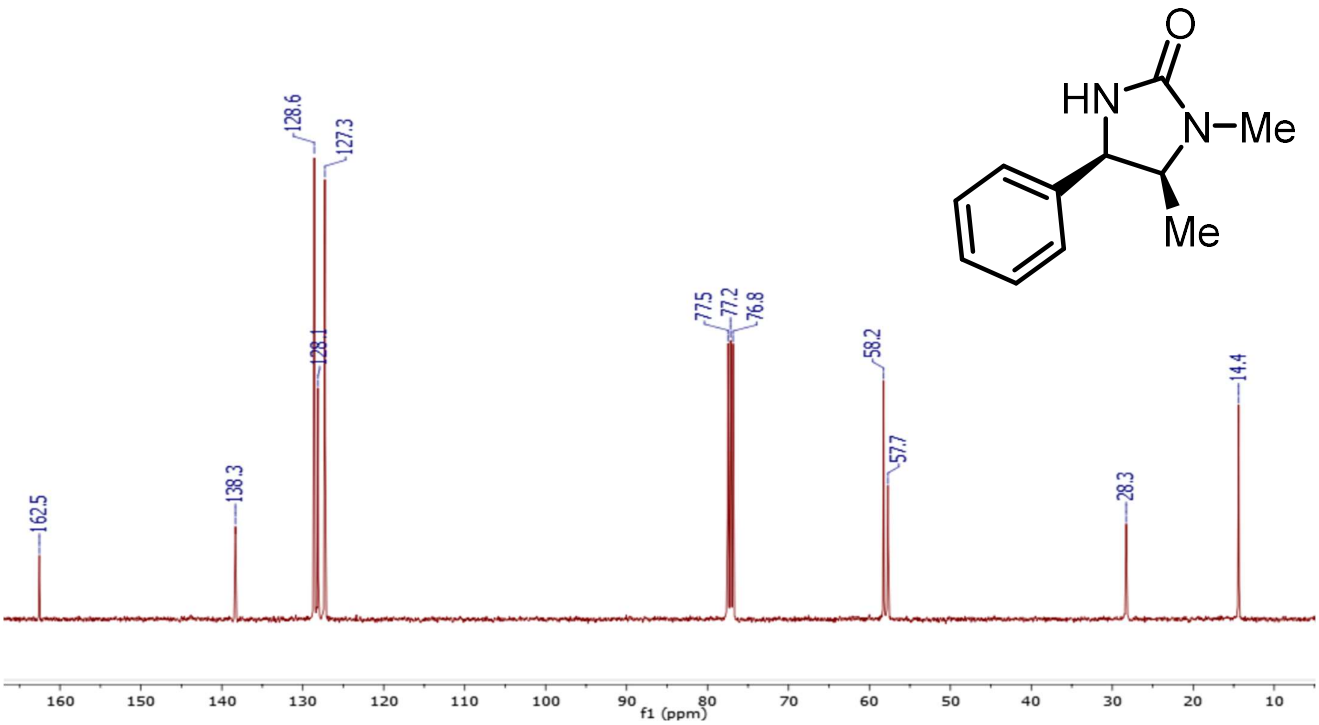

Compound 1:

^{1}H-NMR, $CDCl_3$, 300 MHz

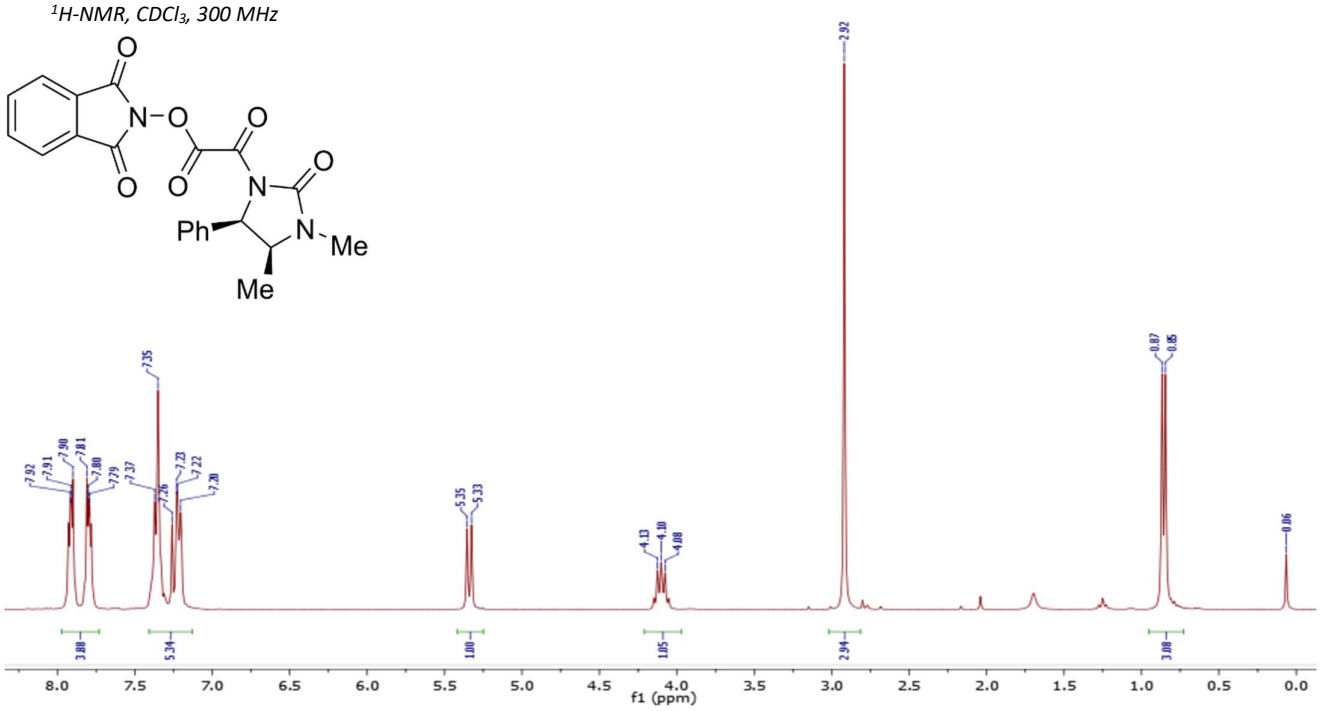

^{13}C-NMR, $CDCl_3$, 101 MHz

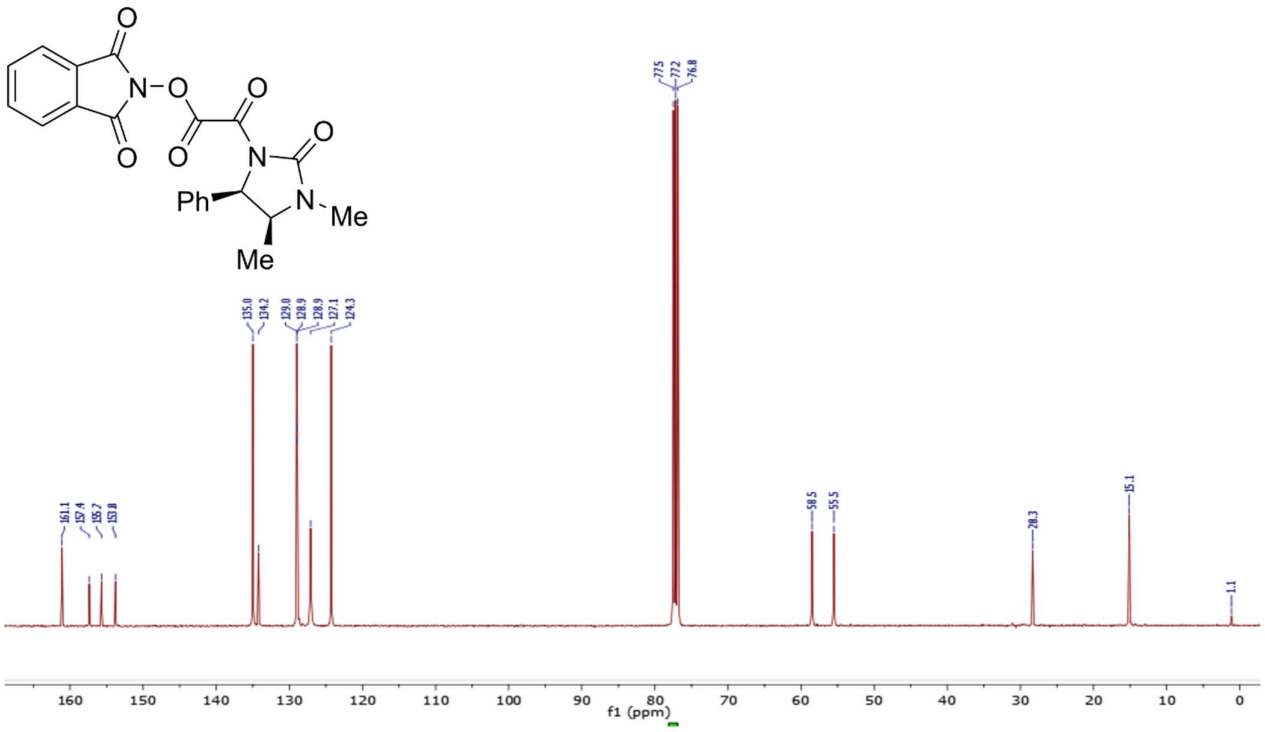

Compound 12:

^{1}H-NMR, $CDCl_3$, 300 MHz

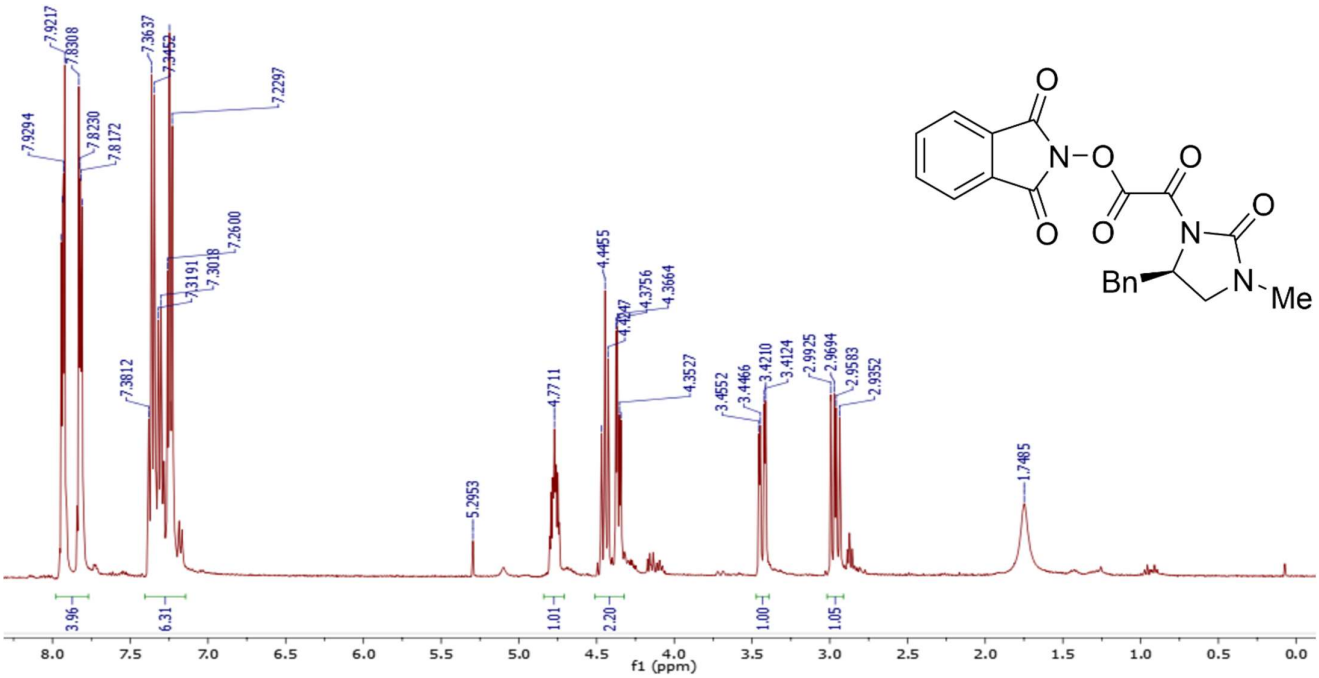

^{13}C-NMR, $CDCl_3$, 101 MHz

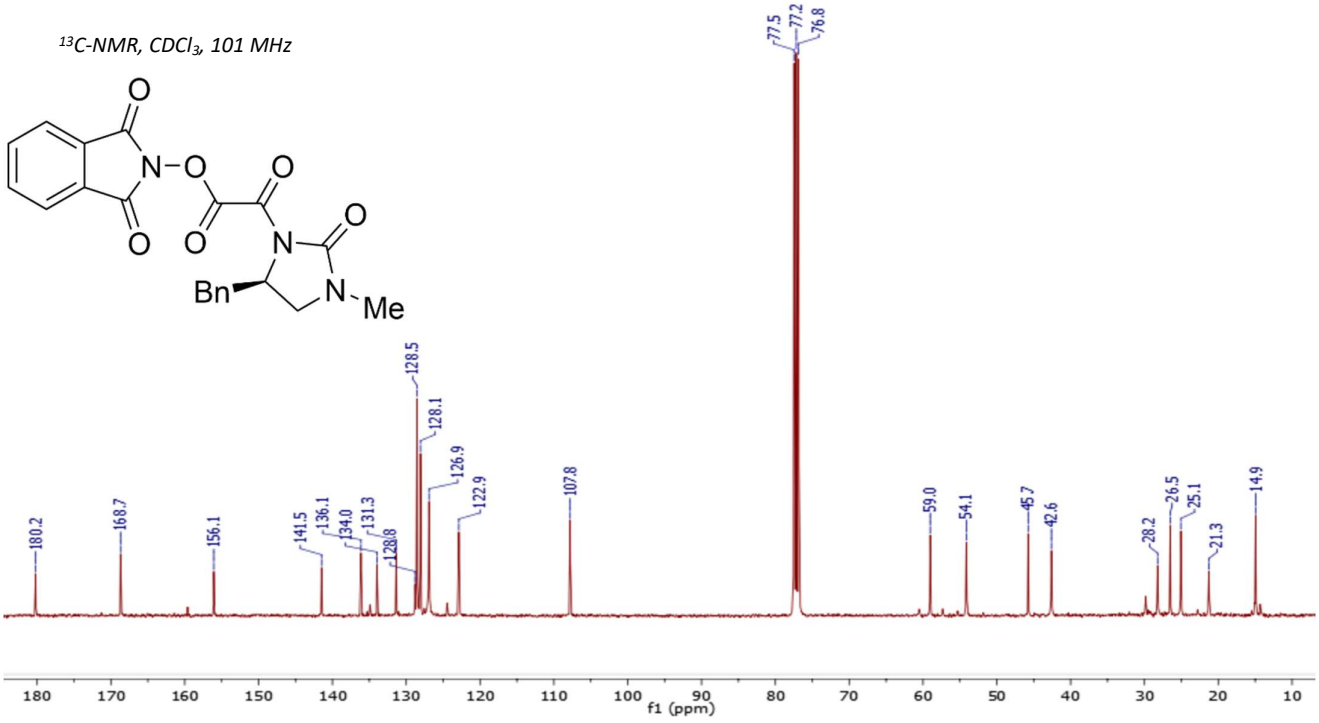

Compound 14:

^{1}H-NMR, MeOD, 300 MHz

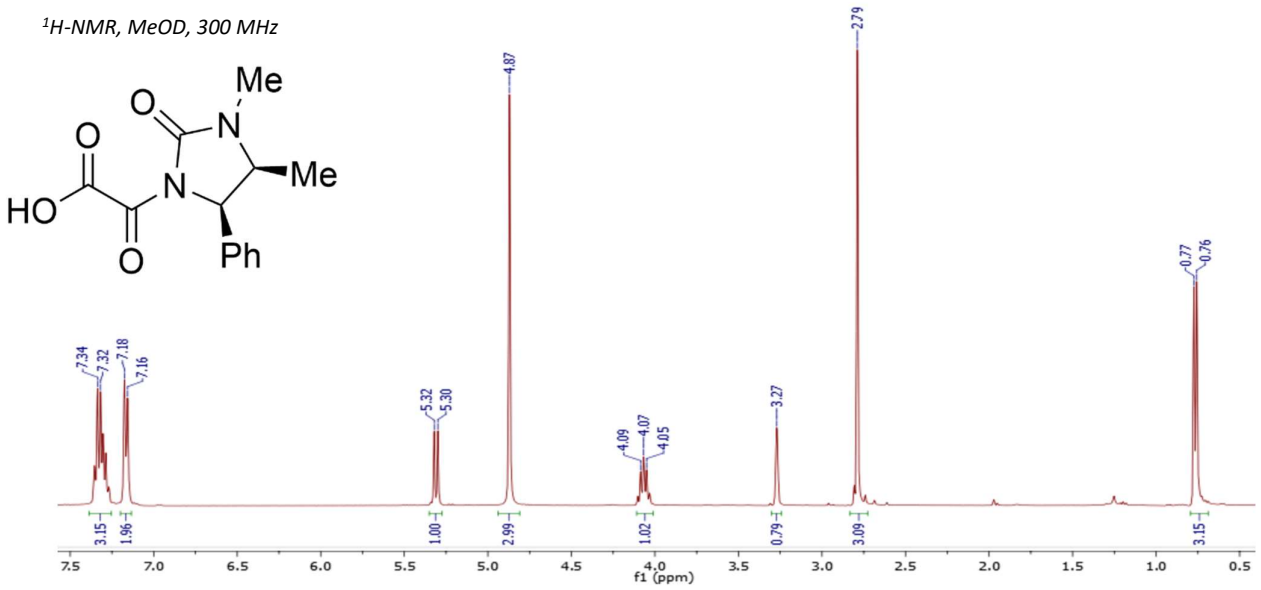

^{13}C-NMR, MeOD, 101 MHz

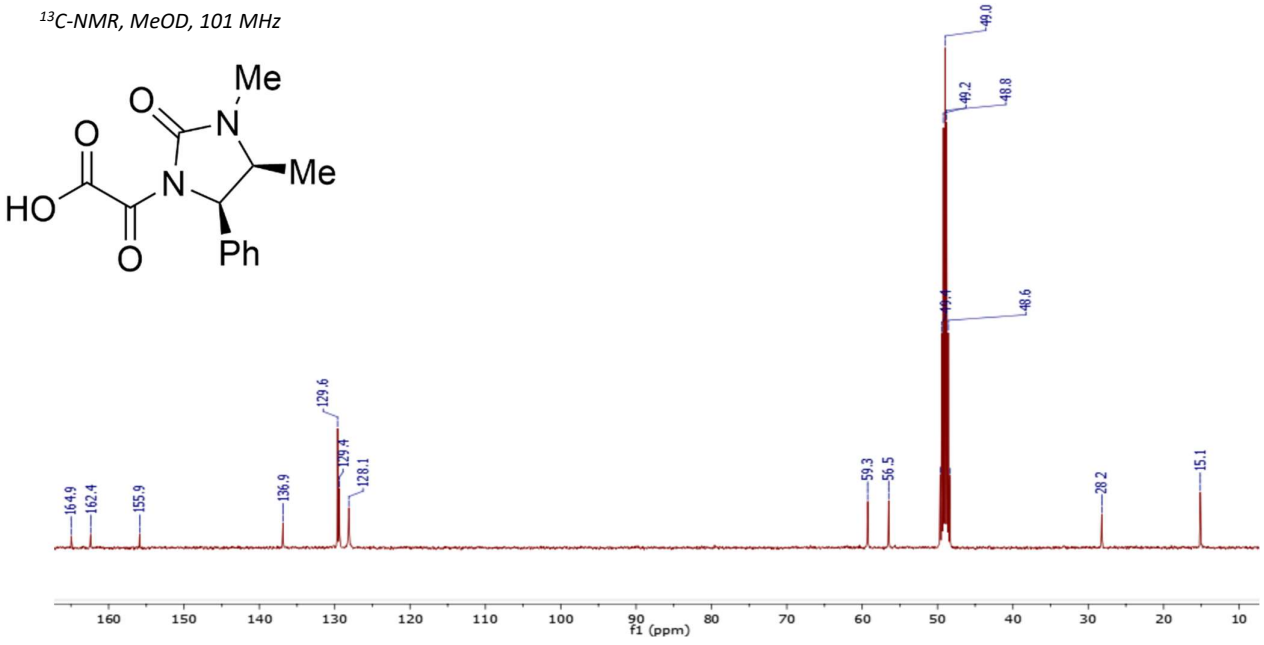

Compound 4a:

^{1}H-NMR, $CDCl_3$, 300 MHz

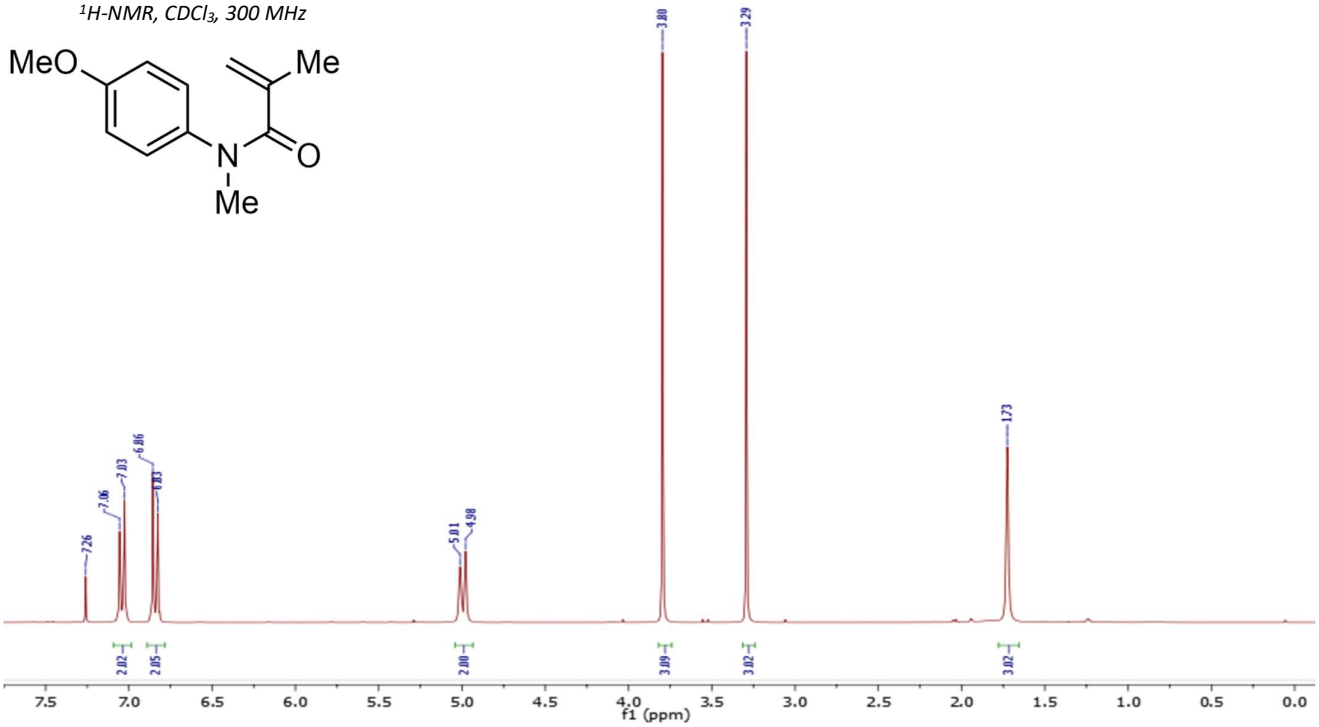

^{13}C-NMR, $CDCl_3$, 101 MHz

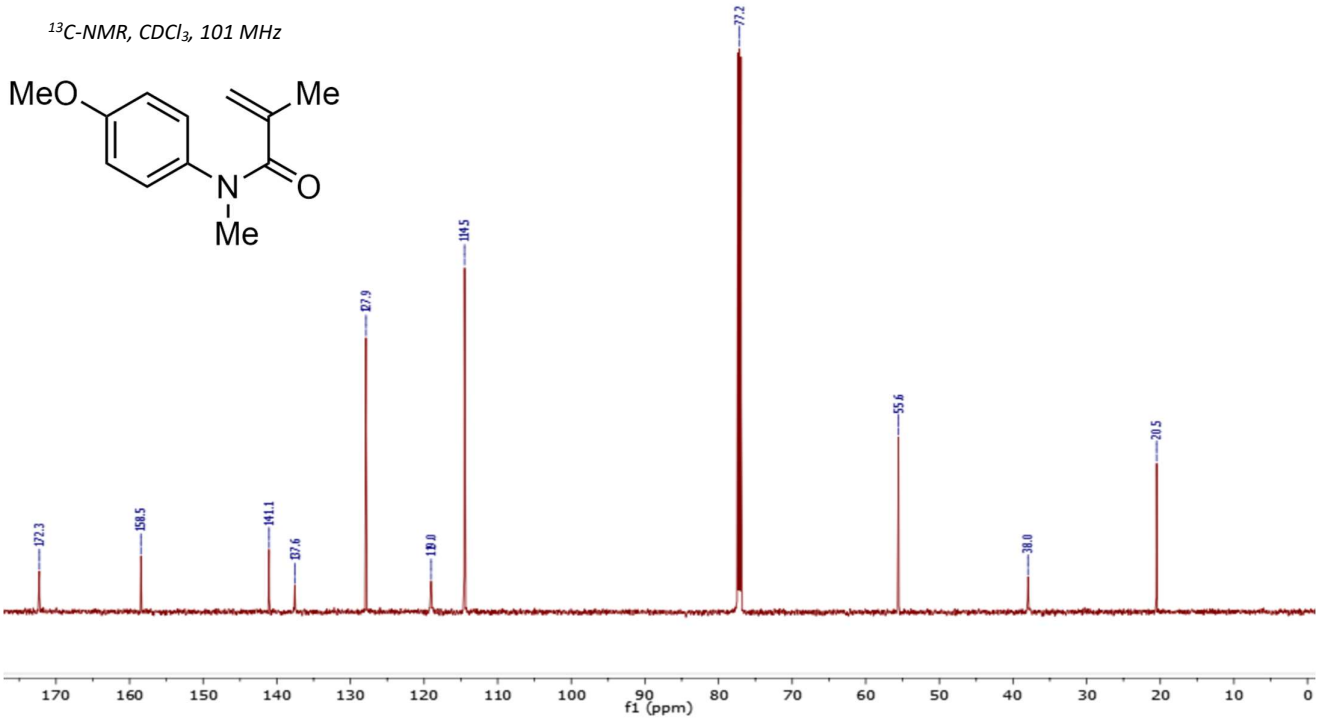

Compound 4b:

^{1}H-NMR, $CDCl_3$, 300 MHz

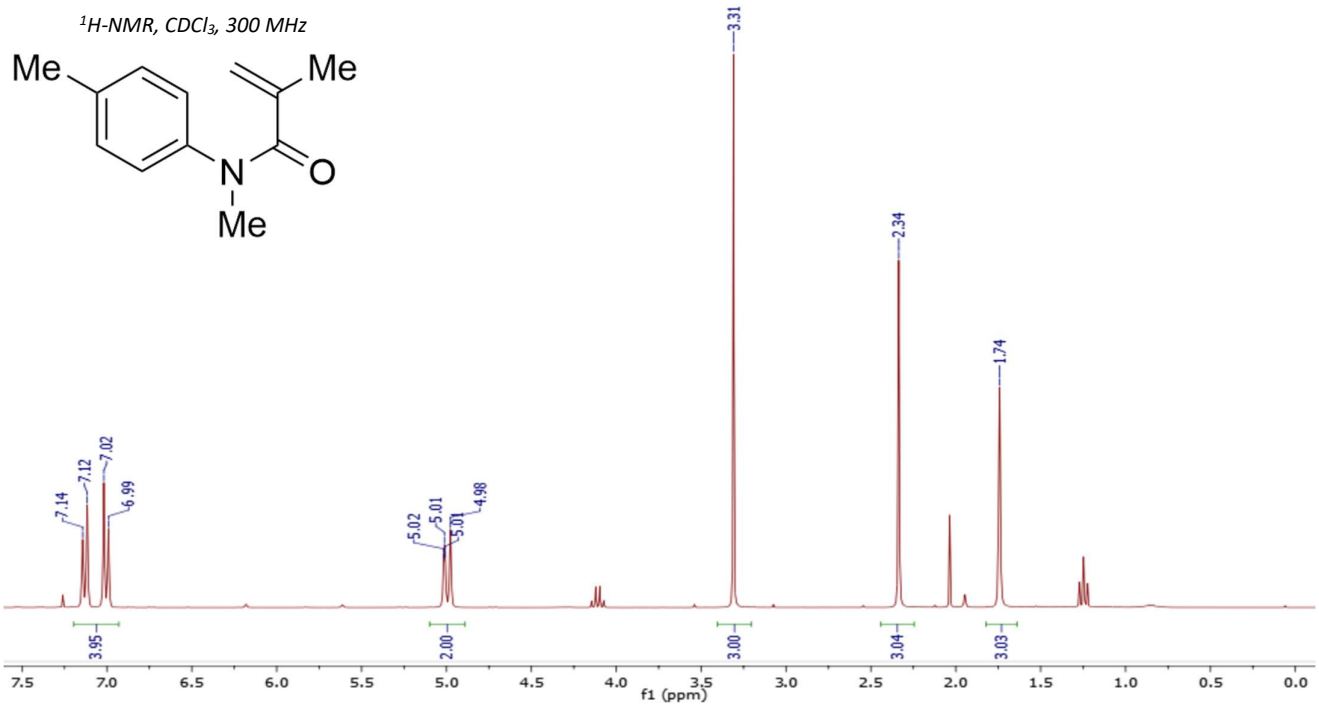

^{13}C-NMR, $CDCl_3$, 101 MHz

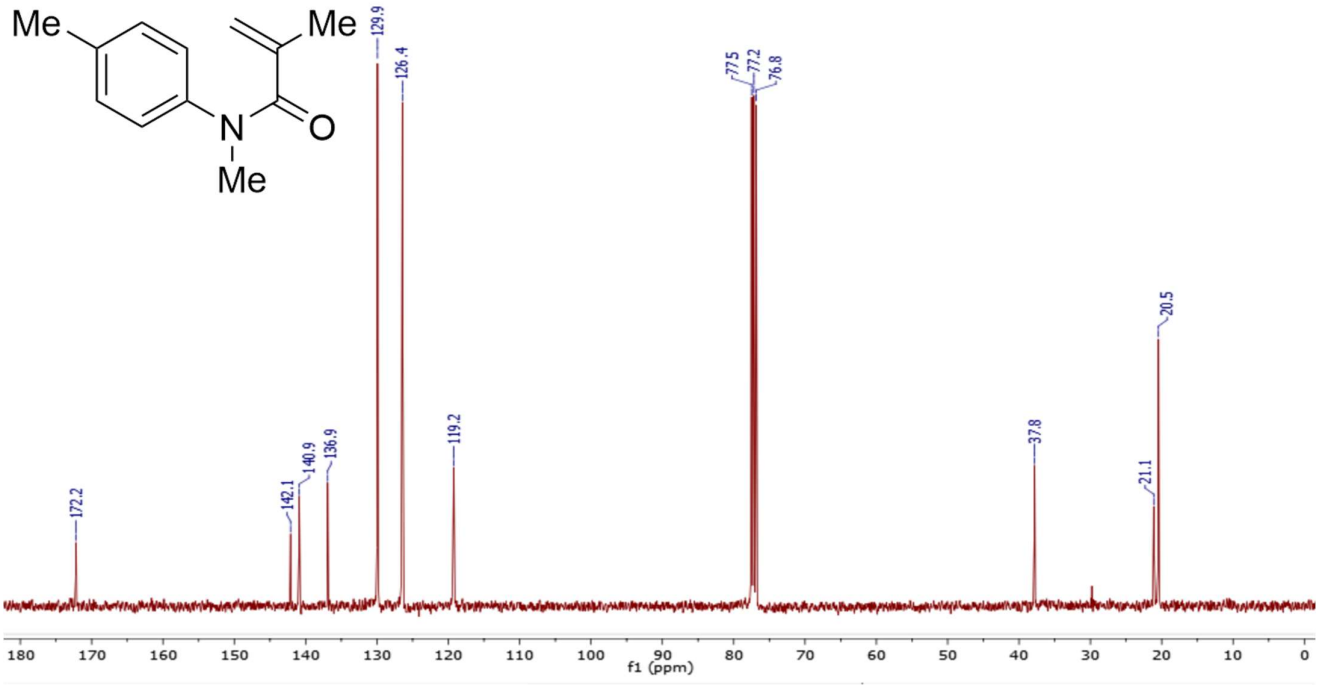

Compound 4c:

^{1}H-NMR, $CDCl_3$, 300 MHz

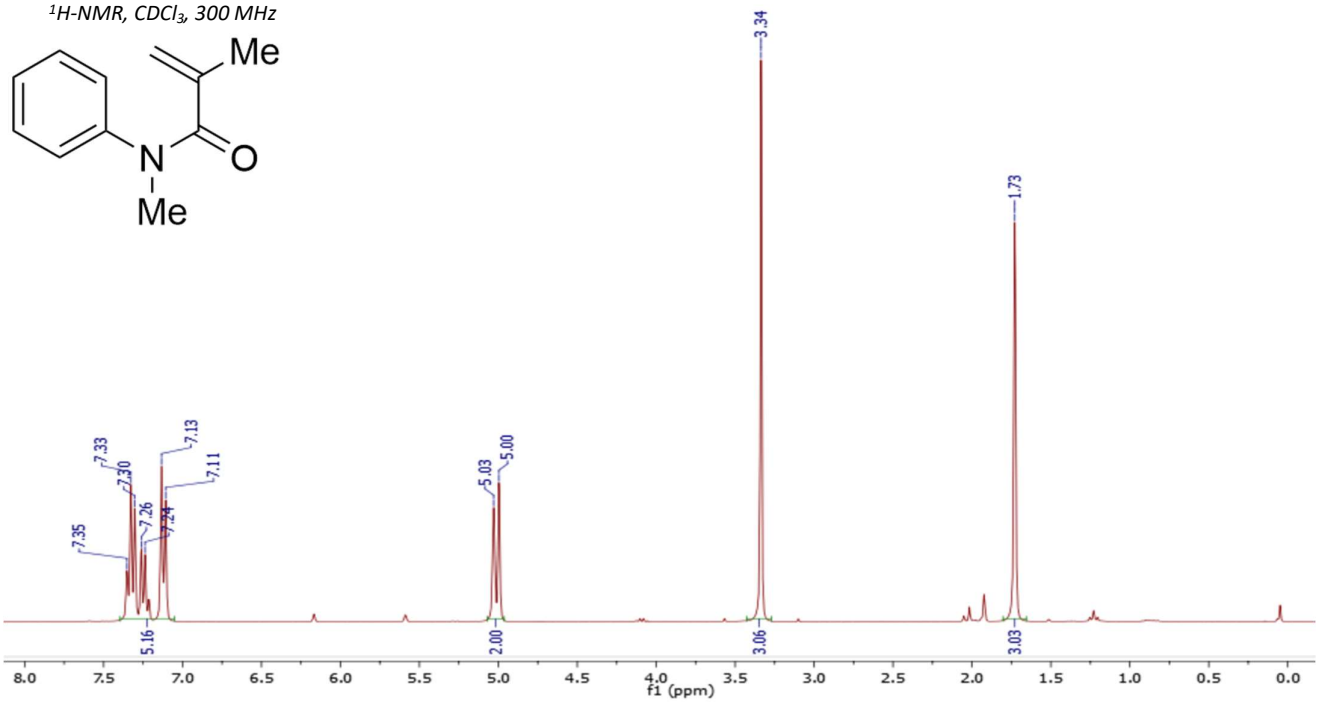

^{13}C-NMR, $CDCl_3$, 101 MHz

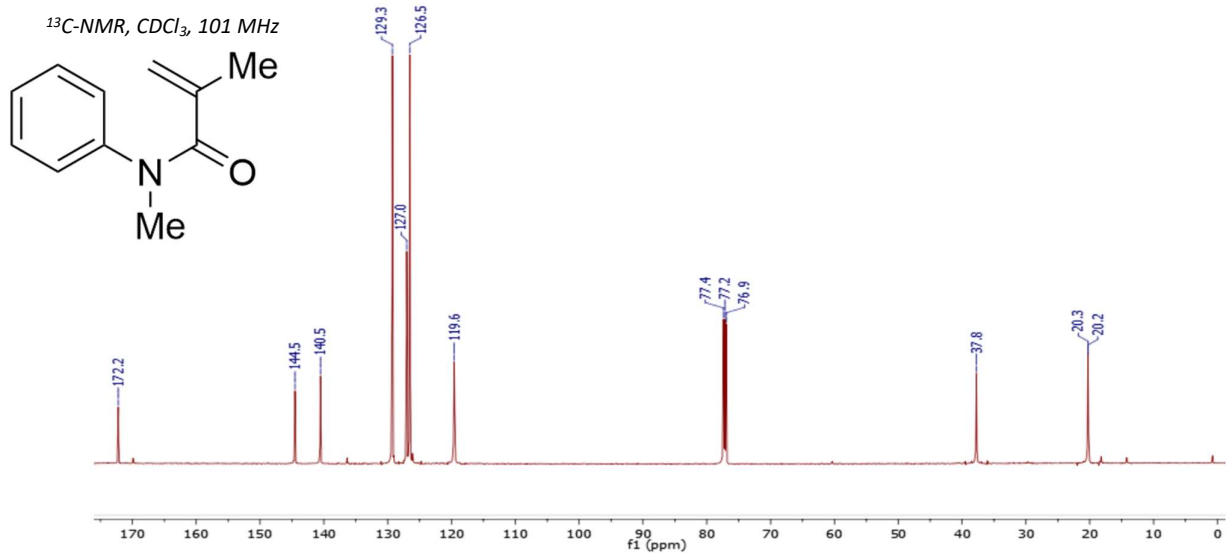

Compound 4d:

^{1}H-NMR, $CDCl_3$, 300 MHz

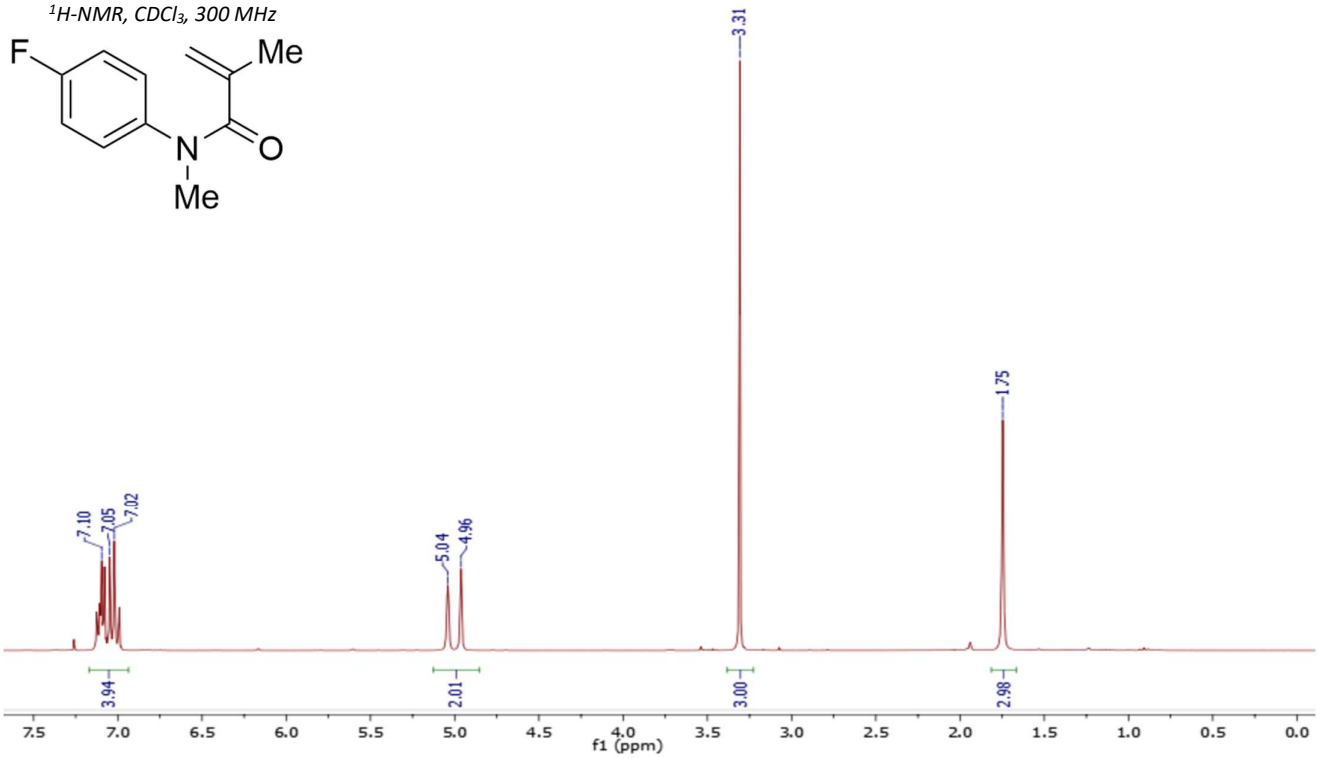

^{13}C-NMR, $CDCl_3$, 101 MHz

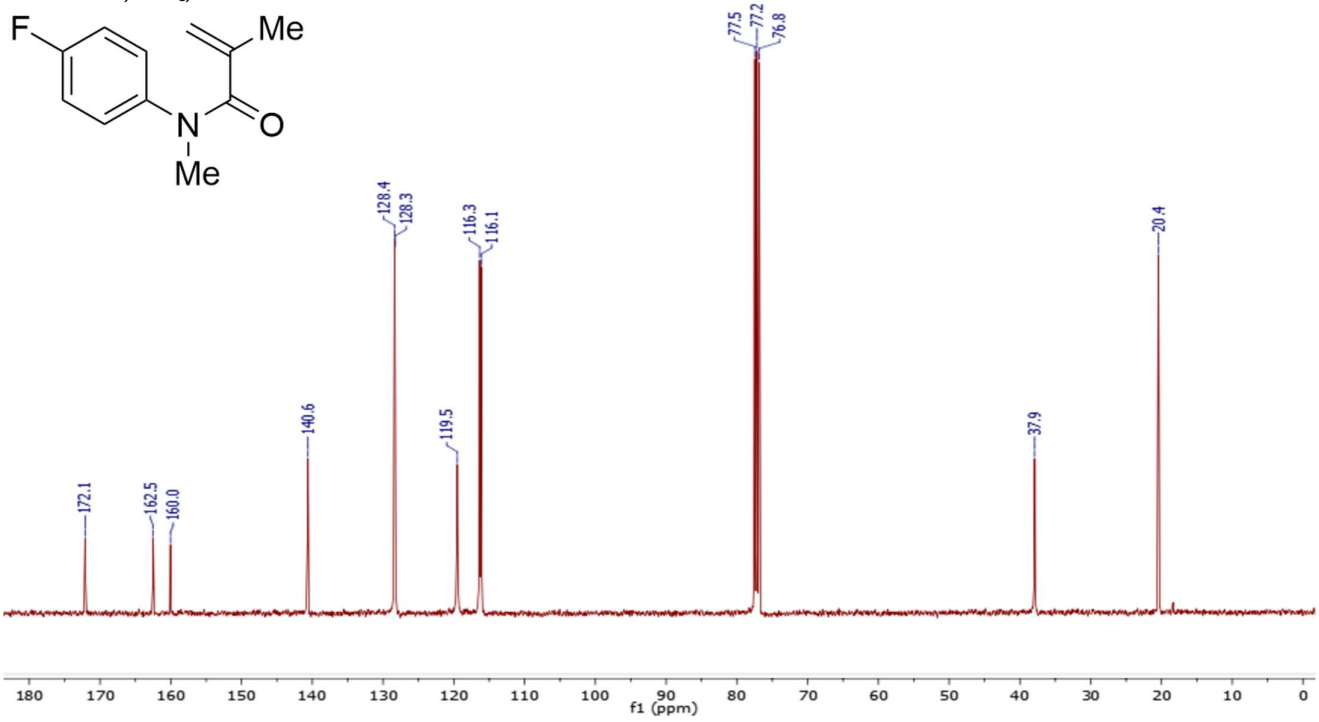

Compound 4e:

^{1}H-NMR, $CDCl_3$, 300 MHz

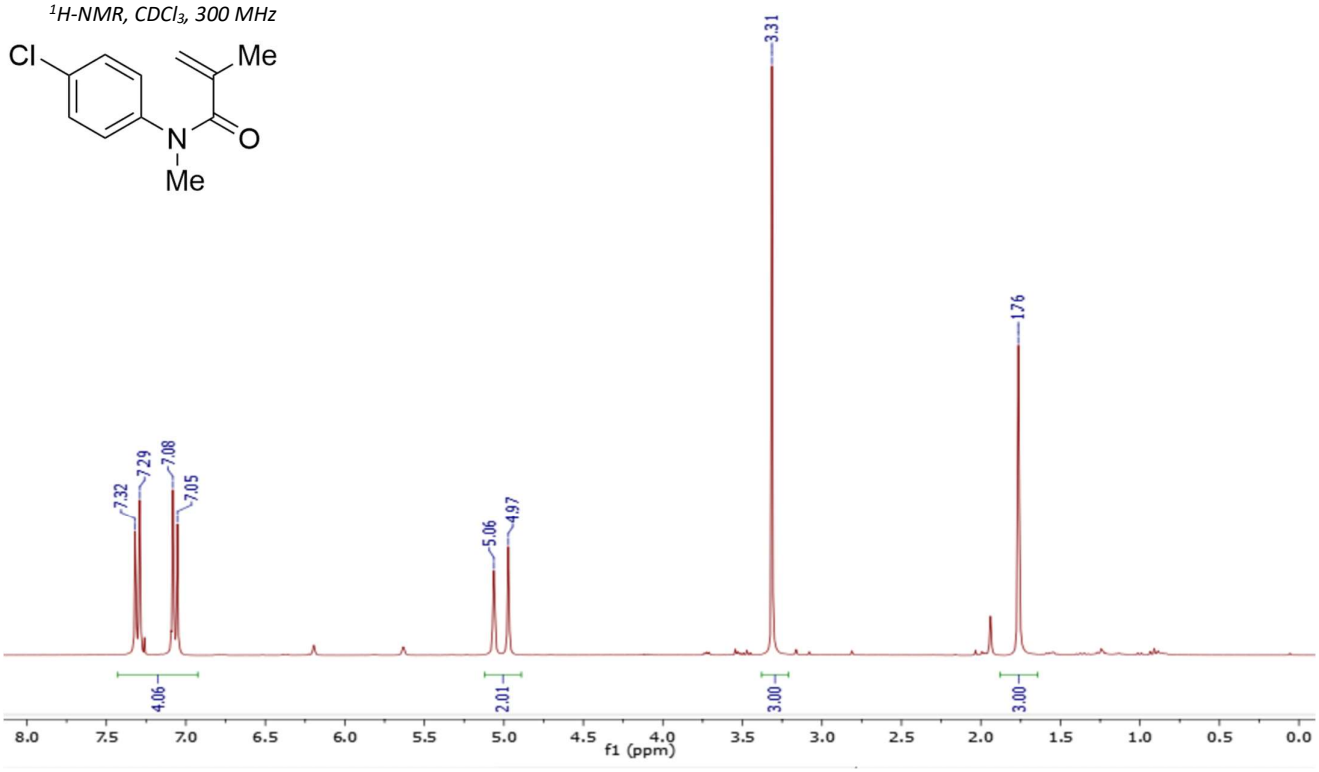

^{13}C-NMR, $CDCl_3$, 101 MHz

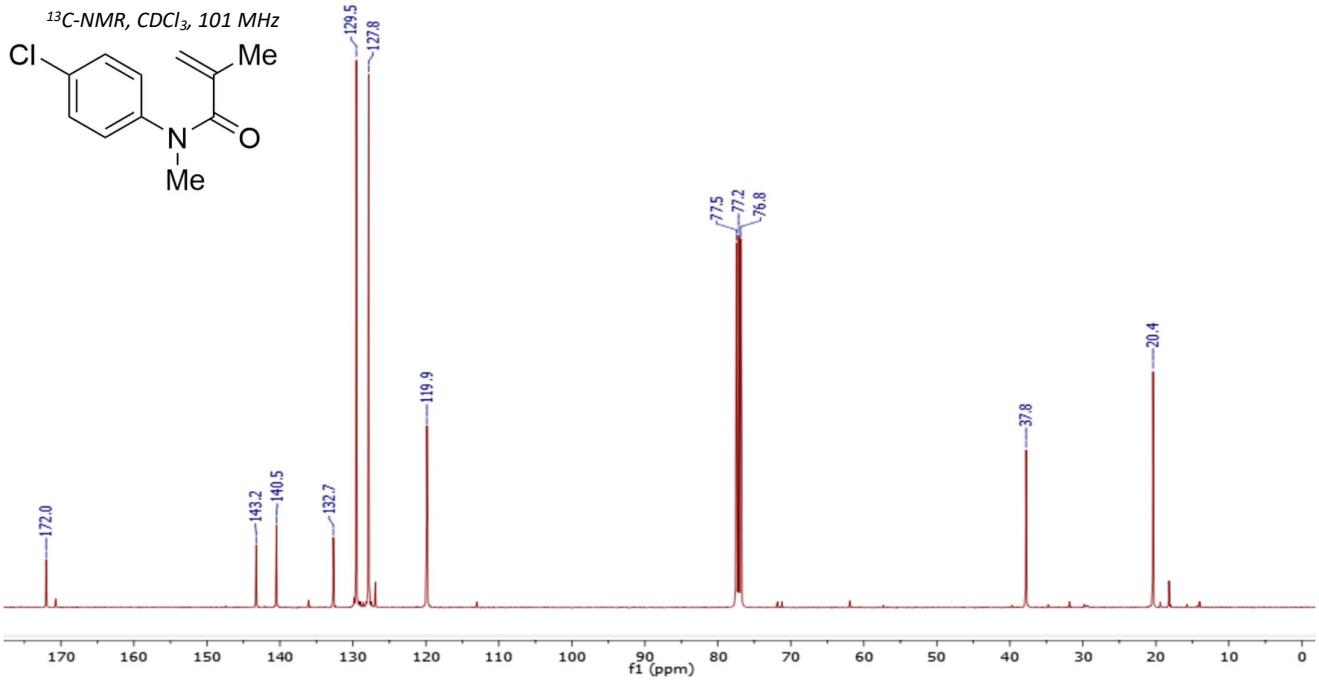

Compound 4f:

^{1}H-NMR, $CDCl_3$, 300 MHz

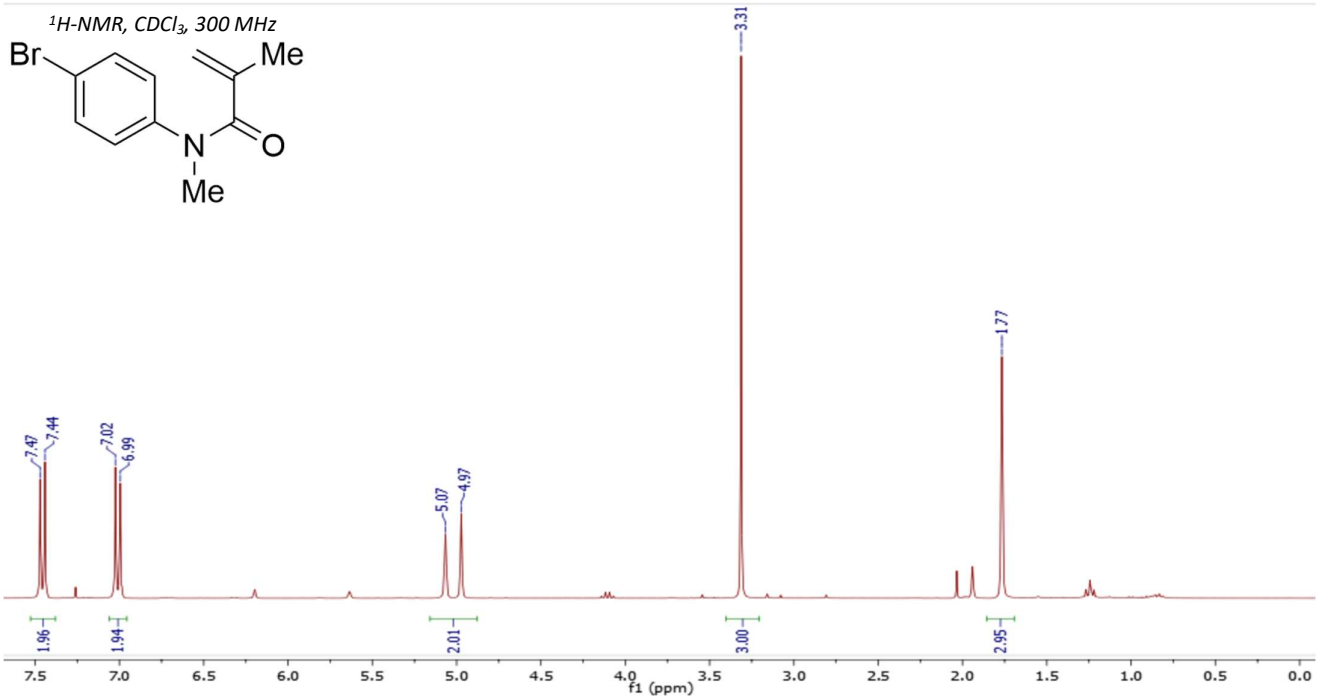

^{13}C-NMR, $CDCl_3$, 101 MHz

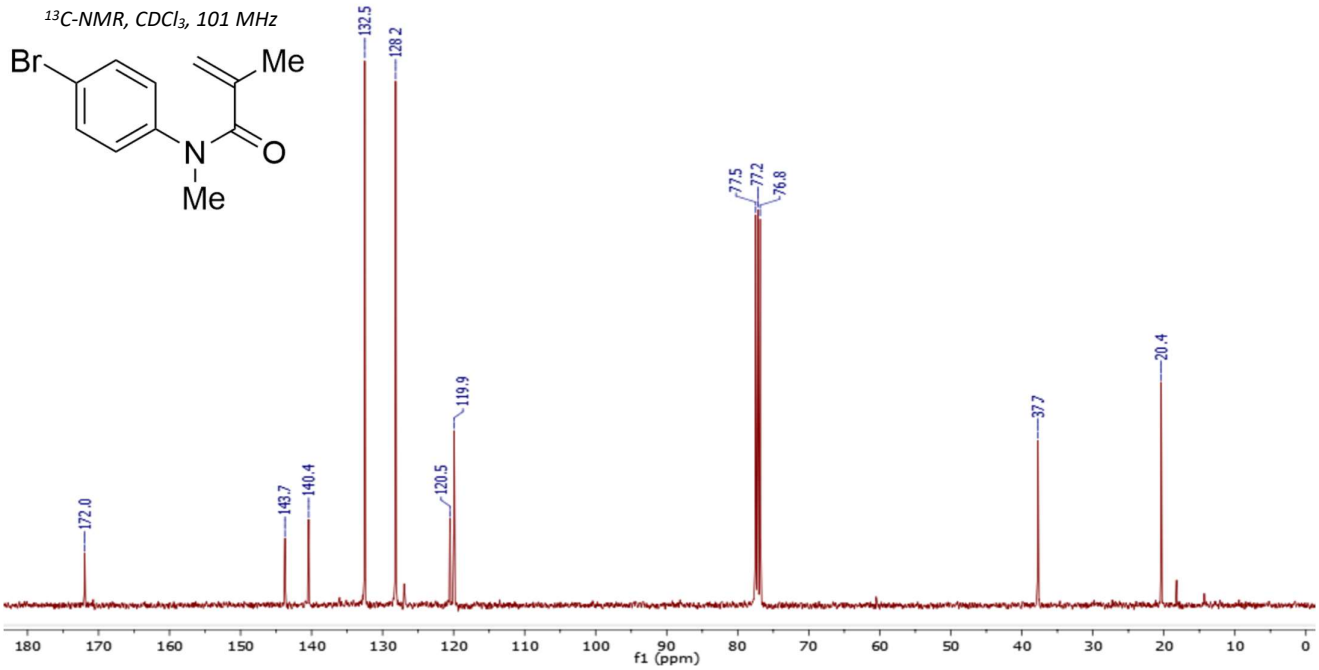

Compound 4g:

^{1}H-NMR, $CDCl_3$, 300 MHz

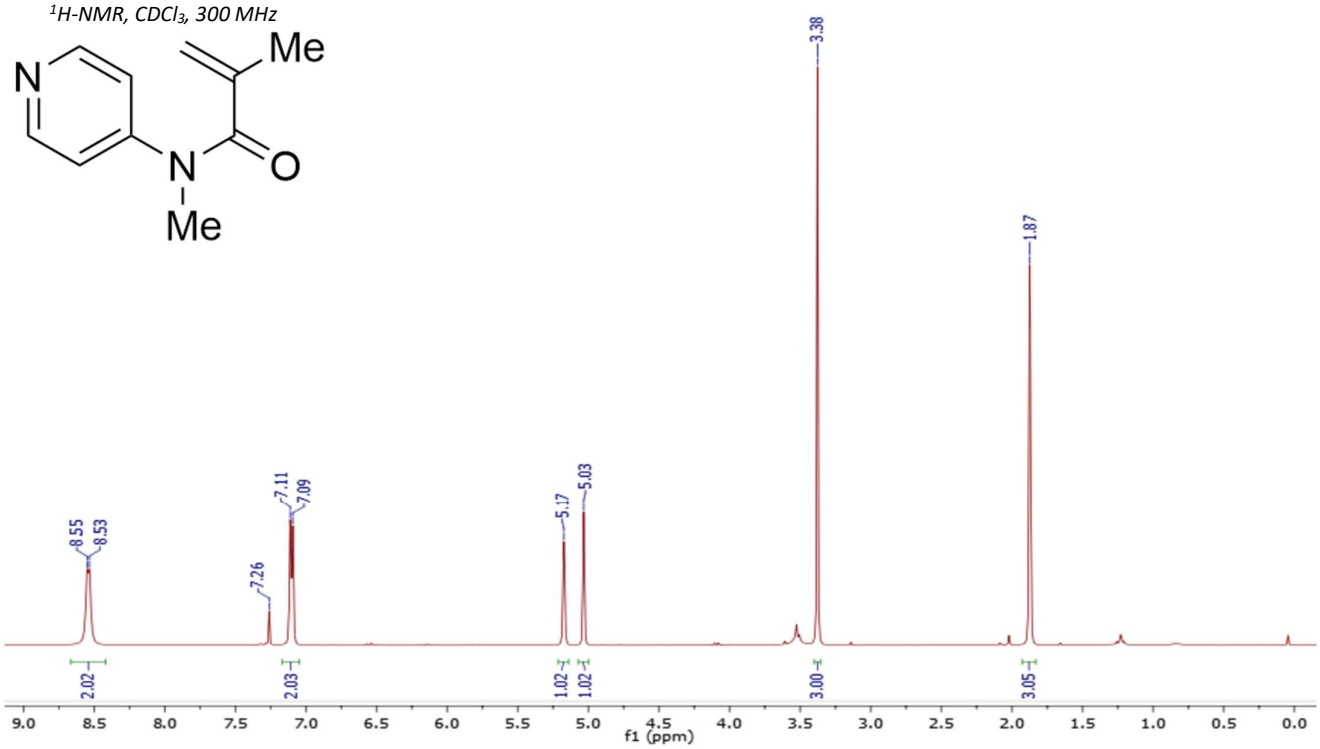

^{13}C-NMR, $CDCl_3$, 101 MHz

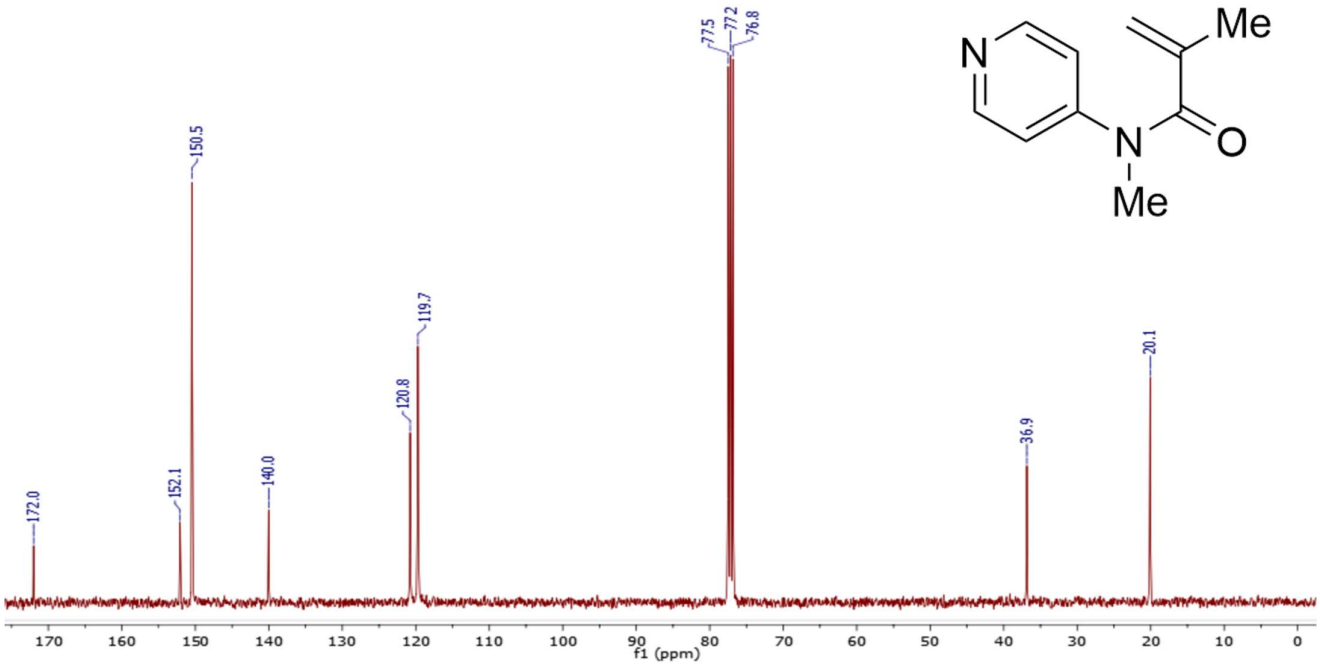

Compound 5a-D1:

^{1}H-NMR, $CDCl_3$, 300 MHz

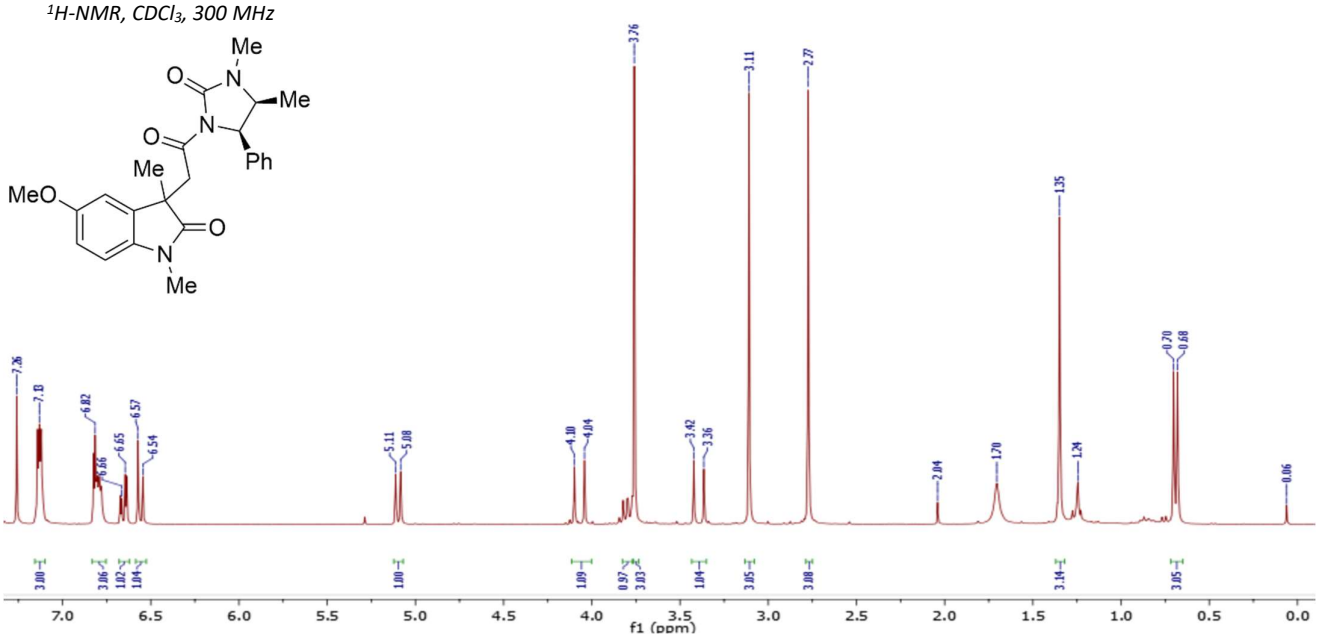

^{13}C-NMR, $CDCl_3$, 101 MHz

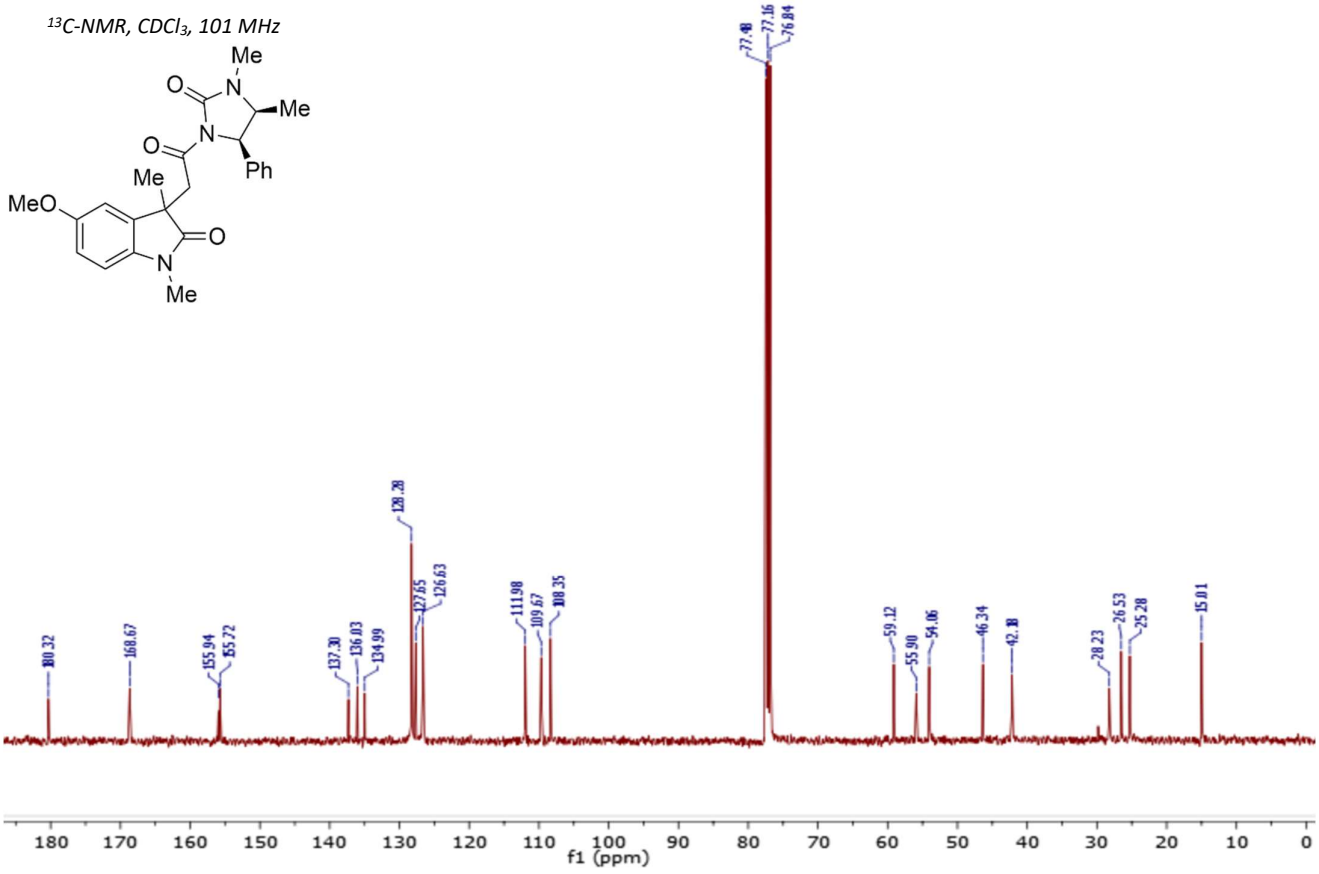

Compound 5a–D2:

^{1}H-NMR, $CDCl_3$, 300 MHz

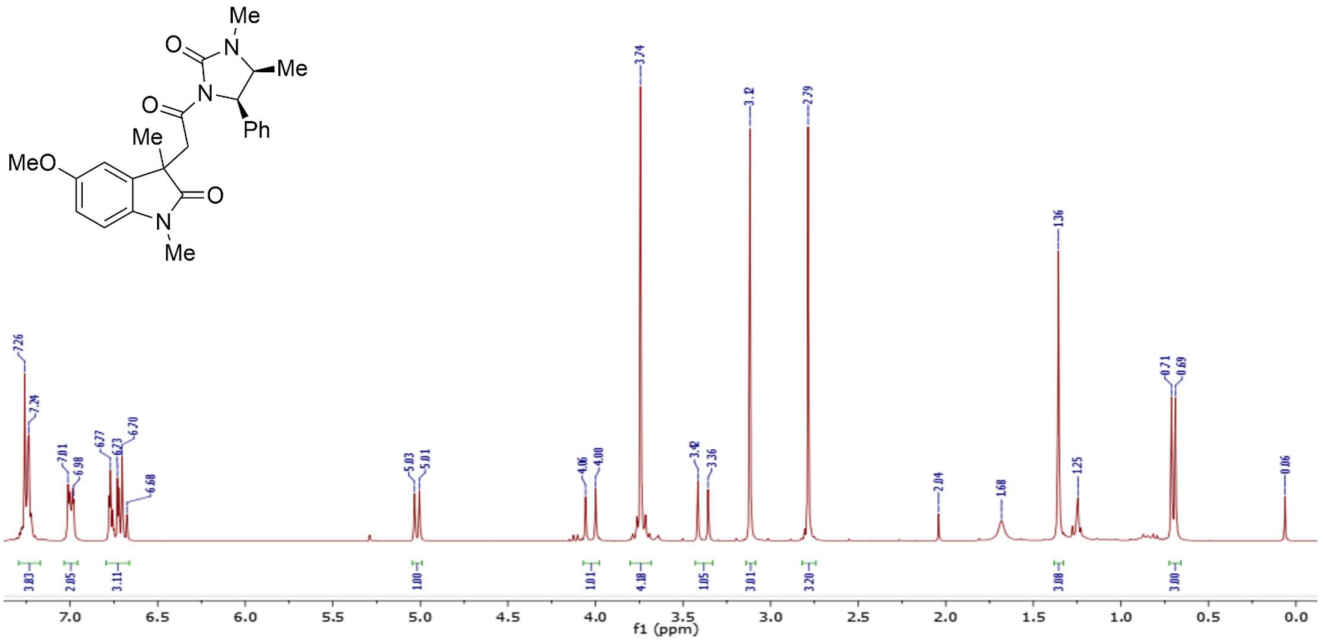

^{13}C-NMR, $CDCl_3$, 101 MHz

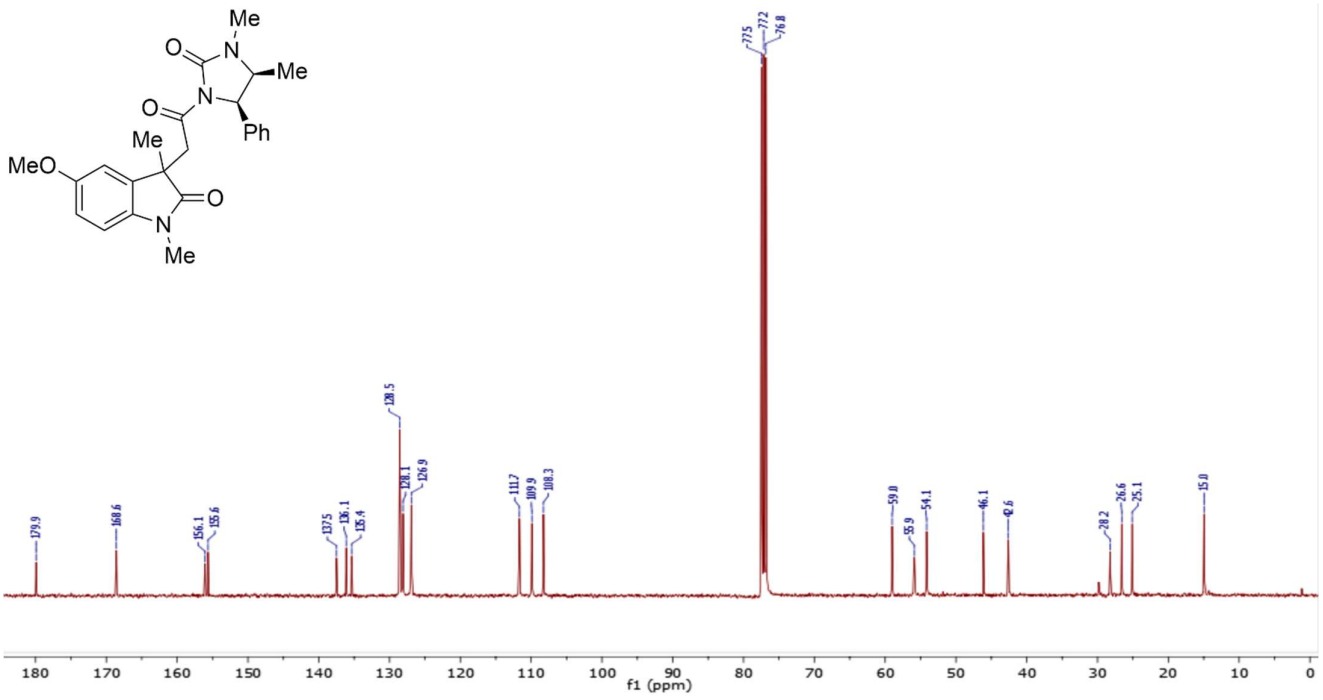

Compound 5b-D1:

^{1}H-NMR, $CDCl_3$, 300 MHz

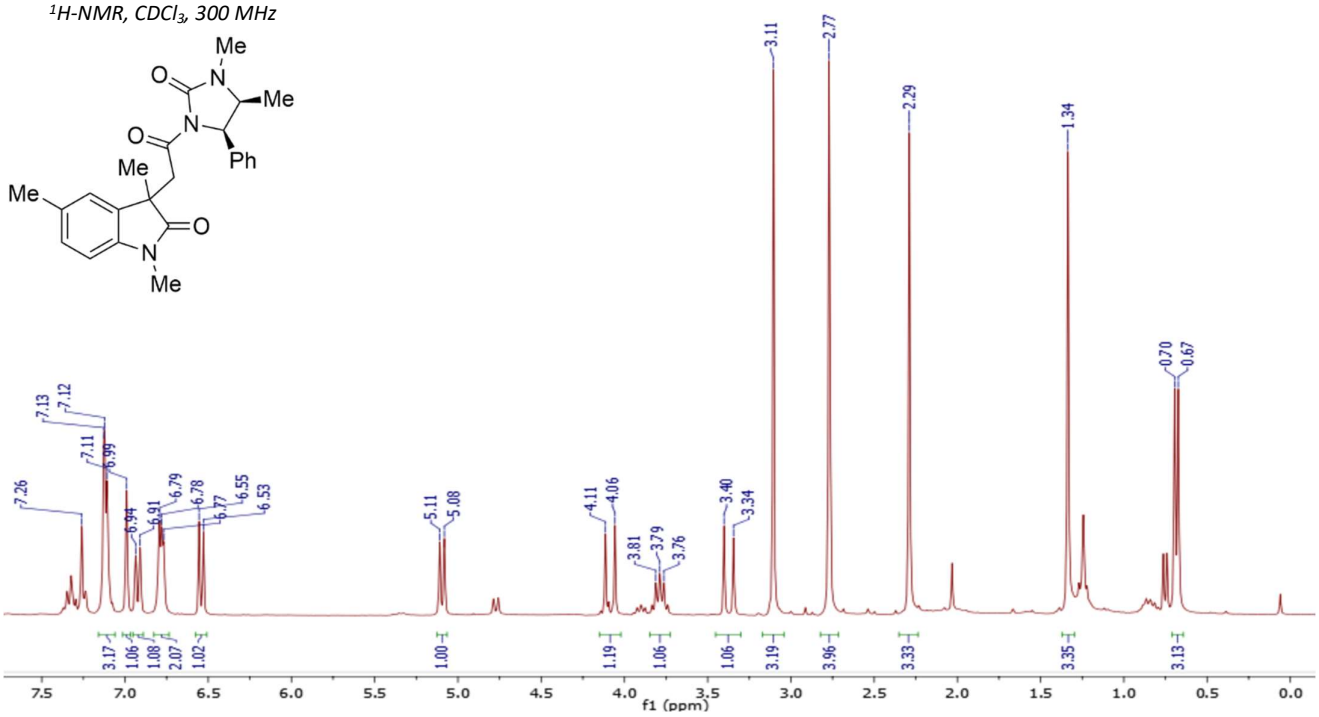

^{13}C-NMR, $CDCl_3$, 101 MHz

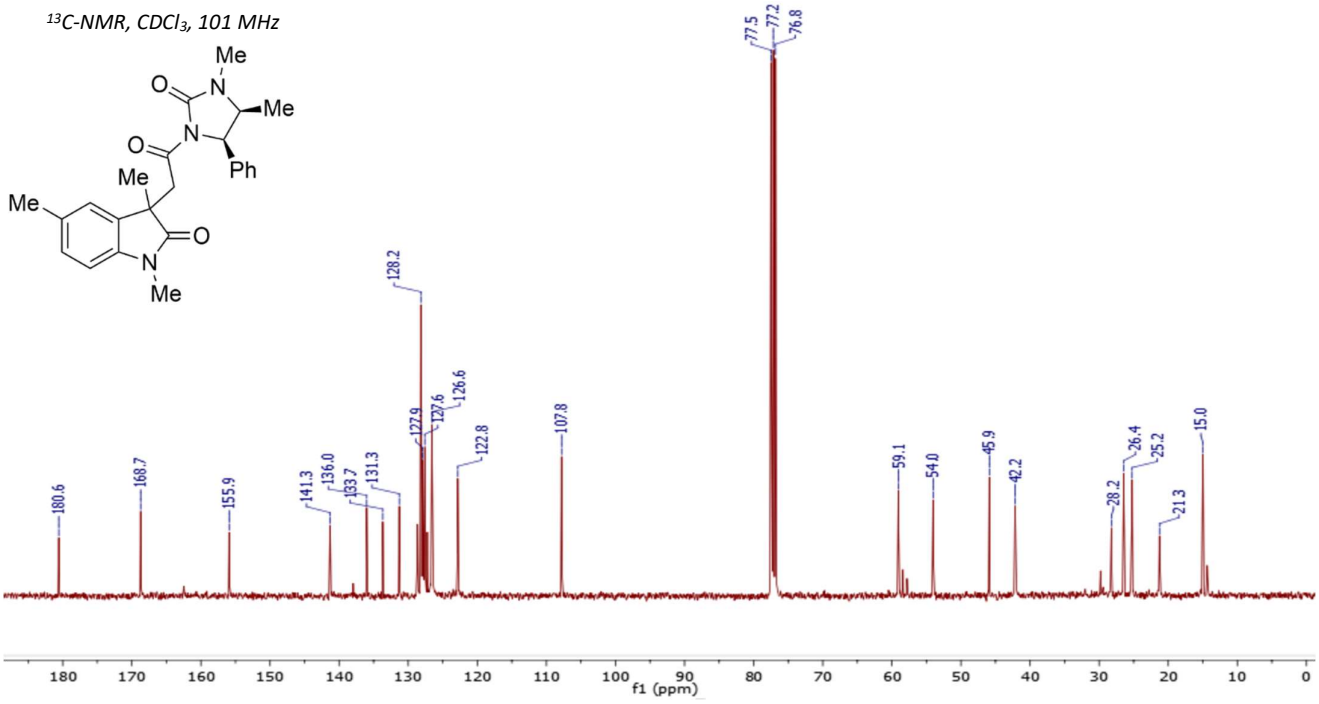

Compound 5b-D2:

^{1}H-NMR, $CDCl_3$, 300 MHz

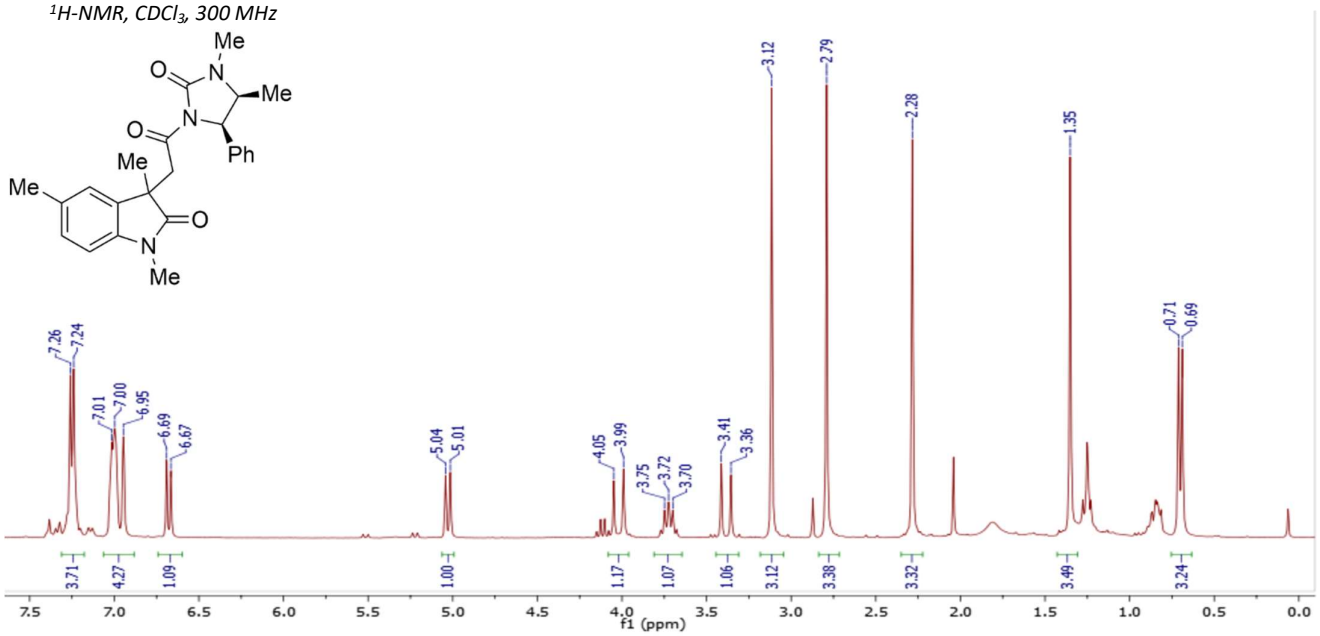

^{13}C-NMR, $CDCl_3$, 101 MHz

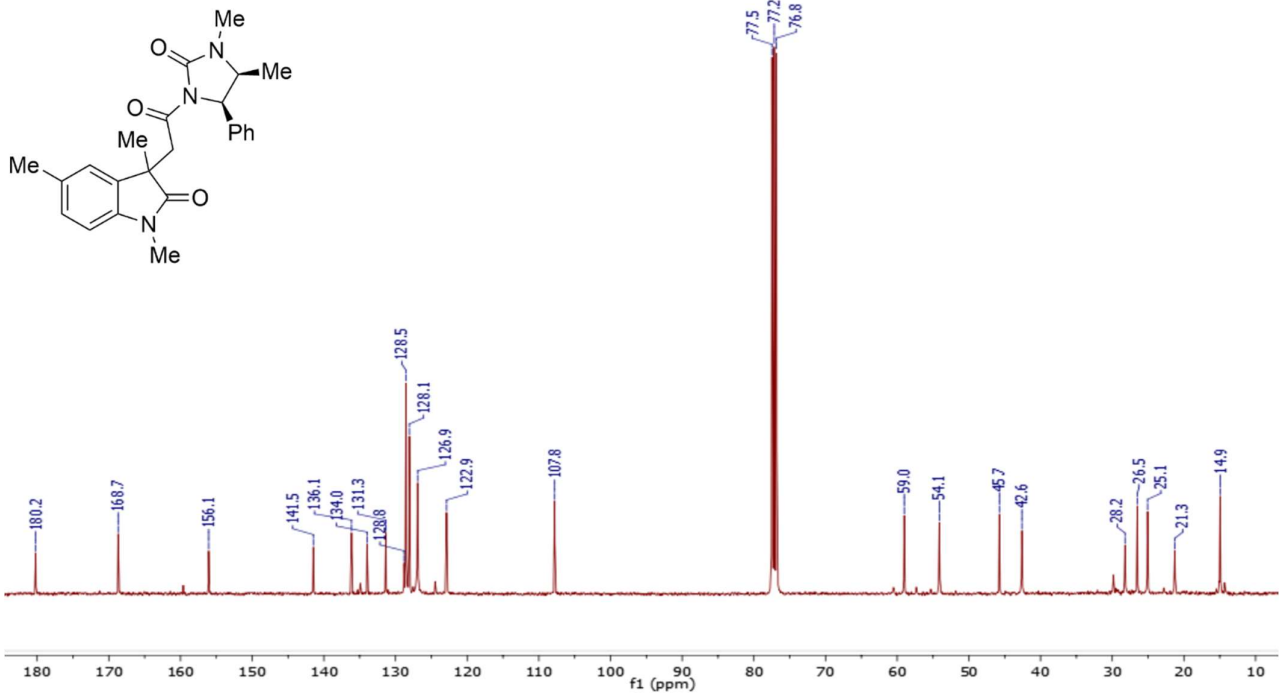

Compound 5c-D1:

^{1}H-NMR, $CDCl_3$, 300 MHz

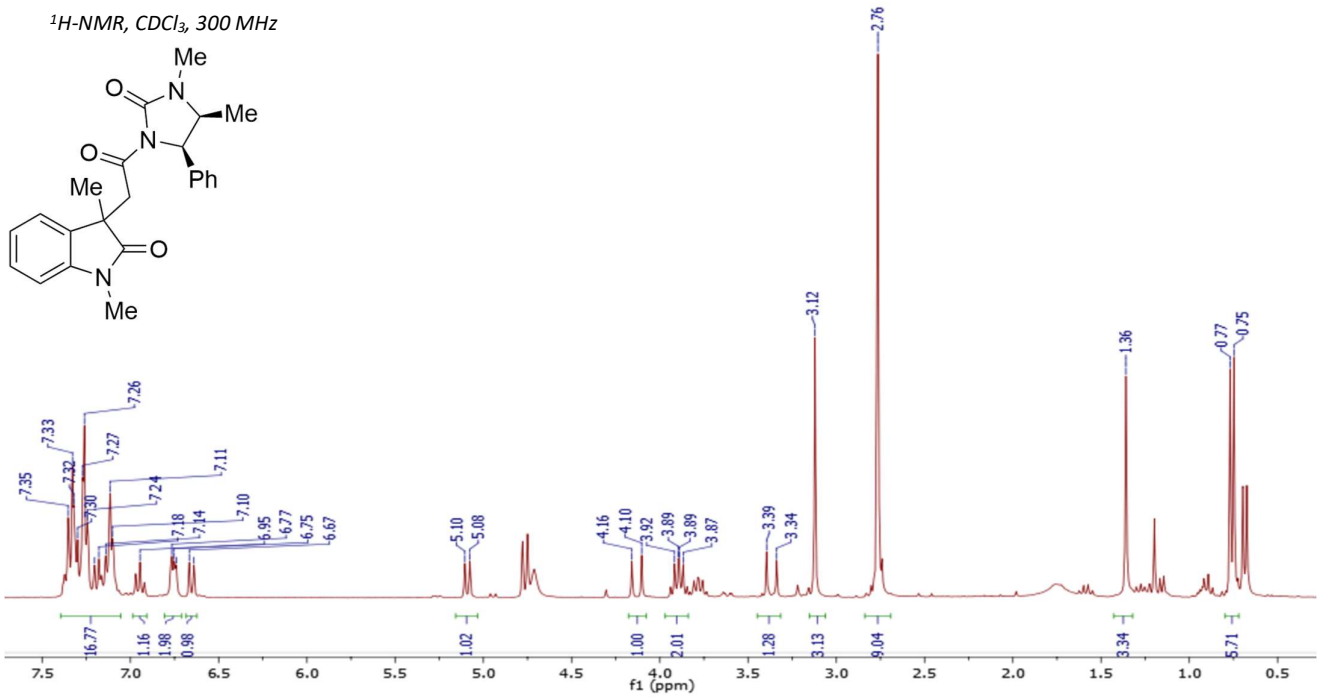

^{13}C-NMR, $CDCl_3$, 101 MHz

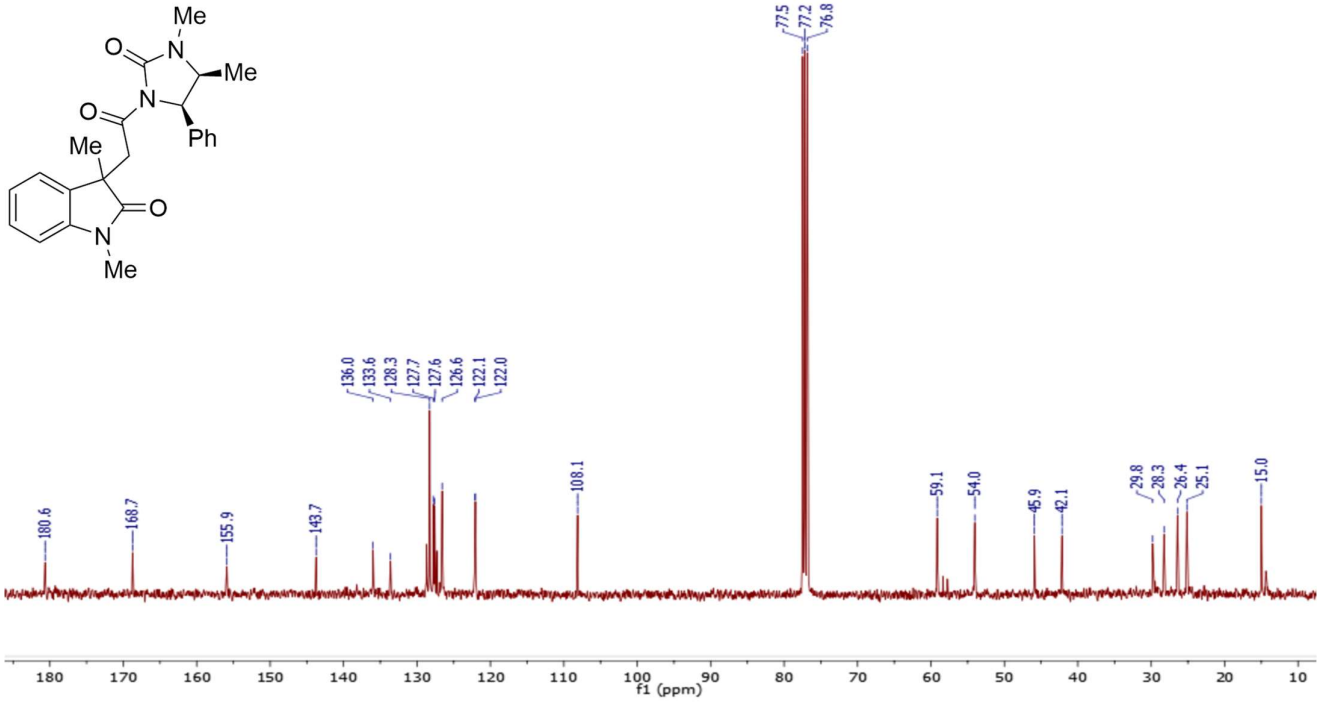

Compound 5c-D2:

^{1}H-NMR, $CDCl_3$, 300 MHz

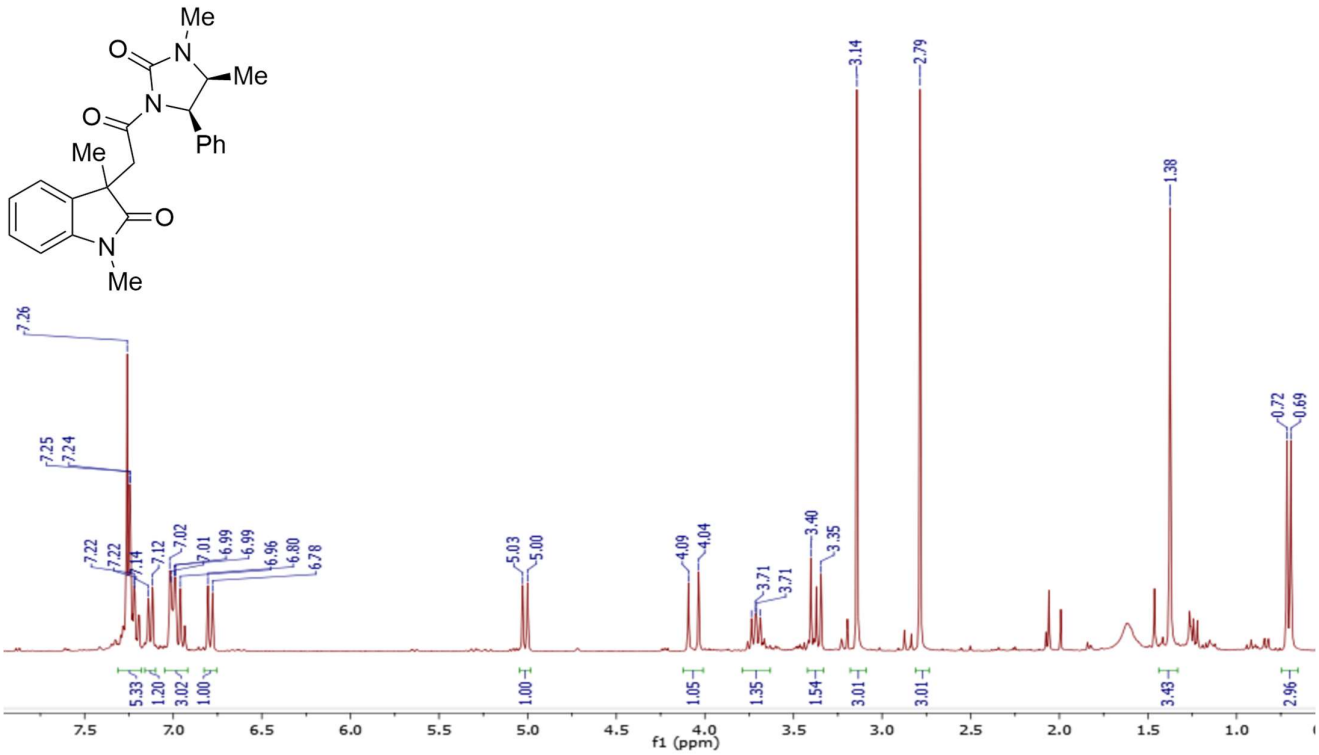

^{13}C-NMR, $CDCl_3$, 101 MHz

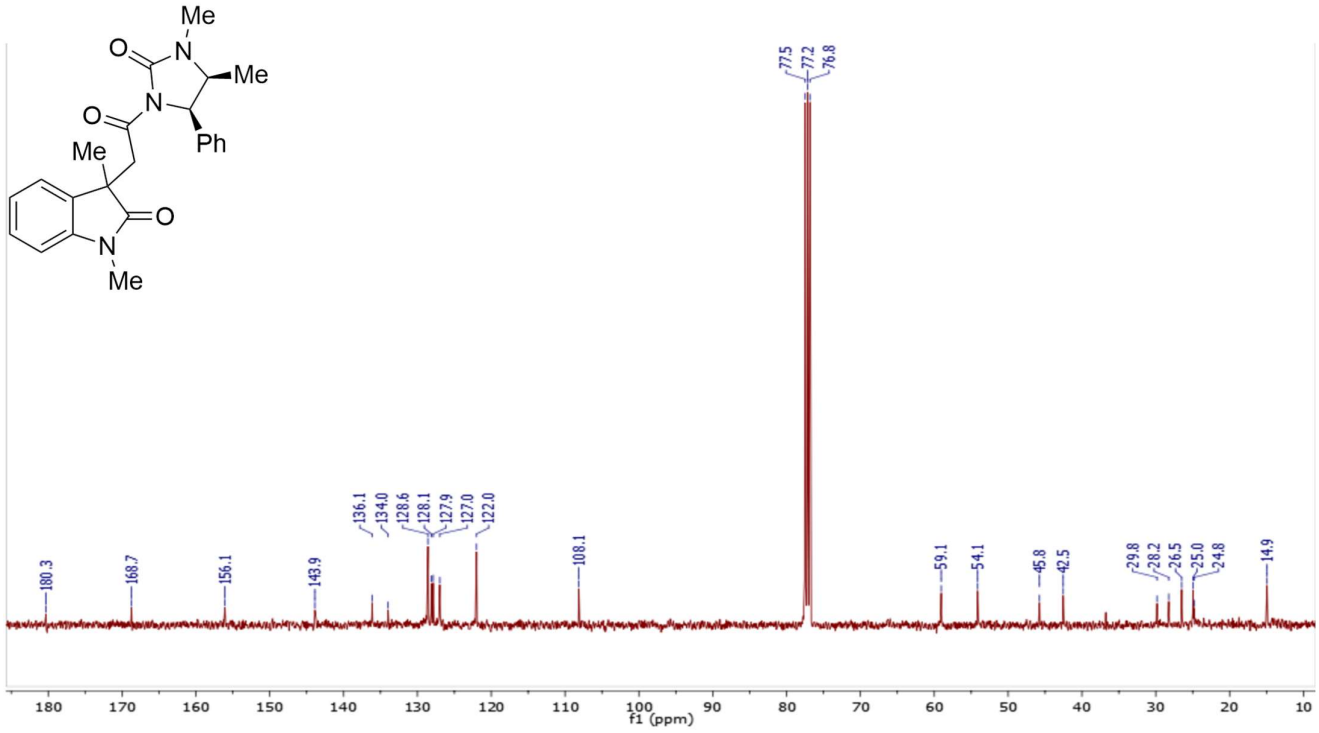

Compound 5d-D1:

^{1}H-NMR, $CDCl_3$, 300 MHz

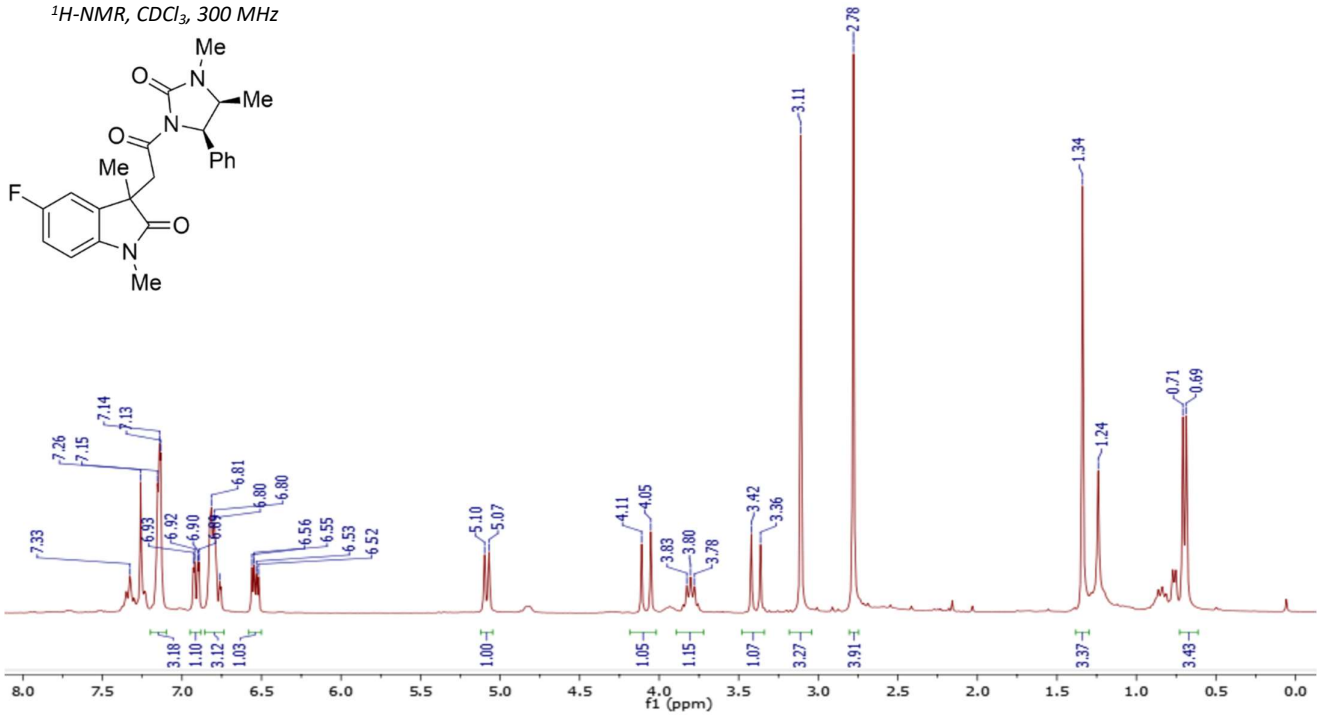

^{13}C-NMR, $CDCl_3$, 101 MHz

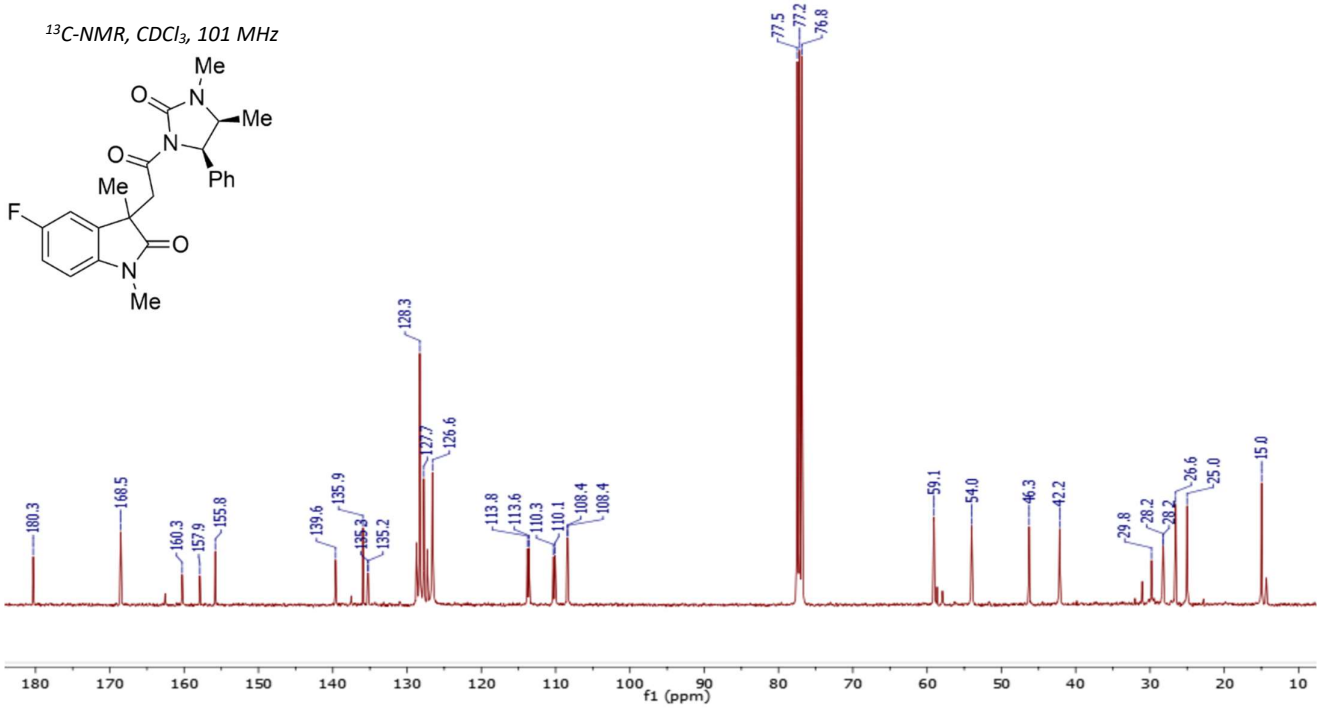

Compound 5d-D2:

^{1}H-NMR, $CDCl_3$, 300 MHz

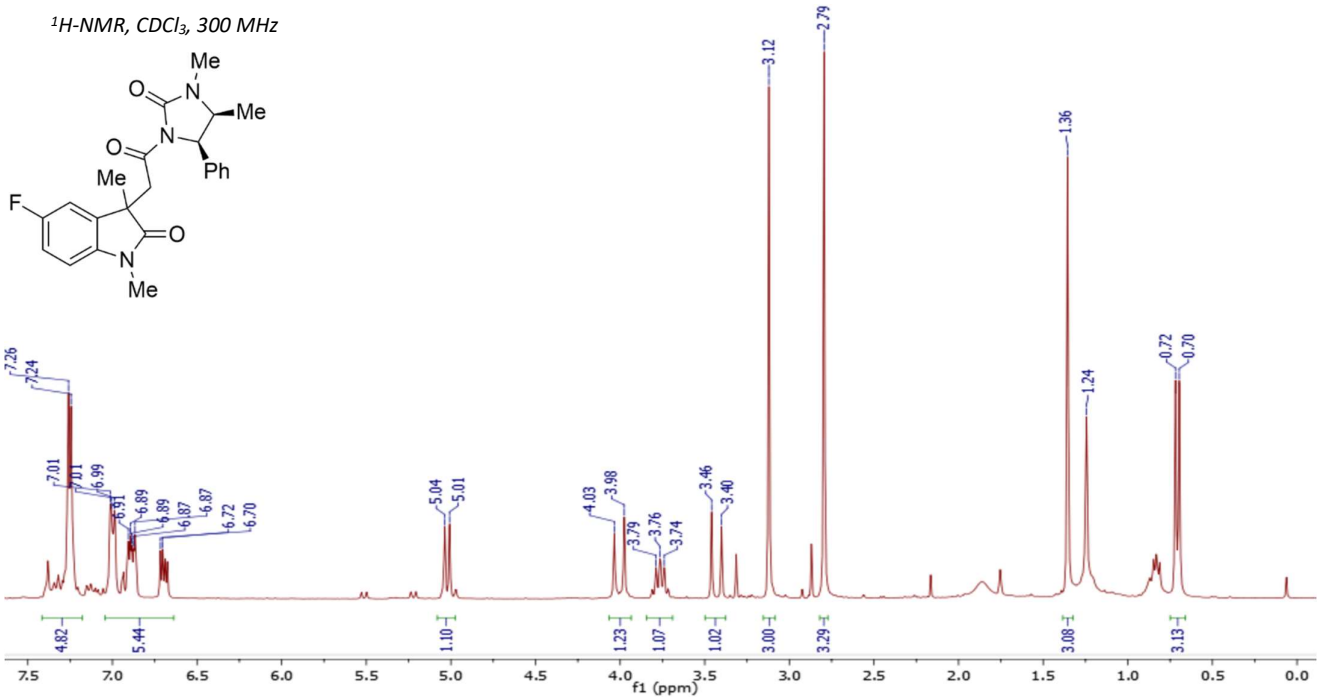

^{13}C-NMR, $CDCl_3$, 101 MHz

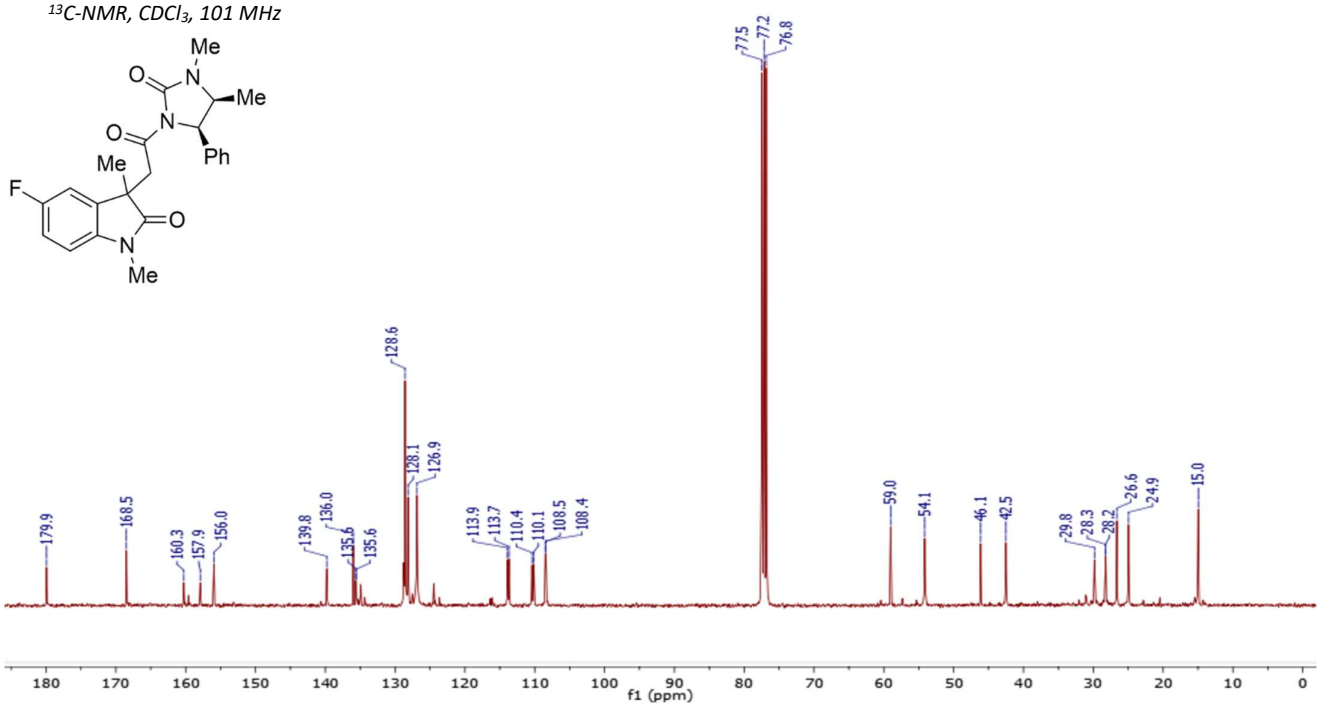

Compound 5e-D1:

^{1}H-NMR, $CDCl_3$, 300 MHz

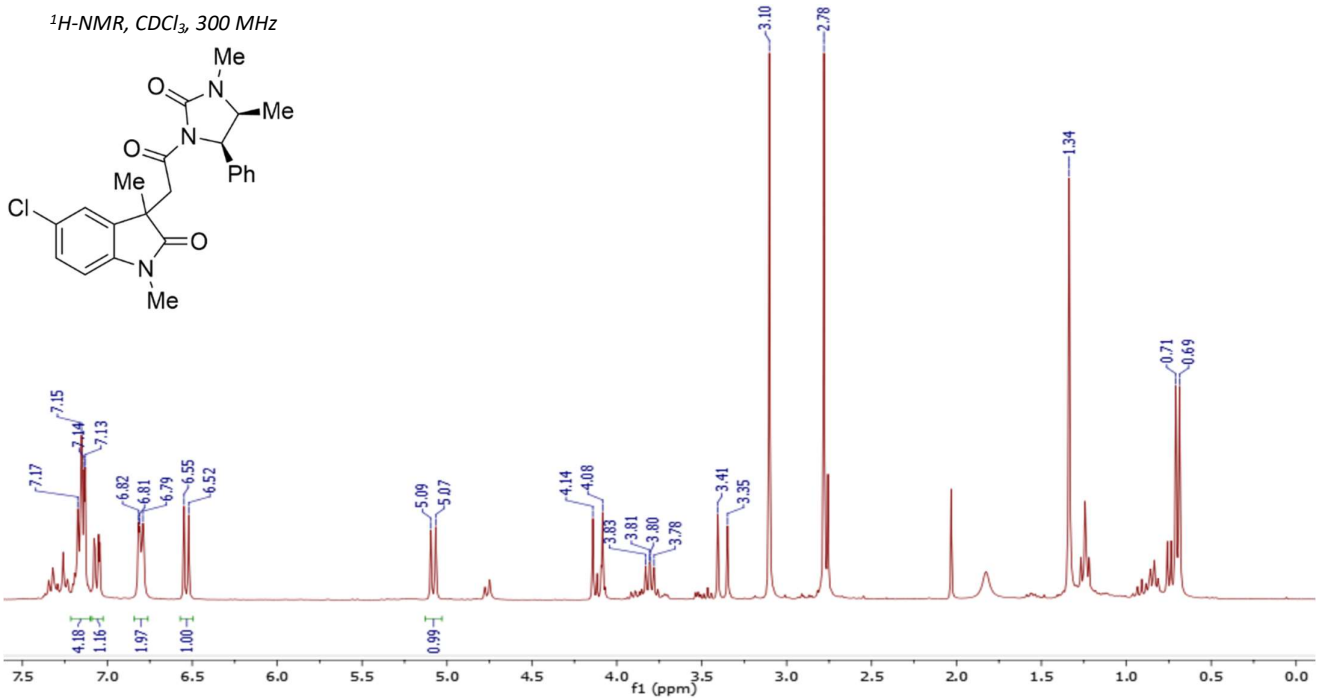

^{13}C-NMR, $CDCl_3$, 101 MHz

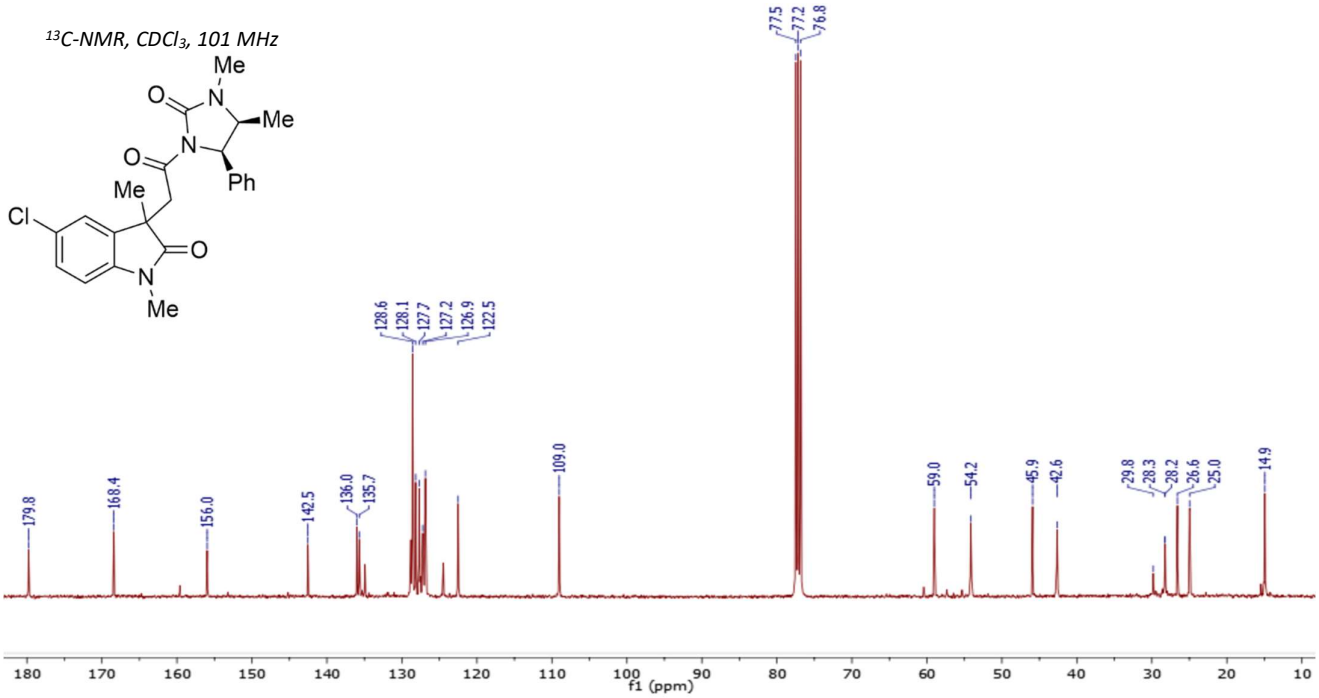

Compound 5e-D2:

^{1}H-NMR, $CDCl_3$, 300 MHz

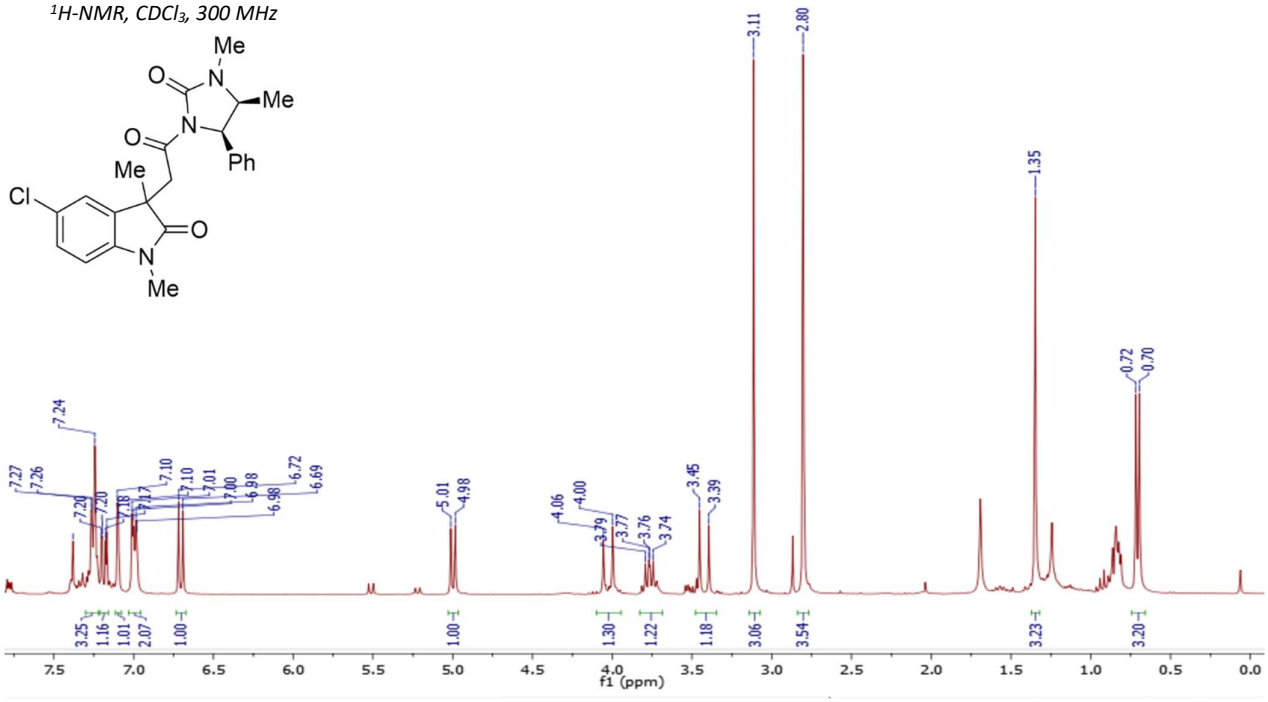

^{13}C-NMR, $CDCl_3$, 101 MHz

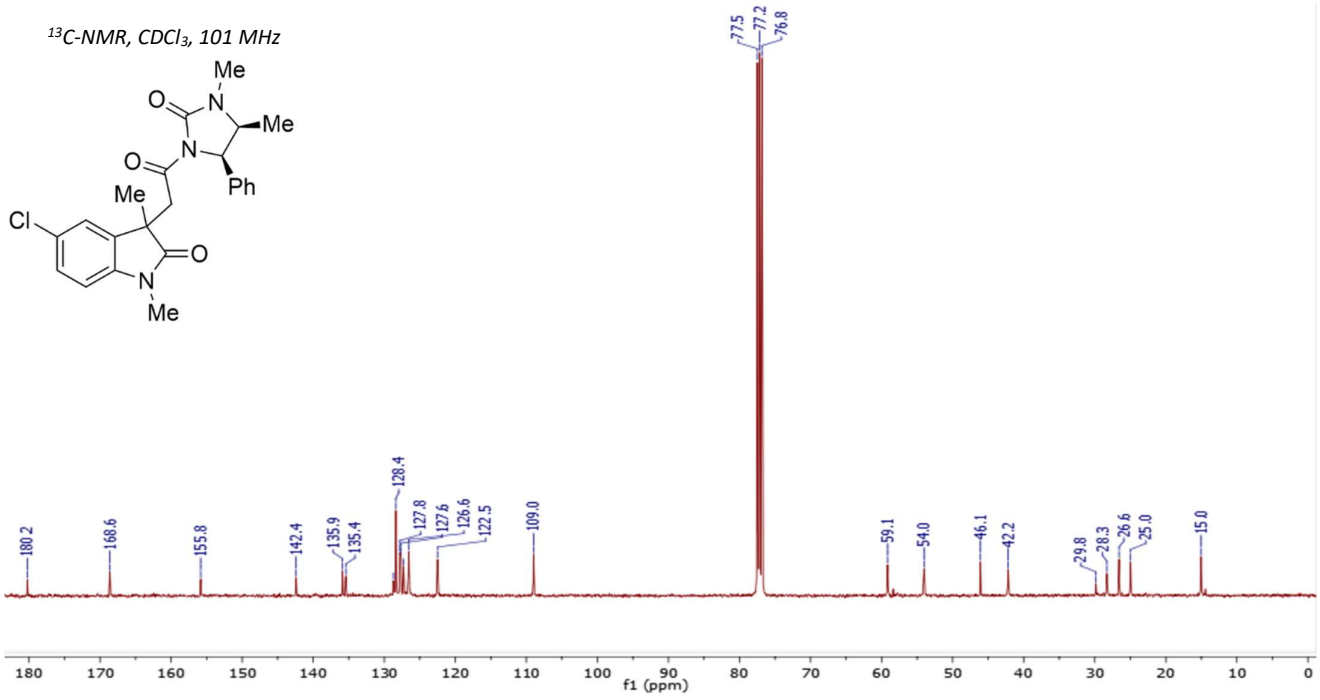

Compound 5f-D1:

^{1}H-NMR, $CDCl_3$, 300 MHz

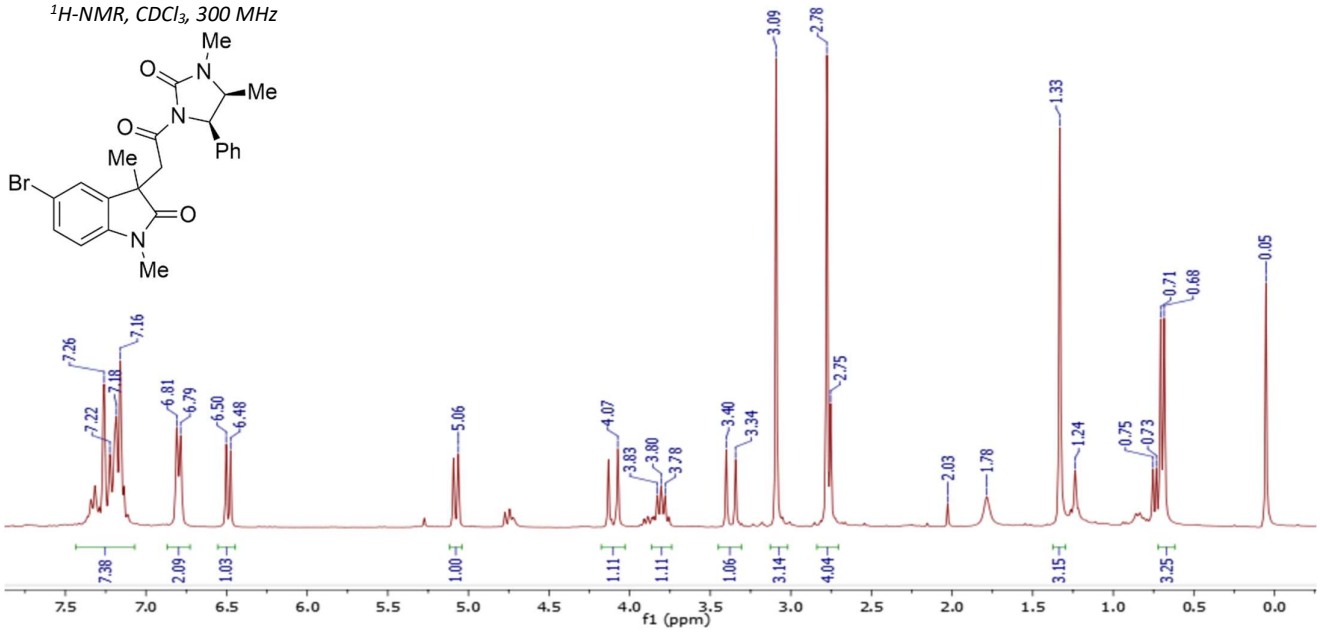

^{13}C-NMR, $CDCl_3$, 101 MHz

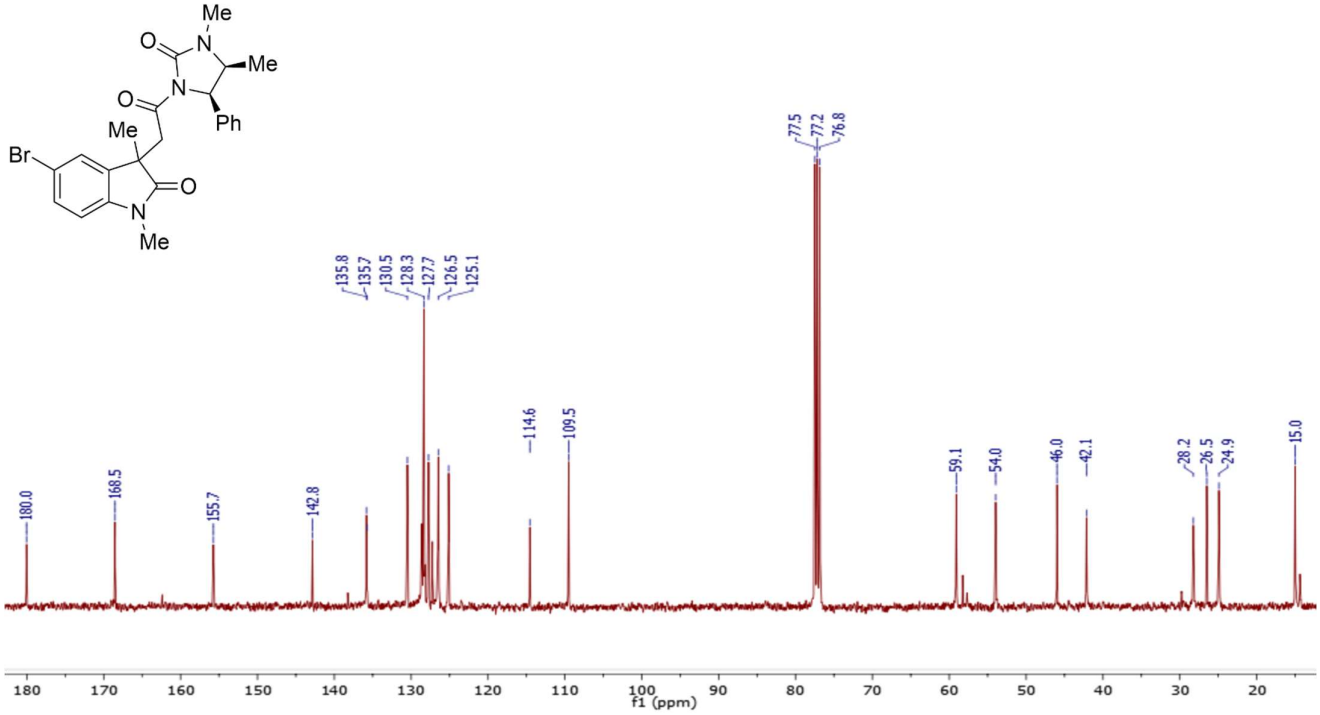

Compound 5f-D2:

^{1}H-NMR, $CDCl_3$, 300 MHz

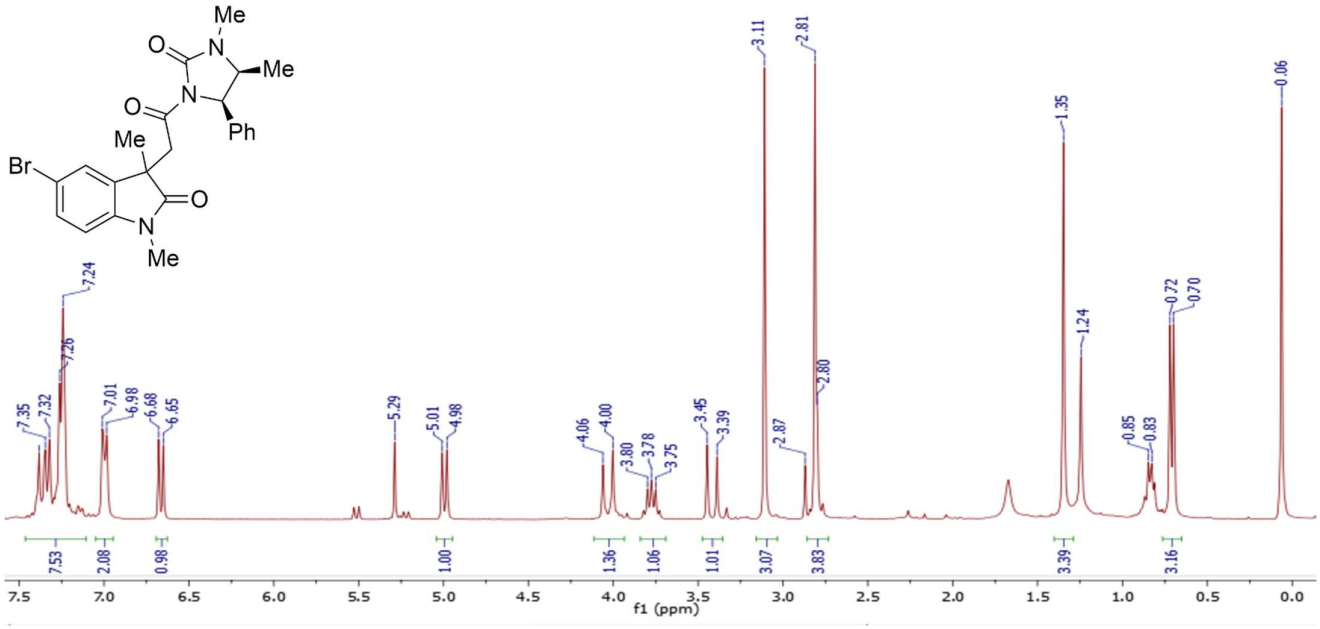

^{13}C-NMR, $CDCl_3$, 101 MHz

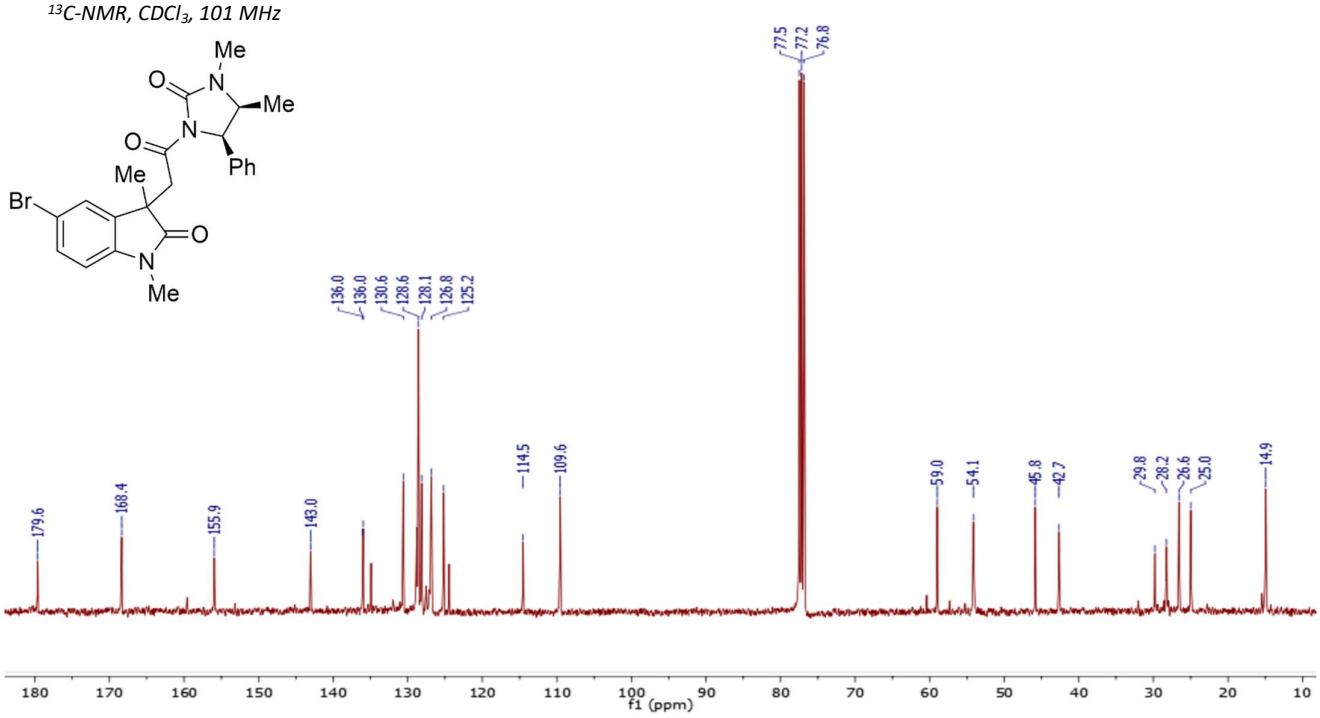

Compound 5g-D1:

^{1}H-NMR, $CDCl_3$, 300 MHz

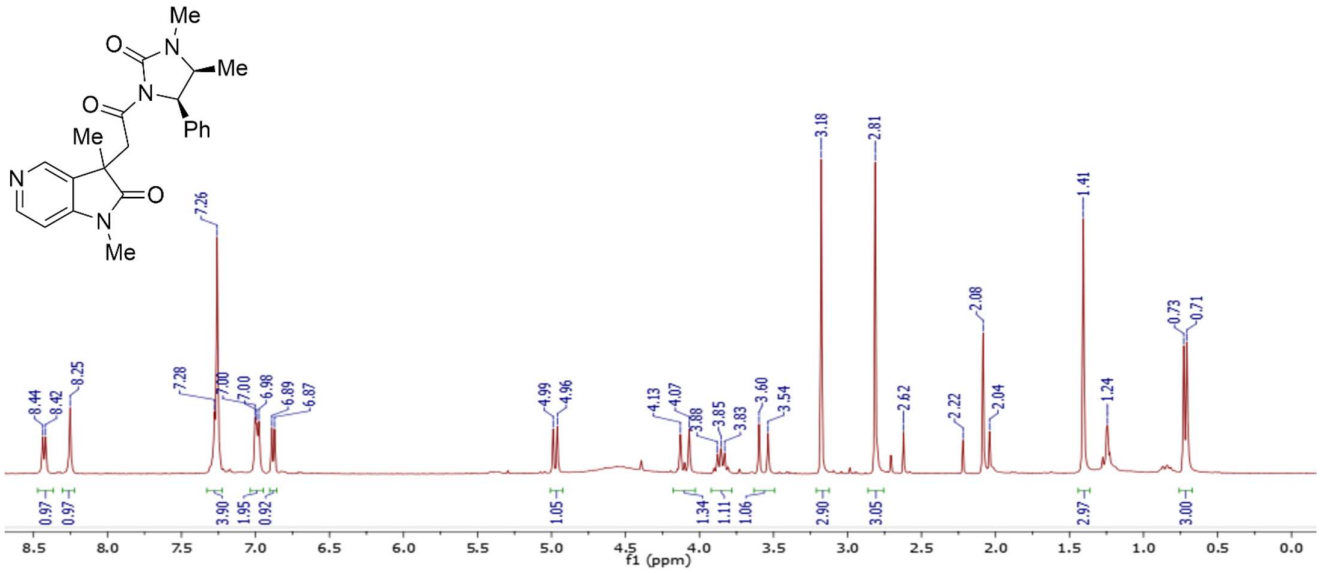

^{13}C-NMR, $CDCl_3$, 101 MHz

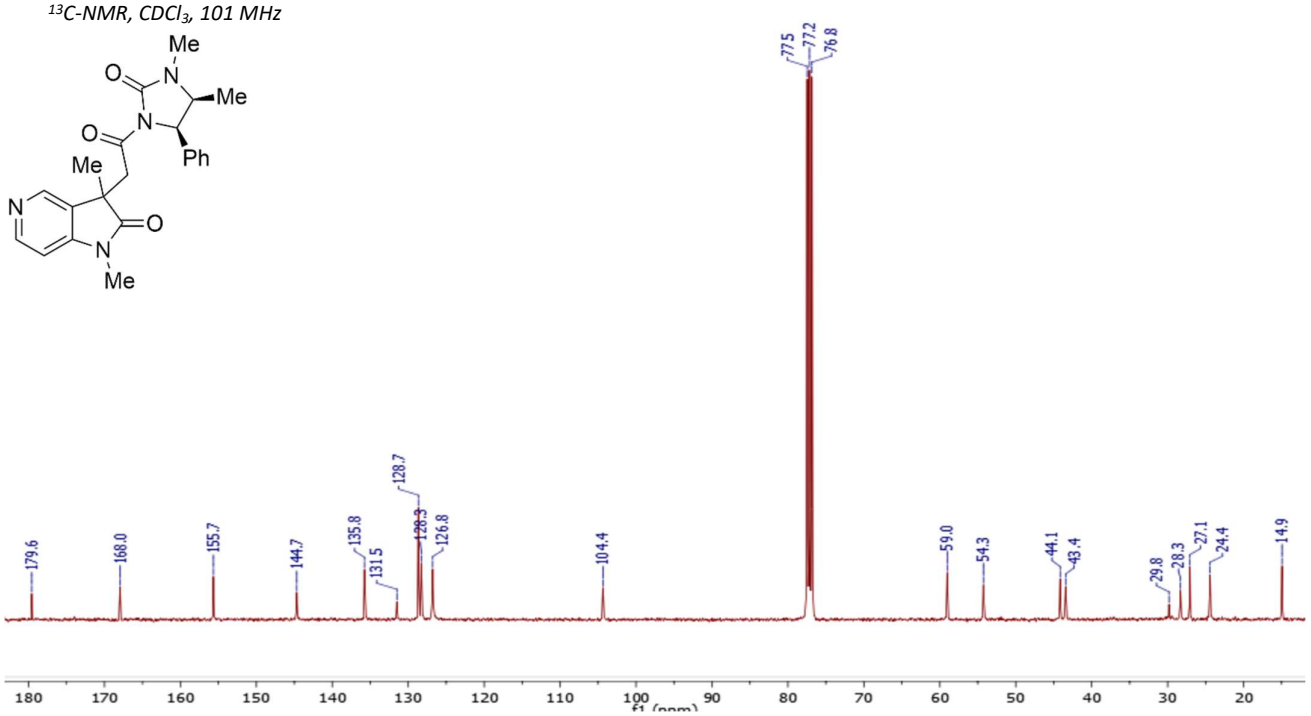

Compound 5g-D2:

^{1}H-NMR, $CDCl_3$, 300 MHz

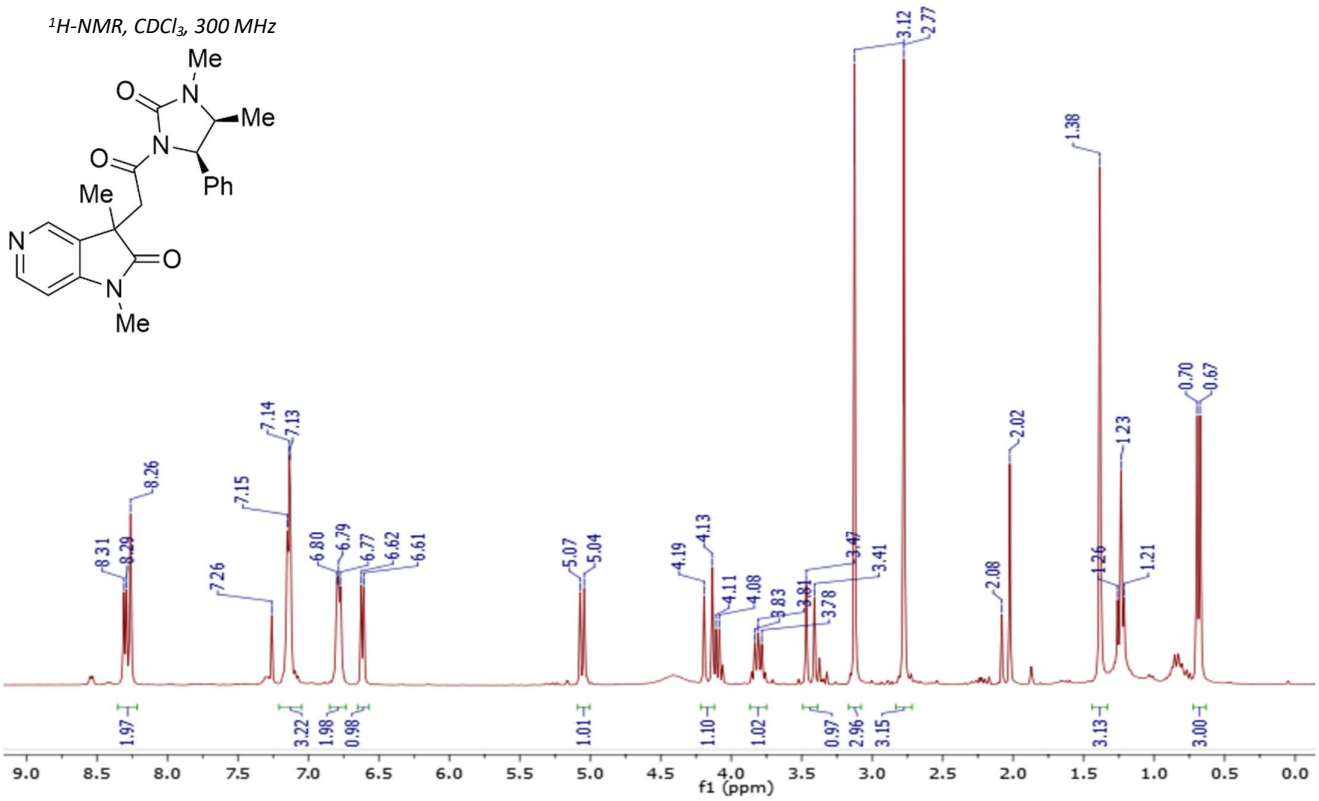

^{13}C-NMR, $CDCl_3$, 101 MHz

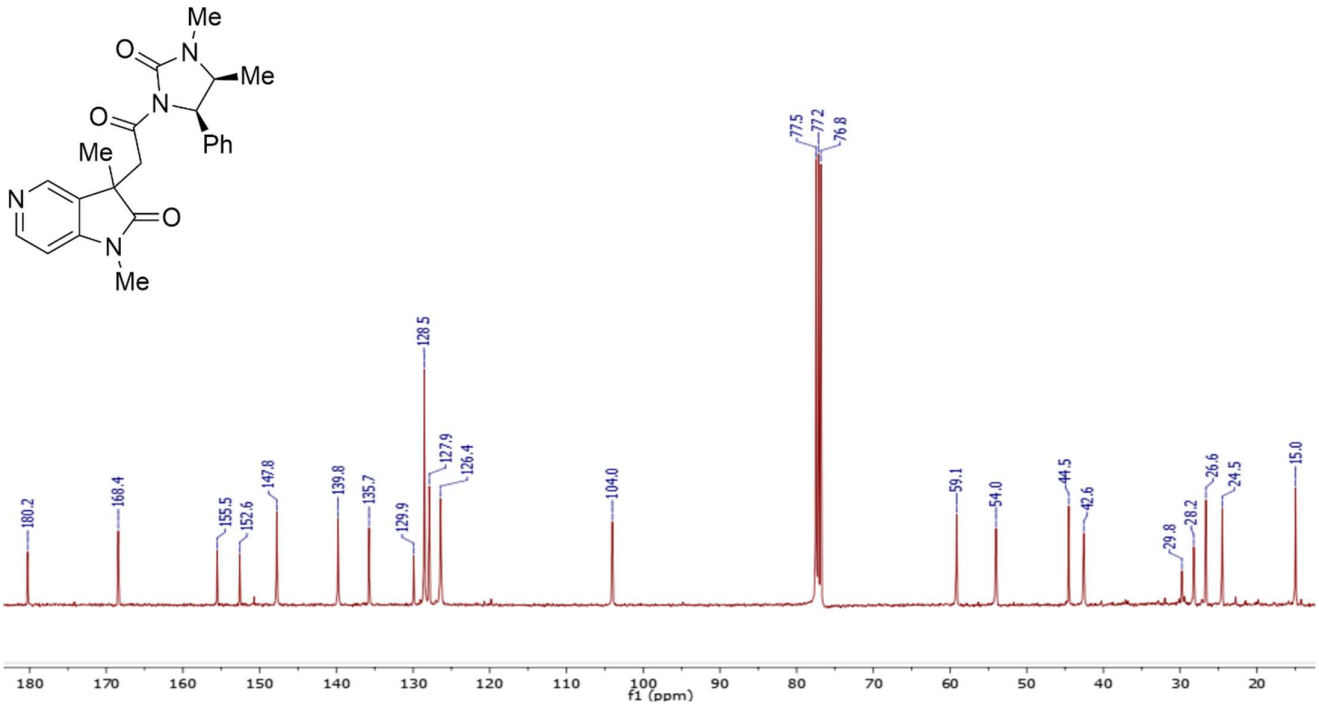

Compound 6:

^{1}H-NMR, $CDCl_3$, 300 MHz

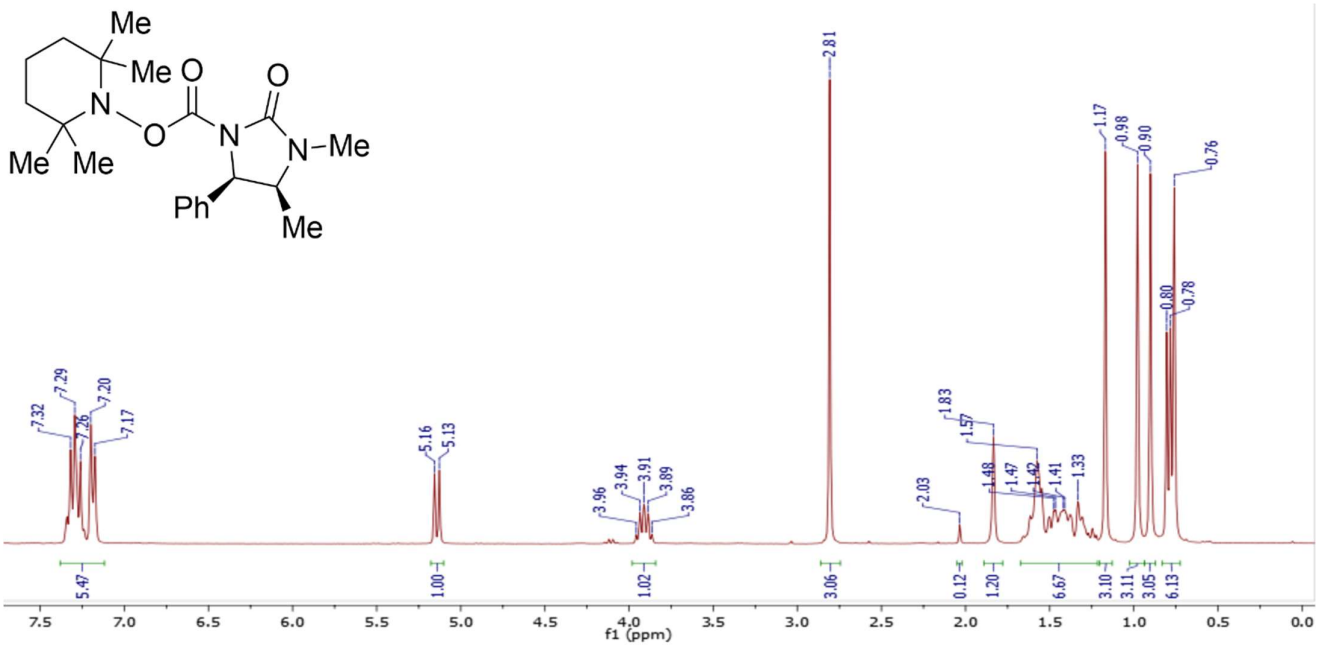

^{13}C-NMR, $CDCl_3$, 101 MHz

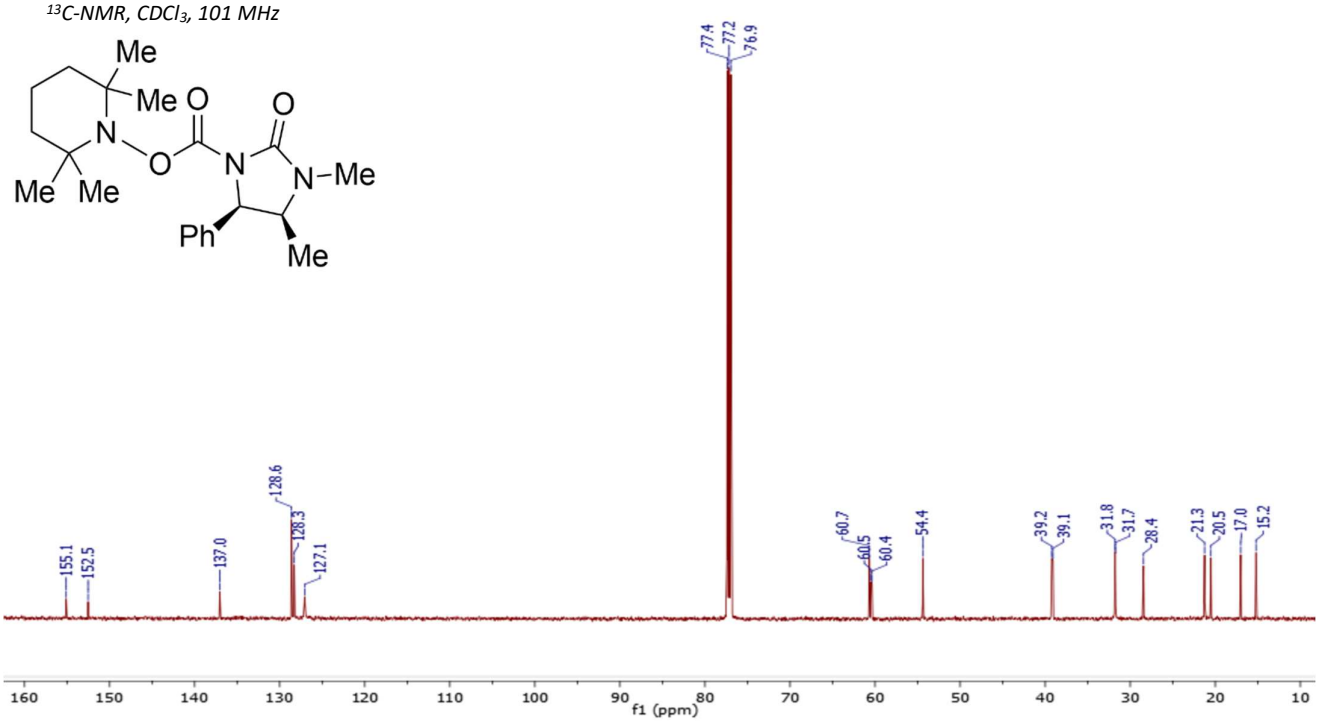

Compound 11:

^{1}H-NMR, $CDCl_3$, 300 MHz

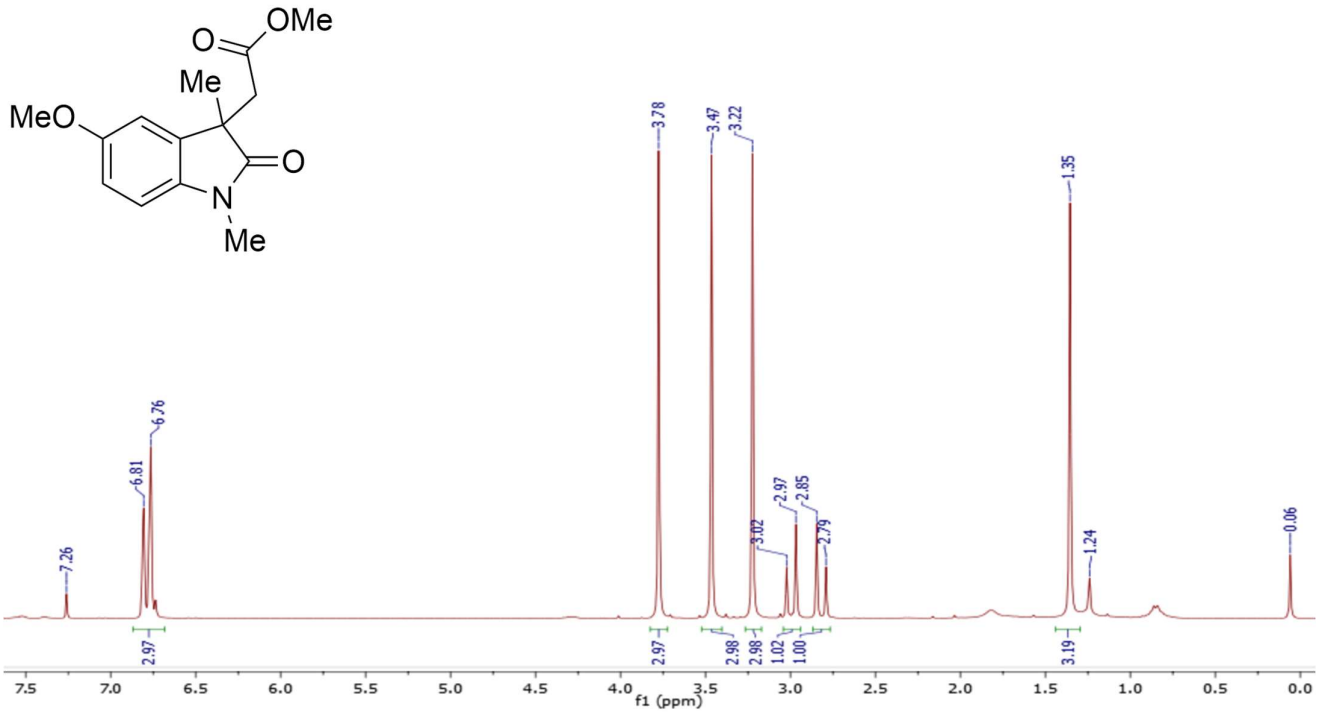

^{13}C-NMR, $CDCl_3$, 101 MHz

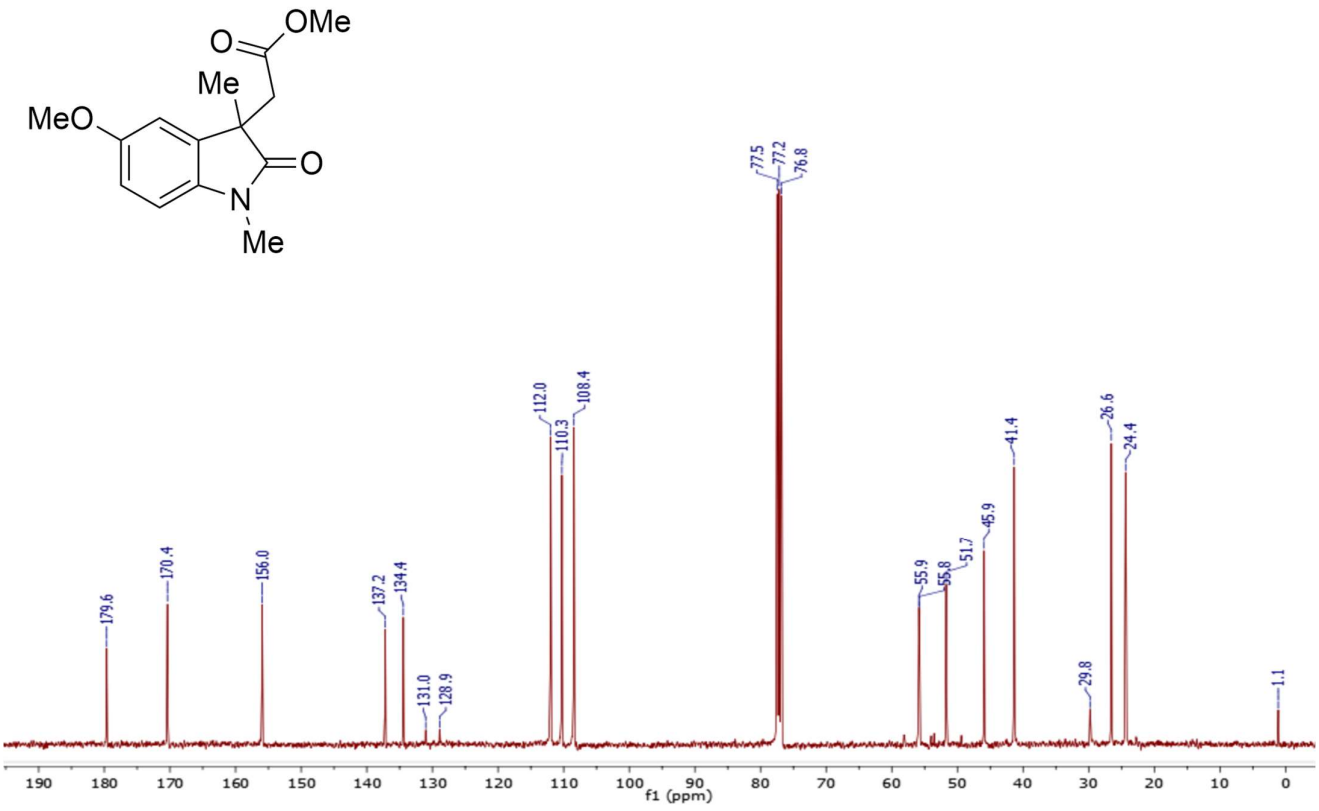

Compound 9:

^{1}H-NMR, $CDCl_3$, 300 MHz

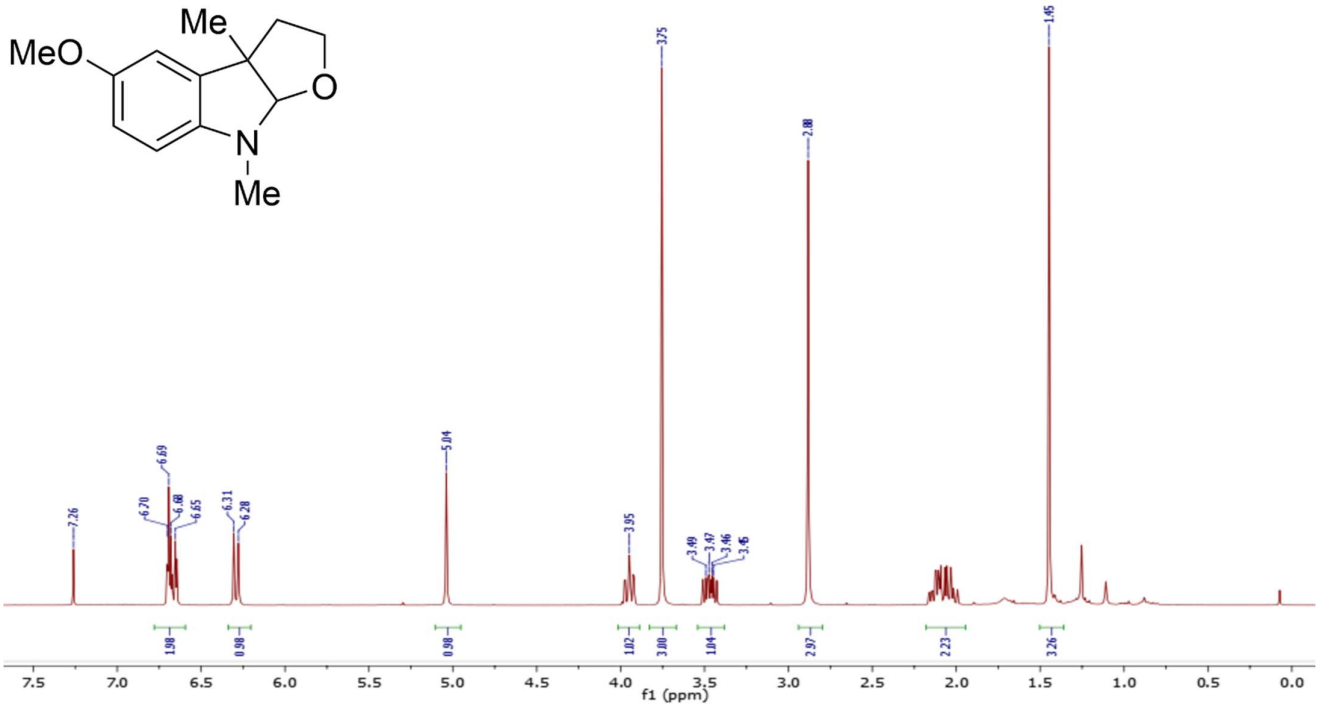

^{13}C-NMR, $CDCl_3$, 101 MHz